Silesian University of Technology
Faculty of Mechanical Engineering
Department of Fundamentals of Machinery Design

DOCTORAL DISSERTATION

Development of industrial monitoring systems with sensor integration, data fusion and information management

Joyraj Chakraborty

Dissertation advisors:

Assoc. Prof. Andrzej Katunin, Ph.D., D.Sc. Eng.
Silesian University of Technology, Faculty of Mechanical Engineering, Gliwice

Assoc. Prof. Marek Salamak, Ph.D., D.Sc. Eng.
Silesian University of Technology, Faculty of Civil Engineering, Gliwice

Gliwice, 2019

Contents

Acknowledgements

I appreciate three year financial support of my work within the Infrastar project financed from the European Union funds. The thesis has been performed within the framework of the European project Infrastar (infrastar.eu), which has received funding from the European Union's Horizon 2020 research and innovation program under the Marie Skłodowska-Curie grant agreement No 676139. The grant is gratefully acknowledged. I would like to extend special thanks to Dr Ernst Niederleithinger and BAM for the sensors and collaboration in the project.

There are many people whose support and assistance played a very important role in the realization of this dissertation. First and foremost, I would like to thank my thesis advisors Assoc. Prof. Andrzej Katunin and Assoc. Prof. Marek Salamak for their patient and precious supervision. Their guidance, knowledge, and support for this research project were the key to completion of this work. I am very grateful to them for leading me to this amazing and promising data science area and demonstrating wonderful scientific perception. I would also like to express my sincere gratitude to Dr Piotr Klikowicz in the Department of Research and Development at NeoStrain for exposing me to the field of non-destructive testing (NDT) and performing FEM calculation for this study. I am greatly thankful to our CEO of NeoStrain Mr. Marek Stolinski, thanks to whom I developed the essential background for NDT research and explored the scientific depth in this field. I would also like to thank Dr Ernst Niederleithinger for teaching me advanced NDT methods and statistical techniques in machine learning and for participating in my thesis committee. Besides, I greatly appreciate the help of my labmate Mr. Łukasz Chmielowski, and would like to thank him for his valuable time and effort in providing crucial discussions and suggestions for this thesis. I am very thankful to my wife Manisha Chakraborty for her love and support. I greatly appreciate her for all the advices. I am gratitude to her for helping me to stay strong in critical moments. At last but not least, I would like to thank our parents Swapan Chakraborty, Kalpita Chakraborty and Sukumar Chakraborty, Archana Bhattacharjee for their unwavering support, and all of my friends here at NeoStrain, friends in Bangladesh and all the ESR's, specially Xin Wang, Amol Mankar, Mariia Nesterova and Joey Velarde for making my academic life very memorable. I specially appreciate valuable advice of my childhood friend Dr Jasim Uddin.

List of important abbreviations

RC	Reinforced Concrete
NDT	Non Destructive Testing
SHM	Structural Health Monitoring
DOFS	Distributed Optical Fiber Sensors
UHPFRC	Ultra-High Performance Fibre Reinforced Concrete
SNR	Signal to-Noise Ratio
UPV	Ultrasonic Pulse Velocity
RMSE	Root Mean Squared Error
CWI	Coda Wave Interferometry
AR	Autoregressive Model
CC	Decorrelation Coefficient
CWT	Continuous Wavelet Transform
STFT	Short-time Fourier transform
UPV	Ultrasonic Pulse Velocity
AE	Acoustic Emission
DIC	Digital Image Correlation
LVDT	Linear Variable Differential Transducer
AROC	Area under the ROC
FBG	Fiber Bragg Grating
FOV	Field of View
WAN	Wide Area Network
LAN	Local Area Network
DAU	Data Acquisition Unit
POD	Probability of Detection
FAR	False Alarm Rate
AUC	Area Under the Curve
ROC	Receiver Operating Characteristic

1. Introduction

1.1 Motivation

In recent years, civil infrastructural health monitoring has gained noticeable attention in the academia as well as in the industry because of maintenance done on bridges due to demands on the safety of the structures. A civil infrastructure such as a bridge is an essential part of public transport links, and constitutes the main attraction in the infrastructure. Therefore, bridges and roads are part of the critical points in all over the world. However, they are expensive to build and maintain, and their unexpected failure can cost a lot (sometimes may be a cause of death). For this reason, the safety of bridges is recognized as a significant problem. Therefore, bridges are expected to have maximum reliability and provide long-term service. To ensure this long-term service, a civil infrastructure should meet the requirement of safety and support. In practice, this can be ensured thorough inspection and maintenance schemes that can be beneficial from the economic viewpoint. Unfortunately, even with the most consistent and thorough visual inspections under the implemented bridge management systems, serious structural damage and bridge disasters still occur. This is a result of a gradual reduction in the level of safety of the facilities operated, of fatigue, accidents, and natural disasters such as earthquakes, typhoons, or floods.

The recent example of such a collapse was Morandi Bridge in Italy. The collapse of the motorway viaduct occurred in Genoa last year on August 14th, leading to at least 43 victims (see Figure 1.1). The Morandi Bridge, a viaduct more than one kilometre long and 45 meters high, crossing the Polcevera coastal river. The website BBC.com noted that this type of infrastructure should have a lifespan of at least one hundred years (*Morandi Genoa bridge: Towers demolished after evacuations*, 2019). Many researchers claim that the collapse was most probably due to the corrosion of pretension cables. Moreover, they mentioned the importance of bridge maintenance during the structure's life and raised the problem of the limited maintenance budget. To prevent the effects of corrosion on concrete structures, it is essential to detect and describe cracks that may appear on the concrete surface as early as possible and, in particular, to estimate their depth and width.

Figure 1.1: Photo of Morandi Bridge after the collapse (Ferraris, 2018)

This incident increased the need to control the technical condition and safety of ageing bridge structures in Europe. Most of the bridges in Europe are now over 40 years old and their service lifetime is becoming a serious issue. Therefore, bridge maintenance has an important economic effect. The monitoring of bridges is recognized as a significant problem. However, still, most institutions consider visual inspection to be-annual monitoring. Visual inspection, though, is not considered as optimal inspection due to the need to detect microcracks and fatigue. Bridges need to be maintained to identify possible damage and its evolution must be followed. Therefore, there are different research projects to be found on crack detection of aged bridges, leading to experiments and models. The development process of concrete fracture/fatigue is not yet well understood. Much has been learned from laboratory tests. However, in situ investigation of the concrete damage is still limited because of challenges in terms of difficulty to access bridges in service, limitations in inspection techniques, long-term monitoring, and detection capability. Consequently, researchers aimed at developing techniques and data processing for long-term structural health monitoring (SHM) by modifying the existing technologies derived from other areas of application in order to facilitate structure management/ NDT techniques with SHM have an increased potential to be part of such SHM systems for safety investigation. It is, therefore, necessary to use reliable NDT techniques, that able to detect damage quantitatively for bridge inspection.

1.2 Importance of the SHM system

Civil infrastructures, like bridges, are capable of safely transferring the superimposed loads to the foundations. However, their structural integrity is degraded by different kinds of operational and environmental effects. Since civil infrastructure is a significant part of the national economy, its strength is very essential in maintaining high levels of structural safety and durability. Hence, an efficient system is urgently required for regular structural assessment and performance of the infrastructure. Therefore, the focus on capability to monitor performance of the large area of structures and on detecting changes, cracks in the structure at the earliest possible stage has increased in recent years due to a number of incidents all over the world, bridges maturing, material deterioration, and limited resource allocated for inspection. Monitoring of changes in the condition of an RC structure and detecting microcracks before they develop into macrocracks, and timely intervention, could stop the premature failure of the structures.

The diagram presenting advantages of using the SHM system for civil structures is presented in Figure 1.2. In detecting damage (e.g. cracks) inside a large concrete structure the only method to validate the result is the destructive method applied to the area of suspected damage. Nonetheless, destructive testing is sometimes not allowed to determine quality of the concrete (also taking a samples is dangerous for the structure). Therefore, there is an increased demand for more precise NDT techniques and, at the same time, for more flexible evaluation and capability to detect the quality of the concrete. There is a clear need to transfer sensing and damage detection technologies from the laboratory environment to routine field applications. The system of diagnosing structural integrity and estimating the nature of damage/change in the structure is usually referred as SHM.

1.3 Organization of the work

The first part of this work discusses evaluation of an automated NDT techniques that can determine adverse changes in the structure with the possibility of visualization of results, based on the integration of sensors and quantify damage evaluation for long term monitoring. The second part presents a feature extraction from newly developed ultrasonic sensors for damage investigation of RC structures. The developed platform was based on advanced signal processing methods, including methods of data normalization and extraction of time-frequency features. The last part of this work presents data fusion techniques to improve overall performance.

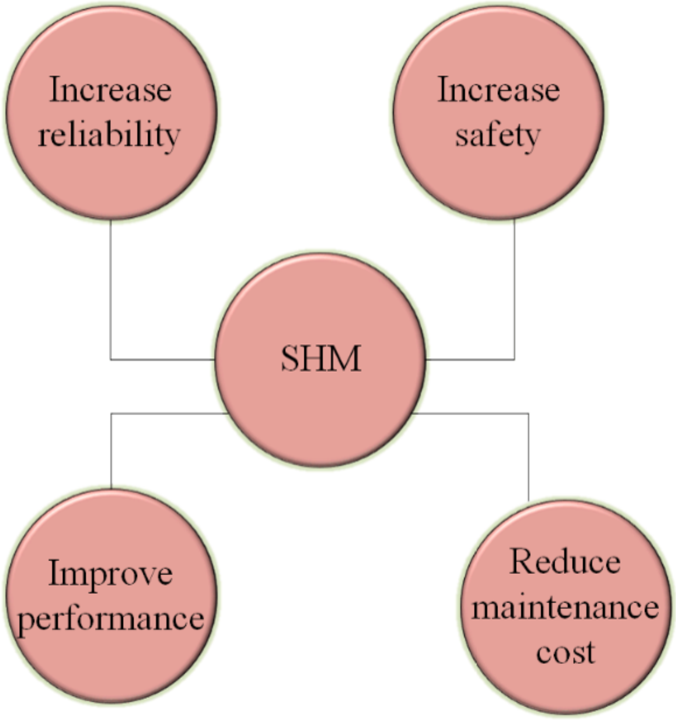

Figure 1.2: Diagram presenting advantages of using SHM for civil structures

This thesis consists of eight chapters. Chapter 2 is the literature review followed by the introduction of bridge structures and different NDT methods. It begins with a brief description of a different types of structure, structural components and their building materials, particularly composite materials made of concrete and steel rods. Afterwards, the types of damage that may appear in the structure are presented. Subsequently, the importance of using the SHM system and types of NDT techniques also discussed. Chapter 3 presents the identified research problem based on the literature review performed in chapter 2. Chapter 4 presents the basic research on the propagation of the ultrasonic wave in concrete and types of ultrasonic transducers their limitations leading to development of new transducers. The procedure of feature extraction from ultrasonic signals is presented. Subsequently, their usage in different applications is also discussed in chapter 5. Chapter 6 includes designing of a new data acquisition system. Then, the test object and experimental setup are described, and signal acquisition for a real object is presented along with the results obtained. Data fusion techniques are detailed in chapter 7. The types of fusion techniques and their usefulness in different applications also presented. The final chapter concludes the thesis by summarizing the work and providing the final conclusions.

2. Introduction to civil structures and non-destructive techniques

2.1 Civil structures

Civil engineering is a discipline of engineering and technical sciences serving to modify the Earth's surface for the needs of human existence (Claisse, 2016). It combines such skills as analysing, designing, construction and maintaining of all civil structures and their components, in particular, such structures and their elements as bridges, roads, canals, tunnels, dams, towers and others. Sometimes also those that are referred to as buildings. Civil engineering and construction in some cases require the transfer of knowledge associated with other disciplines of engineering and technical sciences, such as environmental, material, electrical, mechanical or computer engineering. This necessary transfer of knowledge results from the fact that contemporary civil structures are becoming more and more complex and sophisticated. It forces the use of an interdisciplinary approach to solving all problems related to the durability and safety of these advanced objects. Within the context of the civil structure, the term “structure” directs to anything that is made or built from correlative parts with a fixed location on the ground. This includes buildings but can refer to anything that is designed to carry loads, even if it is not intended to be occupied by people such as bridges, tunnels, towers, windmills, etc (Connor and Faraji, 2016). Most of the civil structures react to static forces, and dynamic influences are usually in the minority. Construction is one of the most energy-consuming and material-intensive branches of the economy, consuming about 50% of produced materials and 40% of energy while emitting nearly 35% of greenhouse gases. At the same time, it is the branch in which the most innovative changes related to automation and robotisation are taking place. There is a wide variation of civil structures just in terms of construction materials. Primary structural materials are, of course steel, concrete and timber. The use of entirely new types of materials, which until now have been used rather in the aviation or space industry, is more and more often noticed. There are new metal alloys using aluminium, titanium or stainless steel. Glass is more often used as a structural material. Recently, the number of structures made of polymer composites has increased significantly. All this is the result of engineers seeking materials that will more easily meet growing investment needs, replace traditional solutions that deplete natural resources, and at the same time improve the durability and safety of structures. The large variety of civil structures and materials used in them discussed above necessitates limitation and orientation of research work. Besides, research must be pertinent to issues that have been set out in the Infrastar project. That is why this project is limited to two types of building structures: bridges and wind turbine towers. For the purpose of this study this range has been further narrowed to RC, the material most commonly used in bridges - RC. More than 75% of new bridges around the world will be made of concrete in the near future. That is why mainly bridges made of RC are analysed in the next sections.

2.1.1 Bridges

A bridge is a kind of civil structure, the construction of which allows overcoming water or land obstacle, built in such a way that under it remains a space. Bridges are used by people and various forms of transport, even animals to safely overcome obstacles. Bridges are of extraordinary importance in strategic and economic terms. Most roads eventually encounter an obstacle that needs to be overcome. This applies to simple nature trails for pedestrians, riders, as well as to canal shipping, the railroad or modern roads. This group of structures includes bridges (over water obstacles), viaducts (over obstacles without water), flyovers (over urbanised areas), and culverts. Designs of bridges depend mainly on the bridge function and the nature of the terrain where the bridge is to be constructed (Chen and Lui, 2005). Bridges are generally classified according to:

- Function — highway, railway, pedestrian bridge;
- Structural material — masonry, timber, steel, concrete, polymer composite bridges;
- Structural system — beam, rigid frame, truss, arch, cable-stayed, suspension bridges.

Main structural systems of bridges are shown in Figure 2.1. The most common bridge structure is the beam bridge, which is the simplest and less expensive form with one or more simple-supported or continuous spans (Figure 2.2). A bridge structure can be divided into two main parts — substructure and superstructure. Substructure (Figure 2.3) is the portion of a bridge structure including supports with abutments and piers supporting the superstructure (Matsagar *et al.*, 2018), while a superstructure is the portion of a bridge structure which carries the traffic load and transfers that load to the substructure. This transfer is usually done through bearings which are devices placed on the top of piers or abutments at both ends of the girder. Girders or beams are horizontal structural elements

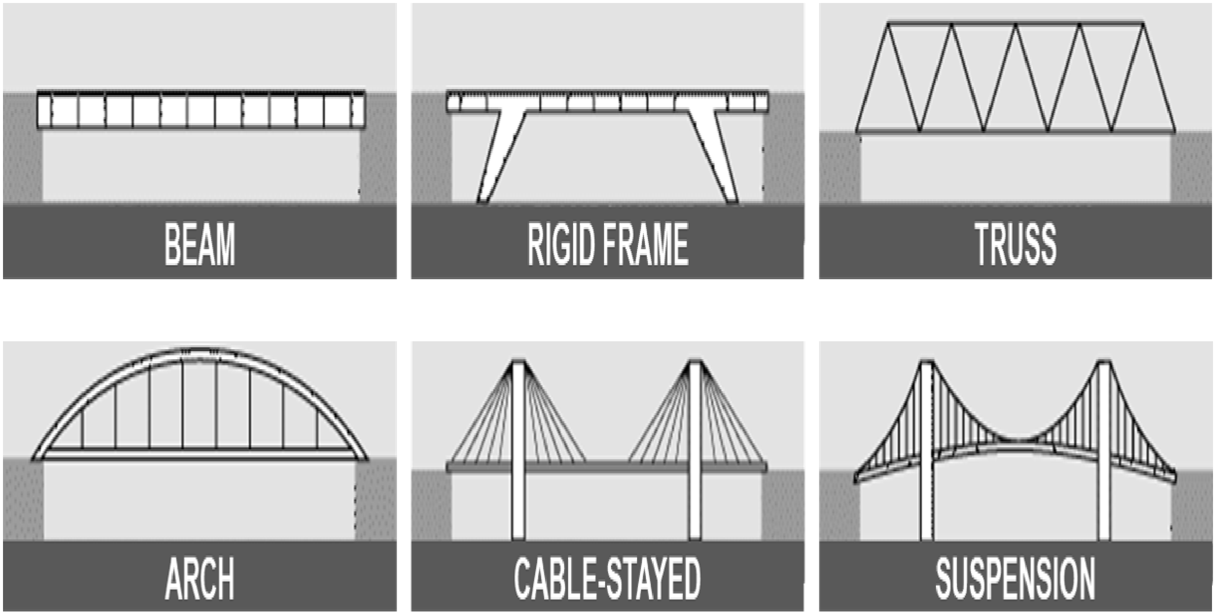

Figure 2.1: Main structural systems of bridges

supporting vertical loads together with the deck or slab which is at the top surface of a bridge. The bridge deck carries traffic loads directly and transmit them to girders.

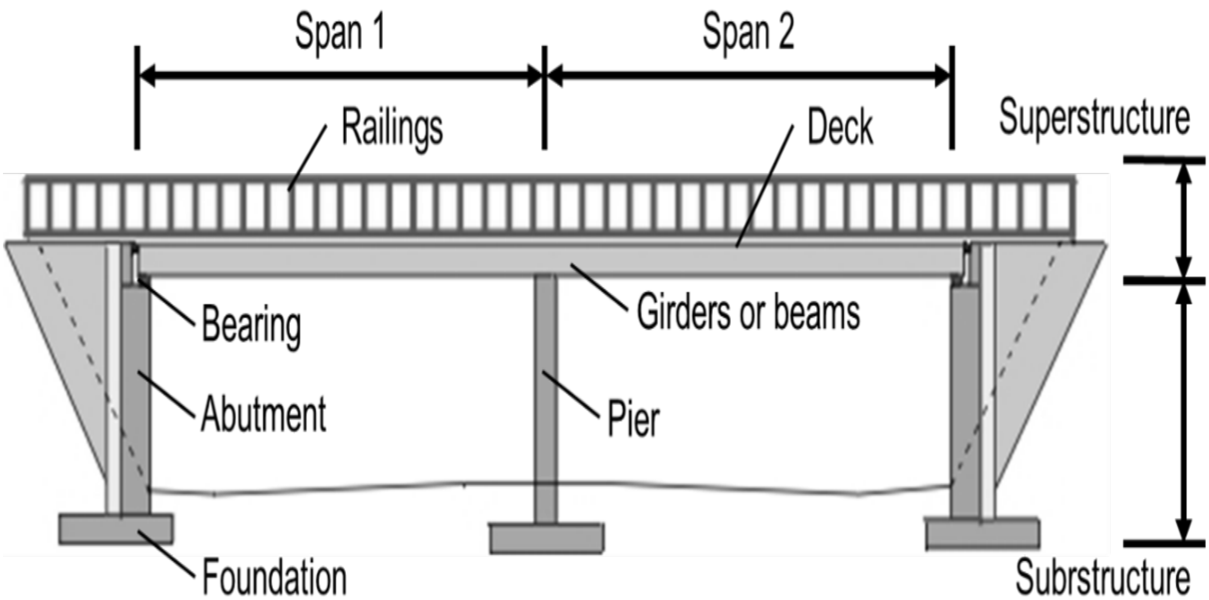

Figure 2.2: Main structural components of a bridge

Depending on the structural system, various types of internal forces may occur in the structural components of bridges causing specific types of stresses and associated deformations. In general, vertical loads and high compression dominate in all types of supports.

The supports transfer enormous reactions from spans to foundations. Only in the case of high piers or pylons, more significant horizontal effect caused by wind, traffic or thermal effects may occur (Zakić *et al.*, 1991). Such a support should therefore be also designed to resist bending and eccentric compression. In some structural systems such as rigid frame or arch the supports may be integrated with the superstructure and constitute a uniform system that requires appropriate modelling. When it comes to superstructure elements,

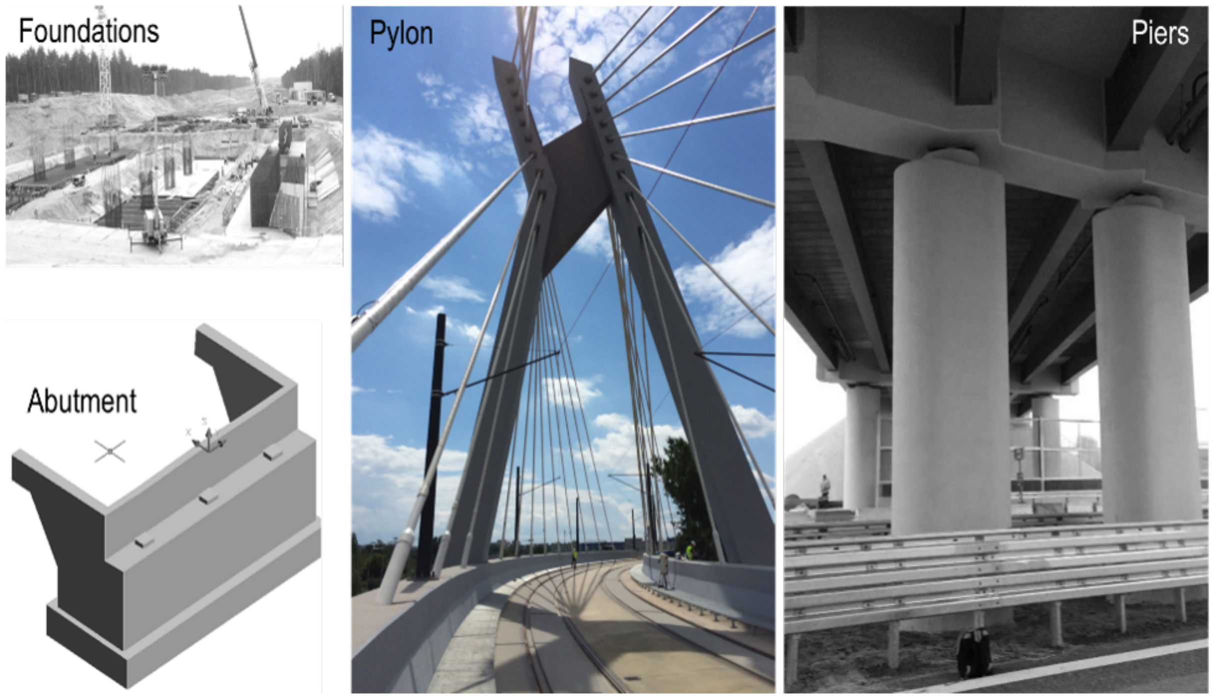

Figure 2.3: Examples of bridge substructures

their static and dynamic response very much depends on the chosen structural system. The simplest solution is, of course, beam bridges mentioned above. Bending accompanied by shear dominates in their girders. The arch bridge has been one of the most often-built structures since antiquity. This is due to the nature of this structure. With properly formed arc geometry, only compressive stresses occur. Thanks to this, in the past it was possible to use materials such as stone and bricks. Modern arch bridges, built mainly of steel or prestressed concrete, no longer need to be so limited in terms of geometry, and that is why designers often choose some very extreme forms. Rigid frame bridges (Figure 2.4) have supports integrated with the girders, which is why they are characterised by a more complex state of stress in all structural components. There is also special horizontal expansion force which must be carried by internal braces or transferred to the soil. Truss bridges are usually plane or spatial rod systems connected in nodes that form multiple triangular structures. The internal forces that dominate them are axial. In the suspension bridge, the girder with the platform is suspended on slender hangers to the main load-bearing cables. The cables are passed through the tops of tower supports called pylons and are usually anchored in the ground at the ends of the bridge. The suspension bridge, on the other hand, also has a girder suspended on tie rods (stays), but these are mounted in pylons to form a triangular girder-stay-pylon system. The girder is bent and compressed, the stay is stretched, while the pylon is mainly compressed (Yilmaz and Wasti, 1984).

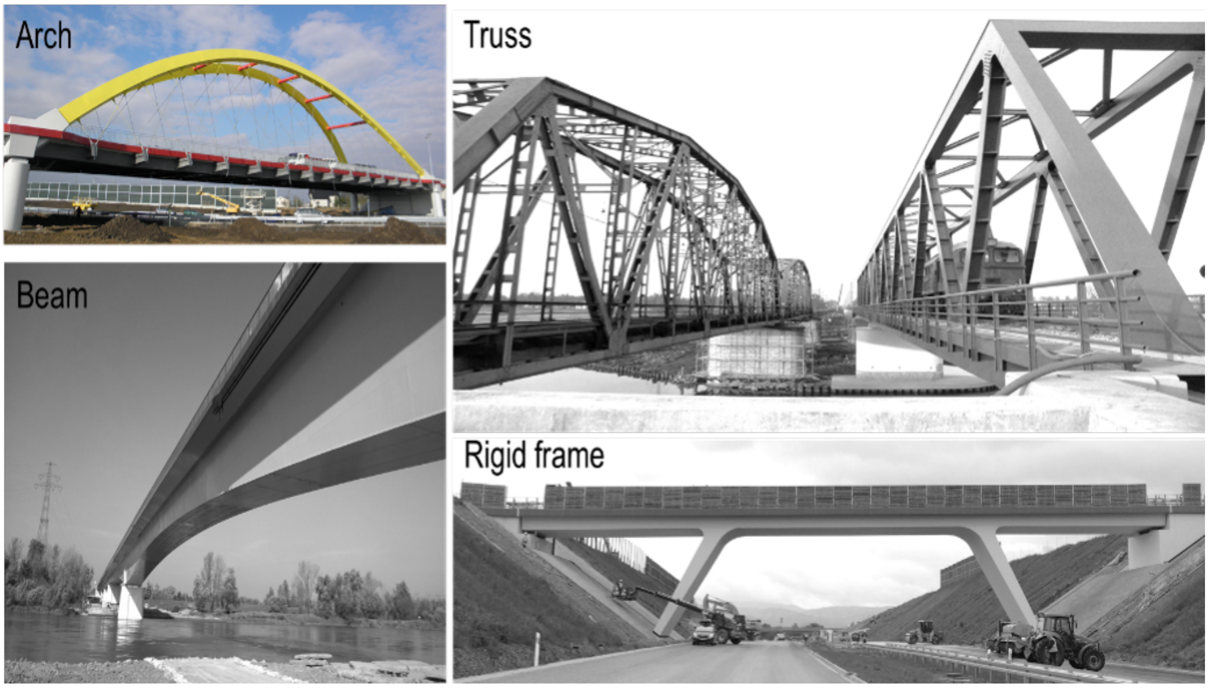

Figure 2.4: Selected examples of different bridge structural systems

Most cases of SHM implementation are designed and installed in the largest and most important modern arch, cable-stayed, suspension bridges. Selected examples of Polish bridges are presented in Figure 2.5. A diagram of the most widespread bridge constructions and their components for SHM is presented in Figure 2.6. Hence, the importance of concrete in modern civil structure like bridges cannot be ignored. Superstructure material is composite, therefore concrete is one of its principal components. It will be discussed in detail in the next section. Therefore, it is discussing in the next section.

2.2 Reinforced concrete as a structural material

RC is a structural composite consisting of concrete reinforced with steel bars. This combination is widely used in construction. Concrete is excellent at transmitting compressive stress, but its tensile strength is very low. Therefore, the steel elements connected to

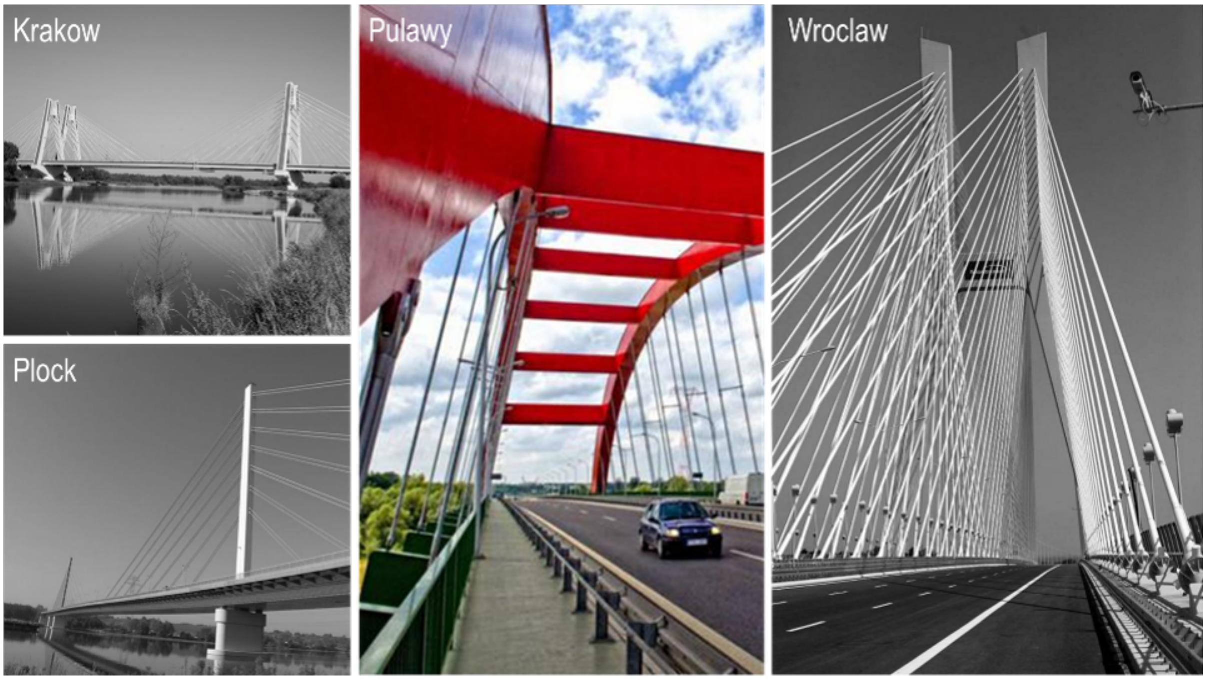

Figure 2.5: Selected examples of Polish bridges with installed SHM systems

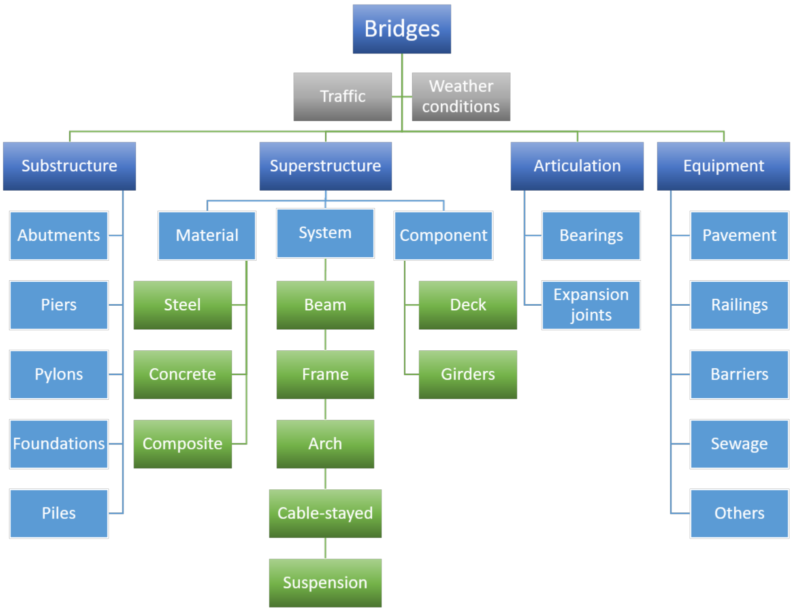

Figure 2.6: A diagram of components of bridges able for SHM

transfer it, mainly tensile stress. Compression reinforcement is also often used nonetheless (Ghosh, 1991). The essential component of RC is concrete, sometimes described as artificial stone. It is a kind of composite created by mixing the binder (cement) and the filler (aggregate), possibly admixtures that give the desired qualities, and water (Mosley and Bungey, 1987; Tsiskreli and Dzhavakhidze, 1970). It is one of the most common building materials in modern construction. Its global production is about 7 billion m^3

annually, which is three times more than wood timber and seven times more than steel per year. Concrete is the most widely used substance on Earth, just after water (Yaphary *et al.*, 2017).

Concrete is such a popular building material because of its properties and versatility. What it amounts to is:

- Easy availability of raw materials from which it is made;
- The right proportions of ingredients;
- The possibility of various applications and shaping;
- Ease of transport and installation due to the fluidity in the initial phase;
- Strength and durability.

Concrete has a long service life and relatively lower maintenance requirements compared to steel or wood. This increases the economic benefits of using concrete in construction. Concrete does not corrode so quickly. It can be tight and frost-resistant. Both the production of concrete and the preparation of the form-shaping formwork can be done in-situ, which reduces transport costs. Concrete is non-flammable and can withstand high temperatures, making it a suitable material for many applications. It is resistant to wind, rain, chemical and biological influences. Of course, provided that there is sufficient tightness (Skalny, 1985).

The idea of combining these two different materials (concrete and steel) emerged because the concrete's tensile strength is much lower than its compressive strength. Steel reinforcements complement these deficiencies. The excellent cooperation of both materials also results from the fact that their thermal deformability is similar (Tabsh and Abdelfatah, 2009). The connection is effective due to the good adhesion of concrete to steel, which is further improved by using bar ribs. The advantages of RC as a structural material include fire resistance, resistance to significant static and dynamic loads, freedom in forming elements, high corrosion resistance (while maintaining the proper cover of steel inserts and correct compaction of the laid concrete mix). Weather resistance can be increased by performing relatively cheap coating protection. These protections are mainly used in the construction of bridges, dams, tunnels, roads, towers.

The essence of RC is the existence of interaction and connection between concrete and steel reinforcement (Figure 2.7). The effectiveness of reinforcement depends on the mechanical properties of concrete, with its uneven surfaces of particles in contact with the steel bar. As a result of mutual deformation of steel and concrete, frictional forces arise that cause the concrete to stretch or compress the reinforcement. In addition, concrete has specific rheological properties occur in the reinforcement. It is shrinkage and creep.

Of course, this is also a load, but working contrary to the classic load, designed and stimulated by an engineer. Concrete shrinkage occurs regardless of the load and is manifested by a decrease in the volume of concrete. It is caused by chemical and physical phenomena, and above all drying out (Grattan-Bellew, 1996). This phenomenon may cause shrinkage cracks, which have a negative effect on the RC structure, reducing its tightness and durability, but also create notches that reduce fatigue resistance. Such cracks can also be identified using NDT techniques or monitored by SHM systems.

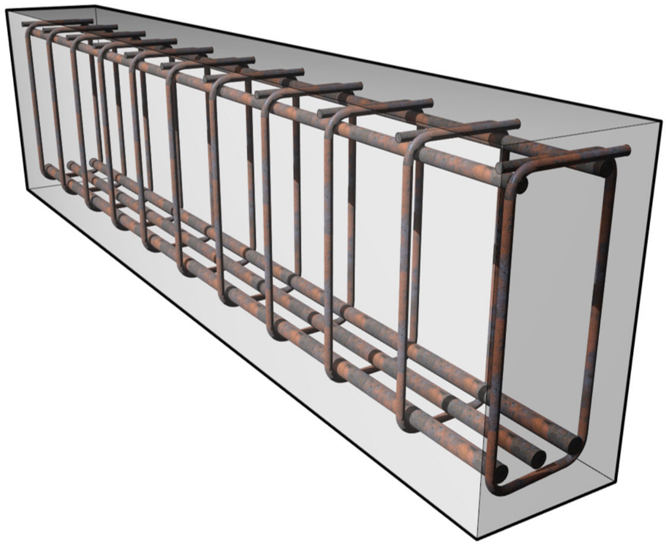

Figure 2.7: The model of reinforced concrete beam (Vasshaug, 2019)

RC is a better structural material than concrete alone without steel bars. The reinforcement reduces the amount and the width of cracks while improving the strength of the entire element. However, it may not provide full crack resistance and has specific strength limits depending on the concrete grade and degree of reinforcement. Increasing the bridge span can always be associated with an increase in beam cross-section and higher consumption of concrete and steel. With a certain span, the use of RC will no longer be effective and economically unjustified.

RC may not ensure full tightness, as it is always accompanied by cracks and microcracks. If water or moisture gets into them, it can quickly penetrate the reinforcement, which may start to corrode. This is the beginning of the entire element destruction process. To avoid such cases, the French engineer Eugène Freyssinet was the first who found a solution by compressing the entire concrete element by stressing the steel tendons concreted in them (Grattan-Bellew, 1996; Menn, 1990). Compression is an active response of the designer to external impacts from self and utility weight. Of course, this is also a load, but working contrary to the classic load. It is designed and stimulated by an engineer.

The structure must safely transfer the combined action of these power systems. The main advantage of introducing compression into concrete is stopping the formation of scratches. The load capacity of the compressed element also increases (Wight, 2015). As a result of pre-stressing, concrete is always compressed and less prone to cracks or damage. The difference between concrete, RC and the prestressed concrete beam is shown schematically in Figure 2.8.

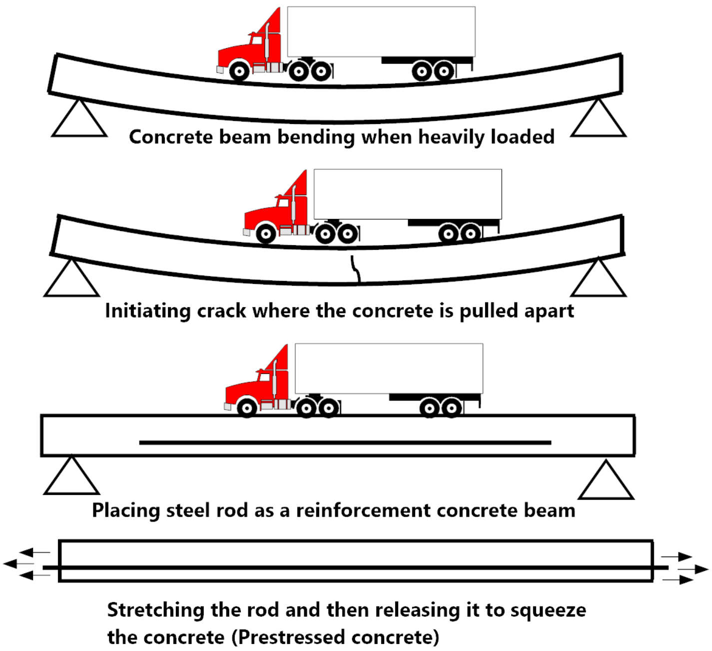

Figure 2.8: Difference between different types of concrete beam

The most commonly used cross-sections of concrete bridges are double-beam and box systems shown in Figure 2.9. The double-beam cross-section has a Gliwice Bridge, which was chosen for in-situ tests described further in section 6.5.

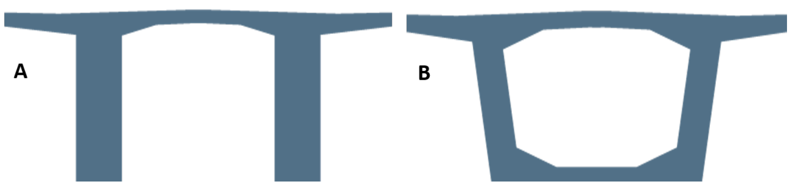

Figure 2.9: Double beam (A) and box cross-sections of bridges (B)

Many scientists and engineers have studied the characteristics of RC elements and their connections under various loads. An exhaustive literature review was carried out to understand the effect of reinforcement on the response of structural elements and the possibility of cracks and damage.

The authors of (Atorod Azizinamini and Hatfield, 1994), investigated flexural capacity and ductility of square high-strength concrete columns under simulated seismic loading. The results shown that the axial load increased bending capacity of columns, but ductility consolidated significantly. Their analysis indicates that the enhancement of volume of transverse reinforcement improves ductility. Tsonos (2004), conducted a full-scale failure testing of behaviour of a RC bridge using a number of new sensors along with traditional sensors. The author proposed to use carbon fibre reinforced polymer (CFRP) bars near surface mounted reinforcements in order to prevent bending failure. The authors of (Galal *et al.*, 2005), proposed a method which provides formulas for the calculation of the shear strength of the RC short columns. They indicated that the nonlinear behaviour of RC short column can predict using lumped plasticity macro models. Hwang et al (2005), investigated to find the relationship of hoops on the strength of RC beam-column joint. Basing on their experiments they indicated that the main function of the joint hoop was to bear shear as a tension tie and to restrict the crack width. Also, it was noted that beam column joint can be used as a shear reinforcement due to their shear strength. Garzón-Roca et al (2011) carried a several experiments to investigate on full-scale specimens strengthened with steel caging also used simulation of the beam-column joint under combined bending and axial loads. Various RC beam-column sub assemblage were investigated. The results have shown that both ultimate load and ductility of the strengthened columns can increase with steel caging. The authors of (Chidambaram and Thirugnanam, 2012), conducted a comparative study on extensive behaviour of the RC beam-column joint with reference to anchorage detailing. The authors concluded that external anhorage system indicates excellent dealing in energy dissipation , ductility and load-deformation parameter comparing to specimens constructed to current design recommendations. The behaviour was better than conventional method of construction.

Bridges are subject to various cyclical repetitive loads, such as traffic, thermal effects, earthquakes, wind, which over time may cause damage and fatigue. Testing and monitoring their technical condition is needed to use these bridges for a long time safely. Damage identification in RC decks and prestressed bridge girders is complicated and difficult. This is due to the fact that modelling and prediction of occurrence of cracks requires a good knowledge of material properties, design assumptions, vehicle load history, and environmental conditions. A combination of structural behaviour during design and actual structural behaviour is essential. It is, therefore, necessary to investigate the types of damage and reasons for damage occurring during the structure's lifetime. It can be useful to design appropriate SHM systems.

2.3 Types of damage in concrete structures

In civil engineering, damage is understood as concrete degradation and abnormal changes in the structural nature of the material e.g., static deformation, strain, propagation of cracks (Nguyen *et al.*, 2014). In the system of categorizing damage to building structures, according to the proposal given by J. Bień (Bień, 2010), three groups of classification criteria can be used:

- Causal criteria - related to the cause or causes of damage;
- Effect criteria - related to effects of damage;
- Cause and effect criteria - combining causes and effects.

Because the causes of bridge damage are in practice often not obvious, and due to the fact that they are a combination of many factors, it seems most rational to accept the effects as a criterion for damage classification (Zakić *et al.*, 1991; Bień *et al.*, 2016). This approach is commonly used in Bridge Management Systems (BMS). It is based on the majority of forms of damage description while reporting bridge inspections around the world.

Therefore, assuming the effect criterion for bridge damage systematics, the following classes of damage are distinguished in Bridge Management Systems (Iffland and Birnstiel, 1993):

1. **Change in the position of the bridge elements.** Not in line with the displacement design of the object or its parts, at which the mutual distances of all points of the displaced structure element do not change;
2. **Deformation.** Geometry changes that are not in line with the design, causing changes in the mutual distances of points of the object or part of it;
3. **Loss of material continuity.** Interruption of the structure material (e.g. scratches, cracks) not in line with the design;
4. **Failure.** Significant damage causing loss of usability of the object or its part and the need to shut it down (failure of the insulation, lighting, drainage system, etc.);
5. **Damage to corrosion protection.** Partial or complete dysfunction of coatings protecting the material of the structure;
6. **Material losses.** Reducing the amount of material of the structure compared to the amount designed;
7. **Material destruction.** Deterioration of the value of physiochemical properties of the material in relation to the designed values;

8. **Pollution.** The occurrence of all kinds of dirt, stains, raids, as well as plant vegetation unforeseen in the project.

However, the modern capabilities of NDT and SHM techniques do not allow all types of identification and observation. Therefore, the problem of their detection and monitoring has been limited in this research only to selected classes and types, and in particular to the loss of material continuity in the form of concrete cracks and fracture. Selected examples of cracks in concrete bridge girders are presented in Figure 2.10 and Figure 2.11. The symptoms (due to overload, corrosion of longitudinal reinforcement) of such cracks (see Figure 2.10) are transverse cracks in cantilever zones, vertical scratches at the top of the girder and horizontal scratches at the bottom of the girder.

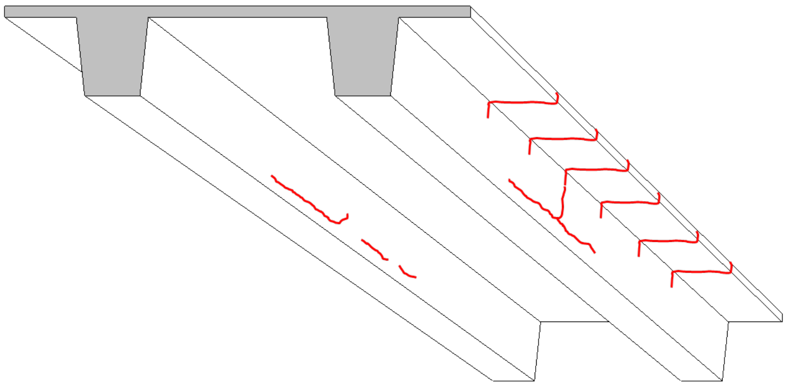

Figure 2.10: Crack due to overload, corrosion of longitudinal reinforcement

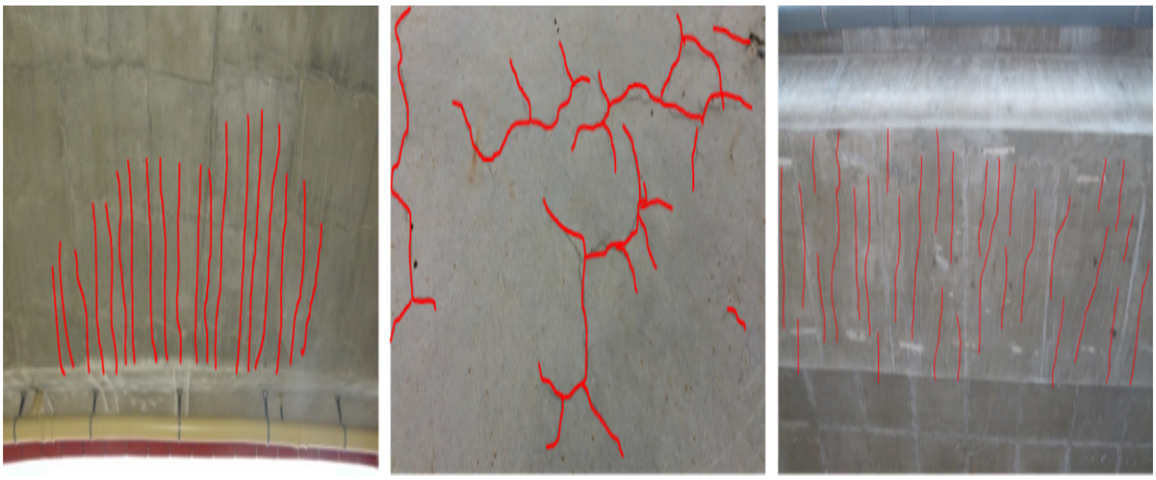

Figure 2.11: Drying shrinkage is the most common cause of concrete cracking

The main reason for cracking in concrete structures is stresses exceeding the tensile strength of concrete. The following are causes that can cause stress in concrete (Figure 2.12):

- External loads - Loads due to traffic, subsidence of supports and soil pressure;
- Internal loads - Shrinkage and creep of concrete or internal pressure of reinforcing steel corrosion products;
- Technological errors - Long technological breaks, errors in compaction mix, improper texture and concrete care;
- Design errors - Incorrect cover thickness, no anti-contraction reinforcement;
- Thermal effects - Temperature changes and local surface heating.

Figure 2.12: Causes of concrete cracking

Temperature has a crucial influence on changes in mechanical properties of concrete. Temperature above 60°C has a noticeable effect in concrete such as reduction of the strength of concrete. Short-time exposure to temperatures of 200°C reduces the concrete strength by 30%, and long time exposure has effects on strength of concrete amounting to even 40% (Jinsong and Qingling, 2019). For standard concrete critical temperature is between 500°C - 600°C, at this temperature concrete breaks up as a consequence of dehydration and cement frame stone crush (Pagani *et al.*, 2014). Therefore, it is recommended that ordinary RC be used below 200°C. For protection against fire, a protective layer of concrete with a thickness of about 10-30 mm is used. It protects the reinforcement not only against corrosion but also the effect of temperature during a fire. In different environmental condition the thickness of the protective layer can increase to ensure its dependable allegiance to the concrete. The authors of (Catbas *et al.*, 2008), presented a reliability estimation of SHM system for a long span bridge. Long-term monitoring data were explored for reliability estimation (Burdet, 2010). The authors show that responses due to temperature have a significant effect on the overall detection reliability. It was indicated that the temperature effect causes temperature-induced stresses on struc-tural elements. However, it is not very easy to conceptualise and subsequently model the temperature effect. Moreover, Xia et al. (2012), presented a case study of temperature effect on vibration properties of civil structures. They shown that the annual variation of temperature has a significant indirect effect on frequencies of material changes (Figure 2.13).

Figure 2.13: Thermal cracks in a thick slab

Regarding reinforced deck, water penetrating the deck might be alkaline, like salt solutions used on highway bridges to melt the ice during winter (see Figure 2.14). The main problem is that the salty water that gets into the concrete deck can come into contact with the steel reinforcing bars within the concrete, eventually causing rust and corrosion, possibly penetrating the structure and resulting in structural fatigue.

Figure 2.14: Deicing salts are a major cause of corrosion of reinforcing steel in concrete (photo courtesy Sigfrid Lundberg)

The messy brown blur observed on the civil concrete structure is caused by rusty water flowing out through the cracks. Another issue is that if there is a resistance crack, and water seeping inside the RC via cracks accumulates during winter, it can enlarge and propagate the cracks so that even more water can get in. Crack investigation allows long term RC monitoring.

For a long and safe use of these concrete structures, their fatigue safety needs should also be considered. However, there are different challenges in reinforced concrete structures fatigue life prediction because of different causes of failure that act synergistically (like long term monitoring data, design conditions, history of loads and temperature variation). A detailed literature review has been completed to understand the fatigue safety impact on structural elements.

Kindrachuk et al. (2015), the authors developed a basic model for concrete using continuum damage mechanics. The model can reconstruct gradual performance deterioration of normal strength concrete under compressive static, creep and cyclic loading in a unified framework. The model was validated by comparing simulation and experimental data for different types of loading. The result shows good connection with experimental and literature, but overestimate fatigue life at high stresses. The authors also indicate another deterioration due to micro-cracks sliding and irreversible closure during load reversals. The authors of (ElSafty *et al.*, 2014), proposed an investigation to repair the laterally damaged prestressed concrete bridge girders using carbon fiber reinforced polymers (CFRP) laminates. They shown experimental and analytical investigations to flexural behaviour of girder under both static and fatigue loading. Their investigation emphasis on static loading and fatigue loading cycles to investigate the behavior under simulated traffic conditions. The authors conclude that with the proper detailing, CFRP systems can be designed to restore the lost flexural capacity, sustain the fatigue load cycles, and maintain the desired failure mode. Tepfers et al. (1984), presented a measuring system for registration of the absorbed energy during fatigue loading. The indication is that the absorbed energy at concrete failure was the same for static load and for fatigue load with different intensities.

The author of (Bastidas-Arteaga, 2018), investigated the effects of chloride-induced corrosion, climate change and cyclic loading on an object and presented a stochastic model that considered effects of all the parameters combined mentioned above. The author performed a reliability analysis on a bridge girder subjected to cyclic loading under different environmental conditions. The results indicated that fatigue load also needs to be considered in analysis because climate change effect reduces lifetime of the structure. Cavalline et al. (2017), compared durability studies of lightweight bridge deck with normal weight bridge deck, taking into consideration the same parameters, such a deck thickness, and geometric configuration, similar age, traffic, and environmental exposure. The result shown that the type of concrete deck was a significant influence factor for observed cracking.

In another study (Simon and Kishen, 2016), a crack growth model was developed by taking into account the effect of bridging stress (aggregates) that exists at the macroscopic scale in cementitious materials. The authors computed the residual strength (considering crack opening displacements) of damaged beams by taking into account the influence of bridging zone present at the macroscopic scale, which obstructs the propagation of crack during the initial stages of loading. This model agrees well with the experimental results for normal concrete.

On the other hand, the authors of (D'Antino *et al.*, 2015) proposed a fatigue loading protocol to observe the effects of different load ranges and different frequencies on an interfacial slip, the decayed energy during cycles, the degradation of stiffness of the interface and the quasi-static monotonic post-fatigue behaviour. The objective of this investigation was to tested Fiber-reinforced cementitious matrix (FRCM) concrete joints under cyclic and post-fatigue quasi-static loading. They observe the effect of different combination of amplitude and mean value on several damage concerning fatigue and post-fatigue behaviour. The results suggest a fracture mechanics approach to relate different frequencies for the intermediate range of fatigue crack growth.

Figure 2.15: Examples of concrete cracks and simple methods of their identification

For various reasons described above, such as overload, manufacturing and design errors, as well as natural destruction processes inside the structure, cracks may occur, which, however, may not always appear on the exposed surface of the element. Knowledge about the existence of cracks is crucial at the construction stage when there are doubts about the quality of construction works and at the maintenance stage, when an inspection is carried out or a project to strengthen the structure is being prepared. Identifying and measuring cracks is a difficult task (Figure 2.15). First of all, access to the structure can be difficult. Bridge pillars can be very high. Bridge girders can also be located very high or located above the inaccessible space of a busy highway, railway line or large river. Therefore, a crack detection system that would inform the owner of the object in such difficult situations would be highly desirable.

Currently, to measure the width of a crack, a feeler gauge, a printed template, a magnifying glass or a microscope may be used (Fu, 2005). When making a measurement, it is crucial to be aware of the fact that concrete changes its dimensions together with temperature changes. The warmer it is, the more its volume increases, which in turn closes the width of the crack. Thus, measuring the crack on the sunny surface of the concrete can show a different result than the same crack in December at -15°C. According to Eurocode 2 (refer (Eurocode, 2005) (section 4)), for durability reasons, depending on the type of reinforcement, load combination and exposure class, the permissible crack widths in the structure should be in the range of 0.2–0.4 mm. In the case of prestressed concrete bridges, cracks even below 0.2 mm may be dangerous, which results from the fact that the prestressing tendons are more sensitive to corrosion. It is also essential to assess crack activity. An active crack is a crack that changes its width but does not necessarily expand. For example, when passing a heavy vehicle over a bridge, the scratches at the bottom of the span may temporarily widen. Crack activity may indicate overloading of the structure under the influence of loads. The easiest way to assess whether the cracks visible on the structure are active is to put a plaster or glass seal on them. However, access to the structure is not always possible. It is also troublesome to observe the condition of the seal in such cases. It is also difficult to measure the depth of surface cracks. The destructive method involves drilling core lace. It is also possible to drill a small hole over the crack and inspect the inside of the crack using a borescope. The non-destructive method involves measuring with NDT devices, e.g. by ultrasonic or impact-echo. If accurate knowledge of changes in crack width overtime is required, sensors (electronic feeler gauges) with specialised equipment for automatic reading and archiving of data can be installed on the outlined fragment of the structure, with the option of sending them remotely. Considering all these difficulties related to the identification and assessment of cracks, and also considering hard-to-reach constructions such as some bridges and tall towers, it is necessary to implement the SHM system, which able to assess the behaviour of the structure and improve its level of safety also taking into account the effect of fatigue. However, fatigue identification is not so simple because it can be difficult to describe what is meant by weakening of a material, and even hard to put it in mathematical terms. Fatigue detection methods are very difficult, not only with respect to a structure, but even to the type of fatigue that is being monitored. It is therefore pleasant to place a sensor that can relate the actual health state of the structure. The main elements of such a damage recognition system include NDT techniques with SHM system.

2.4 Types of NDT techniques and the SHM system

NDT relies on the indirect connection between observed phenomena and measurement parameters. Indeed, effective use of NDT needs a balance of requirements: good understanding of the physical phenomenon, correct testing methods and accurate connecting models for analysis (Büyüköztürk and Taşdemir, 2013; Malhotra and Carino, 2003). In this section, a short review of NDT technologies and their use in SHM system is described. The goal is to provide basic information for a better understanding of the current used technology for bridge monitoring.

2.4.1 NDT techniques

Visual inspection is a common and the oldest NDT technique used in most of bridge inspections (Harding *et al.*, 1990). It can be completed more quickly without special equipment and economically compared to more advanced NDT techniques. However, due to some limitations of visual inspections, the inconstancy of inspection results is normal. According to (Graybeal *et al.*, 2002), the Federal Highway Administration (FHWA) presented an inquiry into the reliability of visual inspections of highway bridges. They found some interesting facts. Their results showed that condition ratings during inspection are flawed with significant inconsistency. It was impossible to identify specific types of defects for which this inspection procedure was prescribed.

There is no specific regulation required to vision test for the person performing an inspection. In many cases, inspectors were not focused on writing down critical fracture findings and fatigue prone details which are important structural components. Most routine inspection results vary. On the other hand, in most cases during in-depth inspections, the inspectors did not reveal the defects for which they were performing the test. It was also found they did not show any problems other than those revealed during routine inspection. This indicate that the accuracy of this type of inspection is relatively poor. Therefore, NDT techniques using different kinds of sensors can be pointed out as more reliable.

The first set of NDT techniques for detecting damage in RC are NDT existing techniques, which can be divided into temperature, optical, electromagnetic and acoustic techniques.

Temperature is an important parameter in monitoring any structure (Figure 2.16). The thermal load is the most crucial parameter affecting bridge behaviour apart from the weight of the bridge and vehicles crossing it. The cycle of sunlight produce temperature gradients and in consequences with other effects can have non-trivial measured response of a bridge to a given load (Priestley, 1985).

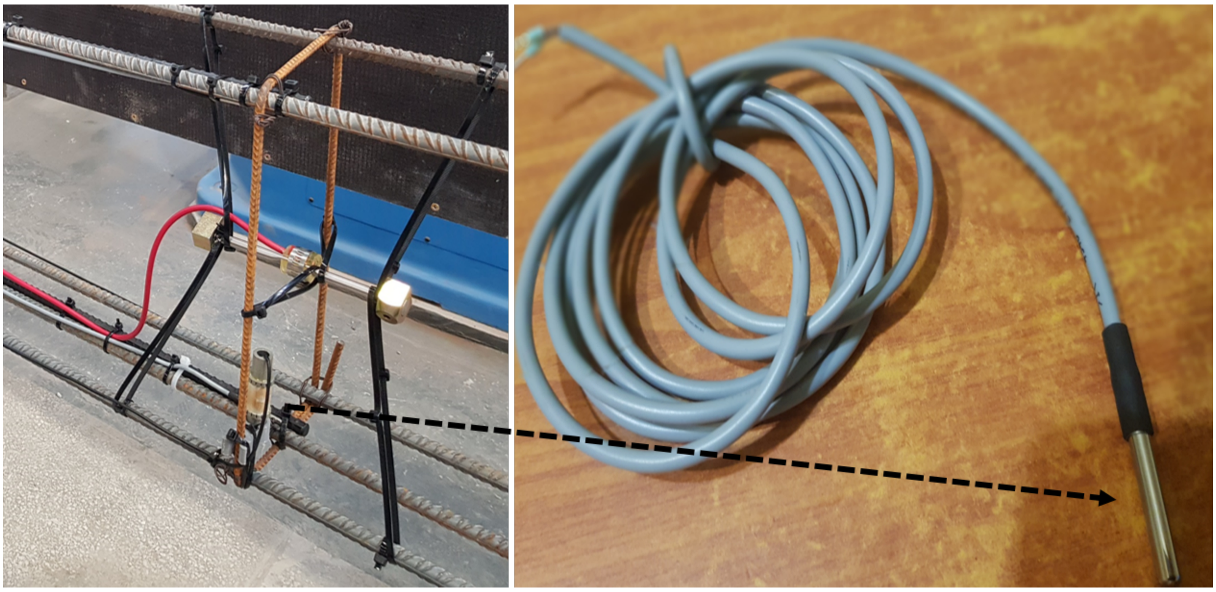

Figure 2.16: Thermistor

Cameras have been used to measure the geometrical properties of the structure. This method is usually referred to as stereo-photogrammetry (Figure 2.17) measuring deflection in the structure under thermal loading, dead and traffic loads, crack lengths and widths, and to monitor damage due to corrosion (Jiang *et al.*, 2008). This is non-destructive, remote sensing technology that can be rapidly deployed in different structures and without elevated costs.

Electromagnetic techniques are defined as propagation of electromagnetic waves in non-metallic (dielectric) materials. In civil engineering, radiography is a commonly used electromagnetic NDT technique that can diagnose both sides of the structure and detect cracks. On the other hand, radar and microwave-based techniques are characterized by

Figure 2.17: Stereo-photogrammetry

high precision in detecting micro-cracking zones, and measuring de-bonding and drawing thermal curvature of the structure (Yun *et al.*, 2013).

Radar interferometry sensor is the strong remote sensing technique used in SHM, capable of detecting small displacements at distance (Maizuar *et al.*, 2017). Radar is the acronym of “Radio Detection and Ranging”, which points at the efficiency of the radar to detect and range objects using electromagnetic waves. The radar emits microwave signals and receives echoes from the structure which taken between it's antenna Field Of View (FOV). Radar interferometry derives from space technology. Since 1990 (Ketelaar, 2009), a satellite-based radar has been capable to utilize the phase information of images to detect ground displacements of a few millimetres at a distance of hundreds of kilometres.

The standard Laser Doppler Vibrometer (LDV) used in many applications as a non-contact sensing technique works on the basis of measuring the Doppler frequency shift of a laser beam after it is reflected from a surface moving relative to the emitter (Figure 2.18). The embedded electronics change the Doppler signal to an analogue voltage balance value, providing instantaneously the velocity value of the target. It can measure velocity and displacement to a resolution of less than one-hundredth of a millimetre, with a sampling frequency in the MHz range. LDVs can measure remotely, meaning that no physical attachment to the structure is required. It also allows for measurement in parts of the structure that are difficult to access. LDV measurements can be done for up to 30 metres without significant loss in accuracy.

Figure 2.18: Laser Doppler Vibrometer

Figure 2.19: Digital image correlation

Optical techniques capture direct images of the surface of the structure, and analyses the object using image correlation. The working principle of these techniques are based on the comparison between fragment of the many images, in order to detect and localize changes in the structure (Nassif *et al.*, 2005). Optical methods include Optical holography, Electronic speckle pattern interferometry, laser shearography, digital image correlation

(Figure 2.19), and tomography (Gajewski and Garbowski, 2014; Kozicki and Tejchman, 2007).

Accelerometers (Figure 2.20) together with strain gauges (Figure 2.21) are traditional techniques used in the SHM system.

Figure 2.20: Accelerometer

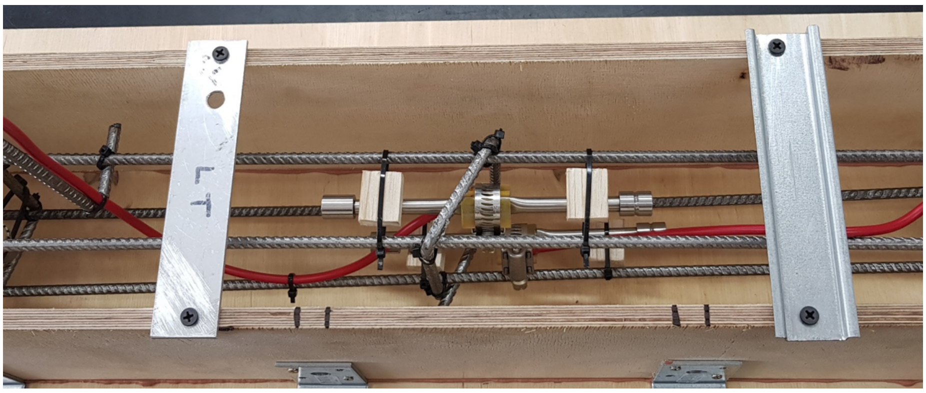

Figure 2.21: Vibrating wire strain gauge

Those are techniques still most frequently used in civil engineering (Li and Ou, 2016). According to Dimension Engineering, “An accelerometer is an electromechanical device that measure acceleration forces” (*Accelerometer Description*, 2017). In accelerometers, the transducer consist of micro electro mechanical system that works based on small mass resting on a sensing element (e.g., made of piezoelectric material). The principle a typical accelerometer uses is acceleration of the frame to which the accelerometer is attached, the effect of the mass produces deformations in the piezoelectric material. When vibrations reach piezoelectric material, it releases an electrical signal which is directly proportional to the forces exerted. Extensive literature reviews on the subject of acceleration-based SHM can be found in (Kwon *et al.*, 2003).

The most common fiber optic sensor for measuring strain is the interferometric FOS (Figure 2.22). Fiber optic interferometers measure various natural parameters of structure

Figure 2.22: Fiber optic sensor

such as strain, pressure, temperature and refractive index, and are widely used (Miller *et al.*, 2017). In a fibre optic sensor, the transmitted light is divided into two beams, one is sent through the measuring strand and the other through a passive reference strand. When the incoming beams are recombined, the relative phase differences can be measured and associated with a given physical value (mostly use for strain or displacement measurement) (Deng and Cai, 2007a). The most used set of NDT techniques for RC inspection are acoustic and ultrasonic methods. Acoustic methods are based on elastic wave propagation with different frequencies inside the cement matrix. The intensity of the signal and propagation time is the most commonly measured parameters. Acoustic methods are widely used in civil engineering to detect crack initiation and growth, defects and material properties (Benavent-Climent *et al.*, 2011; Hoła, 1999). Acoustic emission is based on listening to stress waves, impact echo is based on sending and receiving sound waves, and ultrasonic technique is based on sending and receiving stress waves. The main benefit of the ultrasonic sensor is sensitivity. It can detect very small changes (Lu and Michaels, 2005a).

Recently, new NDT techniques for damage investigation in RC structural elements are emerging such as sensing skin. The authors of (Yan *et al.*, 2019), developed a soft elastomeric capacitive surface sensor for SHM. The sensor can be deployed over a small surface. It is found to be an inexpensive technique with low voltage requirement, easy to install, robust with respect to physical damage and capable of damage localization. It is a very promising technique, nevertheless, it has the same crack detection properties as normal strain gauges, with the difference in durability and robust sensing being the main interest.

The authors of (Hallaji *et al.*, 2014), presented an electrical impedance tomography-based sensing skin for quantitative imaging of damage in concrete. It was shown that the electrical impedance tomography-based sensing skin provides quantitative information on cracks, unsaturated moisture ingress on the cement based material. The technique is still limited to surface inspection. Visual inspection can provide the same information, even if it is not quantifiable as the sensing technique, and a other similar technique can provide the same measurement.

At the moment, those new techniques are still in an initial research phase. Moreover, the traditional techniques (e.g. strain gauges) can provide similar measurements. Electromagnetic technique are sensitive to the condition of concrete, while ultrasonic techniques can detect early changes before total cracking and discontinuity formation. For that reason, Ultrasonic methods are very promising techniques for cracks/changes investigation. Using ultrasonic techniques is a recent development in the area of introducing embedded sensors in structural elements they overcome problems of surface conditions and assure long-term monitoring. They are durable techniques for new structures and old structure. They measure a large variety of features like crack initiation, cracks propagation, and material-characteristic changes. Impact echo also another promising technique, but it required access to both sides of the structure.

FOS technique can provide exciting results with defect visualization. However, their use for structural monitoring is still limited due to expensive equipment, they are not extensively used work in testing and protection of real structures fibre in different environmental conditions.

A summary of common NDT methods that can be used for SHM of a civil structure such as bridges is presented in the Table 2.1 below:

Tab. 2.1: Types of sensors for a common NDT method in SHM

NDT technique	Principle	Advantages	Disadvantages
Visual Inspection	Trained person inspects bridges at regular intervals to cheek the presence of any signs of damage.	Simple.	Hard to locate the microcrack. Crack due to corrosion or fatigue may not be detected.
Vibration monitoring	Changes in the global properties of a structure cause a change in modal properties.	Normally provides global information. Can be applied to a complex structure.	Some changes may be unnoticeable because of the magnitude of a structure
Fiber Optic	Capable to measuring strain and temperature.	Suitable for a large structure.	Costly
Radiographic	Radiographic energy source generates radiation and its travels through both side of the specimen.	Promising laboratory results.	Large size of equipment
Acoustic Emission	AE waves arise from the rapid release of energy from crack initiation.	Highly sensitive. Ability of damage localization.	Difficult to extract a feature from background noise. High sampling needed so a big size of data is needed
Ultrasonic	The ultrasonic transducer sends high-frequency waves to the specimen and receives the pulse.	Highly sensitive. Long range inspection.	Required generation of the source signal

From the literature on different NDT techniques, in terms of structural long-term monitoring efficiency and damage-quantification ability, one can conclude that there are issues with good calibration for optical methods (DIC and stereo-photogrammetry) due to environmental effects e.g., rain, wind, and clouds which cause differences, in contrast, luminosity and environmental conditions. Traditional sensors measure vibrations or strain of the tested object during the test, but complicated integration is needed. FBG is quite a new technique in terms of civil structure monitoring. However, still it is in research phase, and reliability is unknown due to a chance of fibre being broken during the test (possibly due to heavy load), and the cost of interrogators. Also, the FBG technique can be replaced by a large number of strain gauges, their price/quality ratio and capability of long-term monitoring being comparable.

Therefore, it leads to choosing AE and ultrasonic techniques as the most reliable methods for structural safety investigation. Listening to AE events gives information earlier than the opening of visible cracks, but the interpretation of results is always a difficult matter. This is because most AE events occur just before the propagation of microcracks. The lack of significant AE activity at the initial stages of loading causes difficulty in distinguishing between background noise and acoustic events related to the crack. The techniques using ultrasonic sensors are particularly interesting because of the direct relationship between characteristics of wave propagation and the stage of damage to the material. Therefore, it is concluded that ultrasonic techniques are the most reliable in detecting material changes in the structure due to different load conditions.

2.4.2 Sensing and data management

This section presents sensor installation and recent data acquisition and signal processing technique used in the SHM system. It is focuses on the presentation of algorithms that have been used recently in the field of sensors for SHM and NDT for bridges.

The smart sensing concept can be used in civil engineering applications to detect changes in the structure due to material degradation caused by extreme environmental and operational conditions (Salamak *et al.*, 2007). However, it is difficult to find common guidelines for sensor installation on the structure (Hui and Jinping, 2011) (Klikowicz *et al.*, 2016). Nevertheless, some critical points are shared by different fields and should be considered attentively in the design process. The first concern is the installation of the sensors themselves into or onto the host material. On the one hand, it is necessary to ensure a good mechanical contact between the sensors and the structure, while on the other hand, it is important to protect the sensors (like fiber optic sensor, ultrasonic sensor) mechanically. In the event of a strain sensor, it is difficult to add an additional layer of protective cover without altering the sensor reaction. In this case, the sensor has to be fixed onto or embedded directly in the structure. For example, it is possible to glue a Bragg grating sensor to the asphalt or to embed the sensor into a composite material (Miller *et al.*, 2017). In other cases, the strain sensor can be first embedded in a buffer material that is mechanically compatible with the surrounding material. After the sensor installation with all protection systems, the next step is data acquisition. The data acquisition system consists of sensors, data acquisition units (DAU), interrogators, and the main computer, which can work as a server. Sensors capture the signal either electrical or optical – that is converted to digital numeric values which are processed by a computer. Signal processing and filtering might be needed, especially for electrical and optical signals to allow for transmission and post-processing of the signal. There are different systems on the market that require various components and multiple solutions. DAU systems are local servers located in approved locations on the structures, and sensors can be connected to them. Each DAU can be equipped with a time synchronization unit and may have some data processing and data storage facilities, if needed. Data acquisition depends mainly on specific sensor features and a choice to perform structural health recognition. It also depends on the environments where data are captured and on the system architecture. The data acquisition process is completed in the process of transforming electrical signals received from each sensor into a readable format, usually digitized. There are different

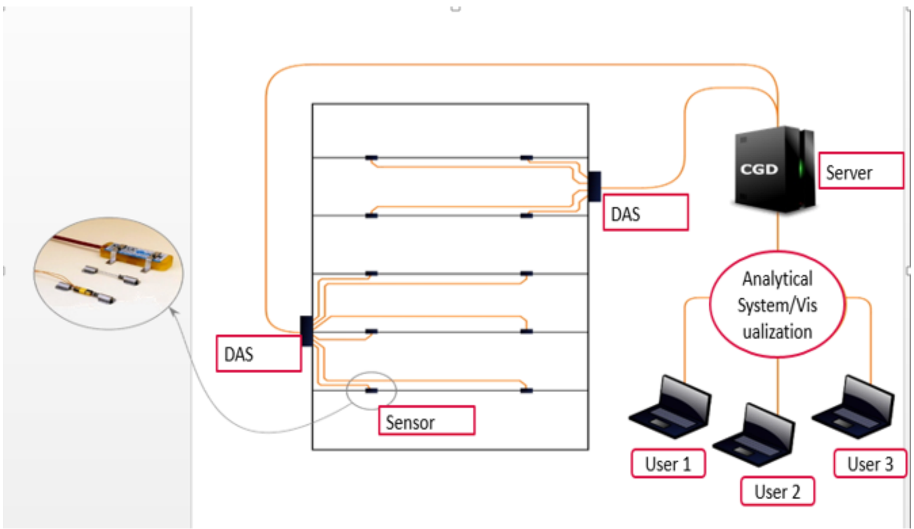

Figure 2.23: Physical diagram of sensors and synchronous data acquisition device

challenges connected with the data acquisition system when monitoring structural health, including the placement of the sensors, the actual data sampling rate, and the number of sensors to be processed (Capineri *et al.*, 2018). All sensors positioned on the structure need to be synchronized. A suitable data communication system needs to be selected. A typical SHM system is either equipped with WAN or LAN (Islam *et al.*, 2018). Large systems are operated with a backbone of fibre optic networks that allow for redundant systems with no data loss (Aranguren *et al.*, 2016). The typical schematic diagram presenting sensors and synchronous data acquisition device is shown in Figure 2.23.

A data communication system transfers the acquired signals to a remote main computer or to an interrogator. Some interrogators are embedded in the data processing unit, and are able to work independently without an external computer. Also, DAS can be located either on the structure or in the main control room. Sensors can be connected via DAU to interrogators or directly to the interrogator. There are many different solutions depending on the technical requirements of the chosen systems.

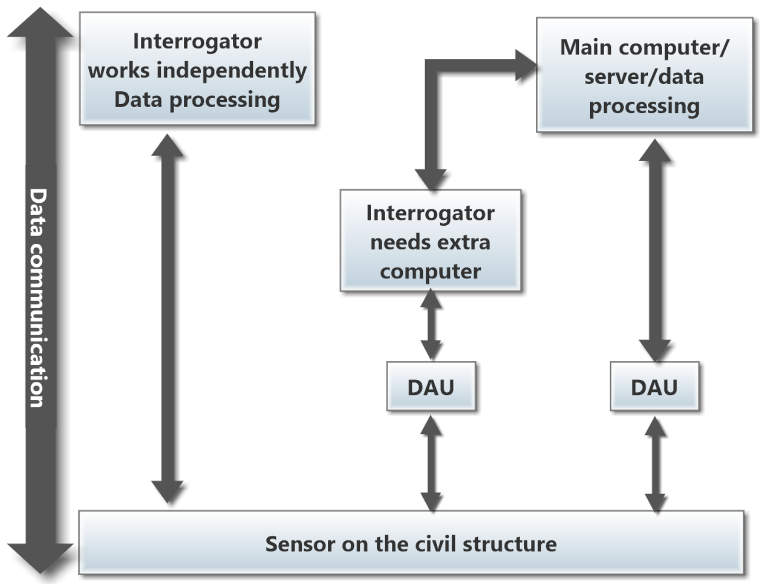

Figure 2.24: The different possibilities for data acquisition systems

Figure 2.24 highlights the different possibilities for DAQ systems. Some additional points are highlighted below:

- Sensors are connected directly to an Interrogator that is able to perform data processing
- Sensors are connected via DAU to an Interrogator that is, in turn, connected to the main computer that performs data processing
- Sensors are connected via DAU to the main computer that performs data processing
- Sensitivity and bandwidth: What is the response of the sensor to inputs, normally over a range of time line?

- Resolution: What is the minimum detectable value of the intended input or the minimum achievable output?
- Cross-axis sensitivity: How strongly does the sensor respond to inputs not aligned with the primary sensing direction?
- Reverberation: Does the sensor have multiple non-linear (resonant) areas that affect accuracy and bandwidth?
- Sensitivity to extraneous measures: Does the sensor respond to unintended inputs ? (Does a transducer (for example Ultrasonic sensor) also respond to different effects yielding "false" signals?)

The sensing system used for real-time monitoring systems can fail in any situation. Firstly, the acquisition process can fail, when the sensors report unexpected values due to the calibration problem. Besides, due to unusual environmental effect on the sensor which may occur at any time and suddenly for a certain period. Depending on the timing of the missing data included in a subset of sensors data, the missing data is classified as missing completely at random (MCAR) when the missing values are randomly distributed by all-time instants (Vateekul and Sarinnapakorn, 2009; D'Ambrosio *et al.*, 2012). The missing data are classified as missing at random (MAR) when the missingness are randomly distributed by subsets and does not depend on missing values in the data matrix (Vateekul and Sarinnapakorn, 2009). Additionally, the missing data are classified as missing not at random (MNAR) when the missing values are not randomly distributed and depend on the missing values. Several methods to minimize the effects of missing data have been developed, estimating the missing values based either on other values correctly obtained or on external factors, ignoring and deleting data etc. The authors of (Vateekul and Sarinnapakorn, 2009), presented the imputation tree (ITree) method, which is a tree-based algorithm for missing values imputation. This method constructs a missing pattern tree (MPT), which is a binary classification tree for identifying the absence of each observation. It uses clustering techniques, e.g., k-means clustering, to impute missing values and linear regression analysis to improve data imputation.

Huang (Huang *et al.*, 2013), proposed a multi-matrices factorization model (MMF) for the missing sensor data estimation, which uses probabilistic spatial feature matrices and probabilistic temporal feature matrix methods to estimate the missing values. There are other methods for sensor data imputation that employ k-nearest neighbour and dynamic time warping based imputation (Hsu *et al.*, 2011), multiple imputation (Pedersen *et al.*, 2017) hot/cold imputation (Smith *et al.*, 2003), maximum likelihood and bayesian estimation (Sun and Butar Butar, 2007) and expectation maximization (Strauss *et al.*, 2003). The data fusion technique can solve this problem without using any additional algorithm for missing data (Rässler, 2004). In general, these methods are used to verify and increase the consistency of sensor data. The individual data processing unit converts data acquired by a single sensor without access to information on the data received from the other sensors. The multiple data processing unit can acquire multiple sensor data in the same processing units use certain control techniques such as data fusion or on a remote processing unit, even immediately on the sensor itself (in the case of smart sensors). The sensor network consists of a dense network of heterogeneous sensors (e.g., strain gages, Fibre-optic, ultrasonic, camera, etc.). Data processing is the next step in the multi-sensor monitoring system used to process the sensor data. Data processing is a depth process, which also depends on environmental conditions (noises), the types of sensors, and the types of data collected (Zhou and Yi, 2013). Therefore, comprehensive data evaluation is a central issue to the successful application of SHM. Data evaluation is a method of transforming raw data into usable meaningful information. The main goals of data evaluation in relation to the monitored structure are, structural identification during construction, operation and degradation, condition assessment, alarm configuration (if required), service life prediction and maintenance planning. Data evaluation may allow for damage localization and quantification as well as for condition assessment. However, now the new research challenge is to integrate data from multiple sensors, to develop local monitoring system that can indicate features based change index of the monitored structure. The features may be defined as user-specified indicator over large data sets, or over pre-computed clusters covering data from one or more sensors. Data fusion and mining can handle these research challenges.

Data fusion and mining is the signal processing technique of extracting patterns of two classes, such as damaged or undamaged from large data sets by combining statistical methods (e.g., statistical pattern recognition) and artificial intelligence. It is an efficient technique for data evaluation which improves the results. Data fusion techniques combine sensor data. They work on three levels: the raw data/signal level, feature level, and decision level. Signal fusion level techniques combine signals from different or the same types of sensors located in different geometric areas. Feature level fusion techniques combine features from the sensors, and merge information from associated databases in order to overcome improvement inaccuracies and capture specific inferences or sequences of observations from a number of various sensors into an individual best estimate of the state of the environment. Decision fusion level is a technique used to analyse decisions from multiple sensors and choose a comprehensive one. Various data fusion methods have been used in the non-destructive evaluation to improve crack detection (Heideklang and

Shokouhi, 2015; Heideklang and Shokouhi, 2013). Gros (Gros, 1997) provides a description of fusion techniques applied to various NDT techniques. Another publication (Mina *et al.*, 1997), examines an aluminum specimen with unnatural cracks in the region of rivet holes utilizing single eddy current probe. The researchers proposed a fusion process that could capture and maintain the details from both the real and imaginary image components. The combination was based on the frequency domain of the acquired images. The adopted linear minimum mean square error (LMMSE) method used to fused the image using a weighting scheme that considered the signal to-noise ratio (SNR) into account. Bao et al. (2019), two eddy current testing systems were presented for structural damage detection using wavelet analysis and Dempster-Shafer (D-S) evidence theory and a combination rule to integrate the signals from these sensors.

In structural monitoring, one of the primary problems is the noise of the signals which interfere with the authenticity and accuracy of the raw data. Sometimes noise which is much stronger than the main raw signal may disturb the reliability and accuracy of measurement, and an initial limit is thus placed on the tackle of small cracks. Therefore, the de-noising should be considered essential in the SHM system (Liggins *et al.*, 2017).

In recent years the wavelet transform (WT), has become a potential tool for de-noising the signals because it is capable of revealing some hidden aspects of the data that other signal analysis techniques fail to detect (Peng and Chu, 2004). The authors of (Yi *et al.*, 2012), proposed an advanced thresholding technique called the sigmoid function based thresholding scheme, to suppress the disadvantages of the traditional hard- and soft-thresholding method in the WT based denoise method.

For bridge monitoring using acoustic emission and ultrasonic technique, one of the challenges is to separate noise from the signal. The authors of (Satour *et al.*, 2013), proposed a wavelet based simple detection threshold on the recording of structural changes. Another author (Unnthorsson, 2013) explains that the threshold technique does not perform well when the AE signal contains strong temporal bursts of high AE activity. Such bursts consist of overlapping transients with varying strength, duration, shape, and frequency. Anubhav presented three signal processing techniques to remove the structural noise from the signal and to estimate the defects (Tiwari *et al.*, 2017). However, there was lack of knowledge on processing of data from real structures. For this reason, the processing technique used for bridge monitoring should be different from the threshold-based technique used for laboratory tests.

In view of the above, more improved data-processing techniques should be developed to extract features from signals used for active or passive measurement in order to detect traffic (vibration) and environmental sources (such as temperature, wind etc.). It is important for SHM system to take into account the environmental effect on structures when choosing sensors and measurement locations. One of the greatest challenges of long-term monitoring is to understand the effect of external changes (environmental and noises) and to handle the amount of data storage. The author of (Mcneill, 2009), the importance of data management for long term monitoring of different highway bridges. It was noted that data management and data-storage systems have to be considered before the installation of the SHM system, or before data acquisition. The publication presented basic SHM with internet connection, standard database and data archiving methodology. Sousa and Wang developed an effective method for data compression and storage. Different methods and algorithms have been compared to find the best data storage technique without losing useful data from the signal. It was found that k-means singular value decomposition technique could guarantee the same level of information even with much smaller databases (Sousa and Wang, 2018).

Figure 2.25: Shows data processing to visualization system

The authors of (Hu *et al.*, 2012; Chen *et al.*, 2016), developed a wireless sensor network based data acquisition system for SHM. Laboratory tests validated the technology before implementing in a real bridge monitoring. The authors suggested that, it is important to ensure the balance of power consumption, communication range and link quality. Consequently, it is necessary to have fundamental knowledge regarding data management for long-term monitoring using strain gauges and ultrasonic sensors. Figure 2.25 shows a data acquisition to a visualization system flowchart.

2.5 Conclusion

The presented studies show that concrete is the most widely used material in the world in terms of volume in many civil, onshore and offshore infrastructures due to its long service life and durability in harsh environments. However, concrete is a material that shows changes over the period of operation. Thus, several factors, such as loading of the structure, the environment, or the attacks sustained over time cause degradation of concrete material. In view of the above, research studies indicated that the SHM system may be beneficial for infrastructure monitoring. In this chapter, SHM system monitoring was presented in detail, and the SHM with automatic NDT techniques in the light of the operational or environmental changes in the structure (such as changes in stress, propagating crack, corrosion, thermal load, etc.). It is well known that several NDT techniques have a number of advantages and disadvantages. However, considering all the advantages and disadvantages, it was concluded that the ultrasonic sensors have the potential to detect changes or cracks in the structure. Thus, previous research study on the integration of a multiple sensor system (such as data acquisition system, a data preprocessing and communication system) in different applications was also considered. Based on the summary of these studies one can observe that the application of SHM systems is comprehensive and necessary for proper operation of civil structures nowadays.

3. Research problem

The interest in the ability to monitor the performance of a concrete structure and detect damage at the earliest possible stage has increased in the last two decades due to aging and material degradation, and limited budget assigned for maintenance and renovation. For such purpose, monitoring with the use of SHM system is a fruitful solution, but it varies as structures have very different requirements. Therefore, the research problem, objective and scope can be formulated for the thesis.

3.1 Identification of research problem

The research described in the introductory section regarding the necessity of diagnosis of propagation of microcracks in reinforcement concrete remains a significant challenge for NDT techniques, despite specific interest in forming such degradation since these cracks may lead to undesirable premature structure failure. This vast majority of SUM research efforts that have been contained and evaluated in the laboratory conditions with substitution of real objects, and the impact of environmental and operational changes in the structure are becoming an increasing concern. Multiple sensors are often installed in the SHM system, as it is hard to detect operational and environmental changes from a single feature of one or a pair of sensors. Therefore, the illustration of the signal/data from each separate sensor may be confusing and may not lead to appropriate detection. This has been the motivation for the undertaken research.

One major methodology to obtain final comprehensive structural health status is to develop more features and feature-based fusion techniques based on the same or different types of sensors with different parameters (information sources), that are sensitive to small changes/ damages. There is a lack of knowledge of whether advanced signal processing techniques, such as time-frequency domain analysis, statistical, matching pursuit, and other, selection of the most sensitive ones to cracks, and their implementation into the fusion algorithm could be useful for the determination of damage-sensitive features.

The research problem boils down to the following questions:

- How to evaluate damage/changes of reinforced concrete decks using embedded sensors?

- How to integrate different NDT techniques in reinforced-concrete structures?
- How to improve the detection capability using data fusion technique?

3.2 Research goal

The main goal of the dissertation is to develop effective signal processing methods and signal synthesis obtained using various measurement systems. The methods should provide qualitatively new information about the condition of the monitored object and contribute to improving the assessment of the technical condition of the examined objects, in particular, concrete bridges. The development of the mentioned methods is based on signals obtained from measuring systems built on real objects (e.g., bridges). This allowed taking into account many critical operational factors that may affect the assessment of the technical condition of monitored objects. The set of developed methods is integrated into the form of an consolidated platform understood as a working methodology with the possibility of visualizing test results. This allowed for the formulation of the scope of the following thesis.

3.3 Thesis of the dissertation

Basing on the identified research questions and goals, one can formulate the thesis of the disseration as follows:
The developed methodology for the assessment of the technical condition of large-size facilities, combining advanced methods of signal analysis and data fusion, will be a new effective tool for monitoring civil structures and early detection of structural changes.
As such, the tasks of the current study can be summarized as the following:

- Definition of structural parameters to evaluate damage/changes of reinforced concrete structure using embedded sensors;
- Feature extraction/damage detection in a reinforced concrete structure (such as a laboratory destructive test, full scale experiment and a real bridge);
- Combining information from multiple sensors to improve overall performance using data fusion techniques applied to real structures.

4. Fundamentals of ultrasonic inspection techniques

4.1 Background

Various methods called NDT techniques have been used for many years. In many cases, they are combined with SHM. More than seventy types of standardized testing methods can be found in the literature (Sun *et al.*, 2011). Although some of them have potential applicability in the considered problem, they are widely used. Indeed, NDT techniques using devices with attached sensors have some drawbacks: the necessity of a considerable number of connections, small coverage, bulky size, complex signal processing, and quite strong local mechanical noises initiated by the sensor elements. For example, strain gauges are commonly used as low-cost measurement devices to measure the internal stress/strain in concrete structures. The problem of application of traditional strain gauges is the difference value of stress inside a concrete specimen, and at a point on the surface of the specimen under axial loading. Also, fiber optic (Deng and Cai, 2007b) and piezoelectric sensors (Yu and Kwon, 2009) have shown excellent performance in measuring internal stresses. The main disadvantages are their cost and capability for long-term monitoring. Another most used set of NDT techniques for reinforced concrete inspection is the acoustic and Ultrasonic Pulse Velocity method (UPV).

For decades, ultrasonic methods have been widely used in civil engineering to detect crack initiation and growth, defects as well as to determine material properties. This chapter provides an introduction to the basic principles of different ultrasonic techniques. Then the principal of wave propagation in solids (like concrete) is briefly discussed. Lastly, the boundaries of traditional ultrasonic techniques are also presented.

4.2 Ultrasonic testing in heterogeneous material

Concrete is a heterogeneous material with non-linear elastic properties. Therefore, ultrasonic wave propagation in concrete is affected by a different factor (e.g. aggregate, moisture content, etc.). Given that each factor itself can be a separate research project, it is not within the scope of these studies to analyze each contribution. Since the purpose of this study is to obtain a better understanding of changes in the real structure, the starting point is to understand the comprehensive strength of concrete. It is possible to estimate this roughly by this assuming that there is a relationship between wave propagation and the stiffness of a material.

4.2.1 Fundamentals of ultrasonic wave propagation

Sound is a dilution of waves of pressure that propagates through a medium based on the way particle oscillates. It can propagate not only compressible media such as air but also water and solids. Sound waves are categorized into four principle modes based on atom oscillate of the media: longitudinal waves, shear waves, surface Rayleigh waves, and in thin materials such as plate. Longitudinal and shear waves are the most common modes of propagation used in ultrasonic measurement (Hellier, 2012; Ensminger and Bond, 2011). In the longitudinal waves, particles of the medium vibrate back and forward parallel to the longitudinal direction or the direction of wave propagation. Since compressional and rarefaction forces are active in these waves sometimes called as a density waves (Ensminger and Bond, 2011). The direction of wave propagation is perpendicular to the direction of impulse and where deformations have a shear character, it is called a transversal or shear wave. As a matter of fact, shear waves are usually produced in materials using longitudinal waves energy. Then the waves that arrive later are diffused wave, because it's coming from reflection and scattering from the material. Their paths are long and complex. This part of the wave is a mix of all types of waves and is called as a diffuse wave. It can be written as:

$$U_u(t) = \sum PA_T(t), \tag{4.1}$$

Where $U_u(t)$ is the diffuse wave field and $PA_T(t)$ is the amplitude of the wave that travelled along each trajectory T. The speed of sound varies in different materials, since the mass of the atomic particles and the elastic properties are different for various materials (Holnicki-Szulc and Soares, 2004). The mass of the atom is related to the thickness of the material, and the elastic properties are related to the elastic constants of the material.

4.2.2 Propagation in elastic material

Elastic waves are stress or strain waves that propagate motion in a medium without transferring matter. In extended isotropic solids, there are two types of elastic waves; longitudinal and transverse waves (Kolsky, 1964; L. Rose and Nagy, 2000). Longitudinal waves are also known as compressional, or P waves. Transverse waves, also known as shear or secondary or S waves (Figure 4.1), are waves with particle motion perpendicular to the direction of wave propagation (Kolsky, 1964; Krautkraamer and Krautkraamer, 1990). Transverse waves are further classified as either Shear Horizontal (SH) or Vertical (SV) depending upon the associated direction of particle motion.

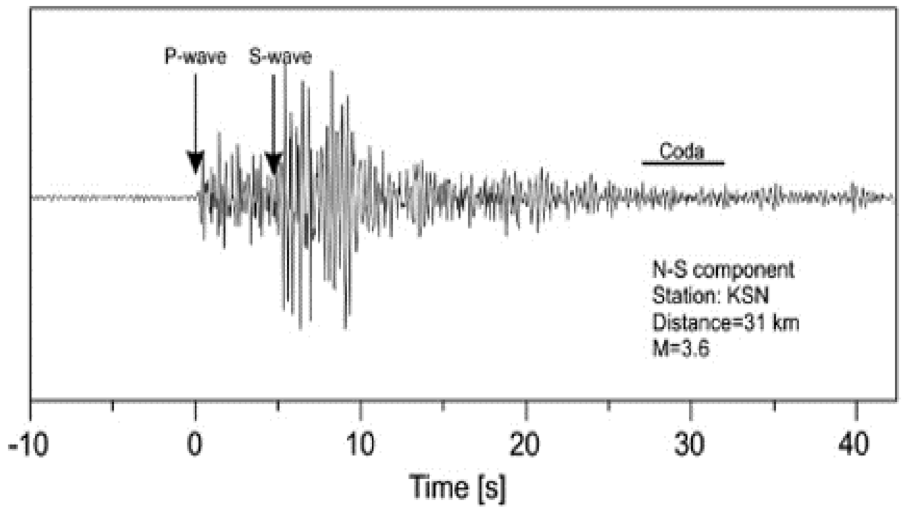

Figure 4.1: Seismogram example taken in KSN, US (Singh *et al.*, 2012)

Such a sound wave is excited by a sinusoidal normal force, which generates periodic pressure and tensile stresses on the component surface. From the excitation center (of the tested material), compression and dilution zones with variable velocity V_l are then propagated alternately at regular intervals in the component, where they generate periodic volume changes. The individual particles of the substance oscillate parallel to the propagation direction of the wave (longitudinally) with the specific frequency. In contrast to the propagation velocity, the frequency is not a substance constant, because it is impressed on the sound wave by the transmitter. For the reasons mentioned, the longitudinal wave is also called the density, pressure or compression wave. It has the highest propagation speed compared to other elastic waves in solids.

The equation for the propagation of elastic waves in a homogeneous, isotropic and elastic solid is written as:

$$\rho \frac{\delta^2 \mu_i}{\delta t^2} = \partial_j \tau_{ij}, \tag{4.2}$$

$$e_{ij} = \frac{1}{2}(\partial_i \mu_i + \partial_j \mu_j), \tag{4.3}$$

$$\tau_{ij} = \lambda\delta_{ij}e_{kk} + 2_{ij}, \tag{4.4}$$

In equations (4.2)-(4.4), ρ is the density of the elastic medium, τ_{ij} the stress on the face perpendicular to the i direction in the j direction, μ_i is the displacement in the i direction, and λ and μ are the Lamé constants (Weaver, 1998).

$$\mu\nabla^2 u + (\lambda + \mu)\nabla\nabla \times u = \rho, \tag{4.5}$$

Rewrite the equation (4.2) as:

$$\rho\frac{\delta^2 u}{\delta t^2} = \mu\nabla^2 u + (\lambda + 2\mu)\nabla(\nabla \times u), \tag{4.6}$$

The Lamé parameters can be written in terms of other more common material properties, E is the young modulus and n is the Poisson's ratio. The velocity of waves is propagating in an elastic medium can be derived from equation (4.6) by application of the divergence are given by:

$$\lambda = \frac{nE}{(1+n)(1-2n)}, \tag{4.7}$$

$$\mu = \frac{E}{(2)(1+n)}, \tag{4.8}$$

This leads to two kinds of waves, a longitudinal wave and a shear wave. The velocity of both wave types can be written as a function of the Lamé parameters. V_l is the velocity of the pressure wave and V_r is the velocity of the shear wave.

$$V_l = \sqrt{\frac{\lambda + 2\mu}{\rho}}, \tag{4.9}$$

$$V_r = \sqrt{\frac{\mu}{\rho}}, \tag{4.10}$$

These relationships are shown in equations (4.9) and (4.10). For longitudinal waves, the speed of the sound in solid material like concrete is given in (4.11):

$$V_l = \sqrt{\frac{E(1-n)}{\rho(1-n)(1-2n)}}, \tag{4.11}$$

The velocity of surface Rayleigh waves is given in (4.12):

$$V_r = \frac{0.87 + 1.12n}{1+n}\sqrt{\frac{E}{2\rho(1-n)(1-2n)}}, \tag{4.12}$$

where V_l and V_r is the velocity of sound for longitudinal wave and Rayleigh waves, E is the young modulus, ρ is the material density, and n is the Poisson's ratio. Equations (4.11) and (4.12) relate wave velocities with elastic parameters. Therefore, the propagation of wave is strongly affected by the elastic properties and density of constituent materials (Grêt *et al.*, 2006).

4.2.3 Reflection and Scattering

If a wave strikes an interface of two media of different impedance, so a part is reflected (reflection) and a part passes through (refraction). The resulting sound pressure of the reflected and the continuous wave results from the sound pressure of the incident in one medium multiplied by a reflection factor or transmission factor. Since elastic waves in concrete are tend to diffraction and attenuation, the elastic waves of relatively low frequency (as low frequency has a large wave-length), and the high energy source is usually needed (Wu and Liu, 1998). If the wave frequency is lower than 20 kHz, the wavelength is larger than the distinguishable size of the structure. It is easy to implement the technique for the SHM system and transient dynamic analysis in this frequency range (Wu and Liu, 1998). If the frequency is megahertz rage (higher than 1 MHz), it is difficult to observe ultrasonic pulse waves on a large length scale, because of the combination of scattering and attenuation. In this case, ultrasonic techniques could be used only on small size specimen in the laboratory. The parameters that impact on the velocity and attenuation of stretch of ultrasound waves are (Wu and Liu, 1998; Fröjd and Ulriksen, 2017): the nature of the load; the age of the concrete (the velocity increases with the time of the concrete); the form and the volume of the structure; the presence of steel reinforcements (the speed increases in proximity of the steel bars); the water/cement ratio; environmental effects, e.g. humidity and temperature of a concrete (Lu and Michaels, 2005b).

4.2.4 Acoustoelastic effect

From the previous sections, one can see how the wave velocity and Young's Modulus derived from stress-strain relationship. The simplified linear elastic assumption would be insufficient for an real structural quantitative test. However, these factor can be reduced using a nonlinear approach i.e., acoustoelasticity theory. The acoustoelasticity theory was developed in 1953 by Hughes and Kelly (Hughes and Kelly, 1953), expanding on Murnaghan's laws of nonlinear elasticity (Murnaghan, 1937). The speed of elastic ultrasonic longitudinal and shear waves propagating through the solid depends on the elastic deformation of the material (Jin *et al.*, 2017). The mathematical description of non-linearity is done taking into consideration the second order effects, expressed by the introduction of a 6th order tensor to Hooke's law (Payan *et al.*, 2010). The equations for elastic wave velocities (longitudinal and shear waves) in a uniaxially stressed medium are given as:

$$\rho_0 v_{11}^2 = \lambda + 2\mu - \frac{\sigma_{11}}{3K}[2l + \lambda + \frac{\lambda + \mu}{\mu}(4m + 4\lambda + 10\mu)], \tag{4.13}$$

$$\rho_0 v_{12}^2 = \rho_0 v_{13}^2 = \lambda - \frac{\sigma_{11}}{3K}[m + \frac{\lambda n}{4\mu} + 4\lambda + 4\mu], \tag{4.14}$$

$$\rho_0 v_{22}^2 = \lambda + 2\mu - \frac{\sigma_{11}}{3K}[2l - \frac{2\lambda}{\mu}(m + \lambda + 2\mu)], \tag{4.15}$$

$$\rho_0 v_{21}^2 = \mu - \frac{\sigma_{11}}{3K}[m + \frac{\lambda n}{4\mu} + \lambda + 2\mu], \tag{4.16}$$

$$\rho_0 v_{23}^2 = \mu - \frac{\sigma_{11}}{3K}[m + \frac{\lambda + \mu}{2\mu} n - 2\mu], \tag{4.17}$$

where ρ_0 is the material density v_{ij} is the velocity of a wave propagating in a particular direction. σ_{11} is the stress in particular direction. λ and μ are Lamé 's parameter, and l, m, n is Murnaghan 's parameters. This equation, describing diffuse ultrasonic wave can be used for evaluation of non-linear parameters in concrete.

As previously discussed, Hughes and Kelly's classical theory of acoustoelasticity can be used in evaluation of concrete structure as a homogeneous isotropic medium. Ultrasonic wave velocity and attenuation are rapidly increased by initiating cracks and can indicate as damage index (Fröjd and Ulriksen, 2017)(Stähler *et al.*, 2011). Attenuation and velocity changes are almost linear with initiating cracks. Previous studies of ultrasonic wave behaviour in concrete have shown that (Larose and Hall, 2019; Stähler *et al.*, 2011; Zhang *et al.*, 2011; Zhang *et al.*, 2012), under different load variation the observed phase was almost linear.

4.2.5 Temperature effect

Research studies of ultrasonic NDE conclude that temperature variations influences the ultrasonic velocity in composite structure e.g., bridges (Cegla *et al.*, 2011). The ultrasonic wave velocity changes due to temperature variation e.g. just a 20°C cause changes in ultrasonic propagation velocity by 0.5% (Scruby and Moss, 1993). In reality, it is difficult to compensate slightly thermal expansion when the temperature increases or decreases sharply. One can observe the variations of thermal curvature in the structure due to daily temperature. However, the thermal curvature mostly changes within 1°C, which requires a longer period. Fortunately, it is easy to dissociate the deformations related to the temperature or the traffic-induced distortions, due to the fact that the effects of traffic occur at frequencies much higher than temperature variations.

Nevertheless, such sharp temperature changes can influenced damage detection estimation. Previous research showed that ultrasonic signal is subject to stretch or distort due to temperature changes (Croxford *et al.*, 2007; Weaver and Lobkis, 2000; Zhang *et al.*, 2012). Rozsypalová et al. show that, ultrasonic waveform is distorted as the specimen cools or heats in the room temperature (Rozsypalová *et al.*, 2018). To remove the temperature effect from diffuse ultrasonic wave, several temperature compensation methodology have been proposed in the literature. Most of the SHM system using active monitoring employ algebraic difference between the current time-signals and a baseline (in that case, the structure is considered as undamaged) time-signal to compensate temperature. The subtraction of baseline time signal is named as a baseline compensated signals. The authors (Salmanpour *et al.*, 2016; Alguri *et al.*, 2017; Michaels, 2008; Moll *et al.*, 2019) have proposed compensating multiple baselines due to temperature changes in the structure. Moll et al. (2019), the authors proposed optimal baseline selection method to compensate temperature effect.

However, the temperature effect on ultrasonic wave velocity is considered negligible, unless the tested element is exposed to extreme temperatures (Zhang *et al.*, 2013). This is why in this study uses the embedded methodology. Previous research studies showed that near surface changes have less influence on the ultrasonic wave velocity (Niederleithinger and Wunderlich, 2013). Yet, simple baseline subtraction method was used in this studies to minimize the temperature influence.

4.3 Ultrasonic transducers

4.3.1 Traditional ultrasonic transducers

The UPV method is most commonly used to detect the quality of concrete, the position of crack or depth inside both reinforced or masonry structures (Komlos *et al.*, 1996). The UPV method is based on sending and receiving sound waves inside the cement matrix. The measured parameters are the elastic properties of the material. Ultrasound pulse waves in structure which is also known as a pulse echo and pitch-catch sensing method Figure 4.2(A) and 4.2(B). It can be used in many applications for the purpose of damage detection/evaluation, source localization, material characterization, and more. The ultrasonic inspection method consists in sending high frequency sound waves, usually above 20 kHz, introduced into the material. The measurement of the ultrasound transmission functions is carried out in active way. For this purpose, the equipment consists of two transducers, one for transmission, and another for reception (Peterson *et al.*, 1995). The transducer heads are attached to opposite sides of each other on tested structure, and the received signal is measured after excitation of a short pulse from the transducer. The extracted parameters are different in different structures due to different concrete formulation. Therefore, the measurement concept has to adjust ultrasonic measurements to a specific concrete structure (Concu and Trulli, 2018).

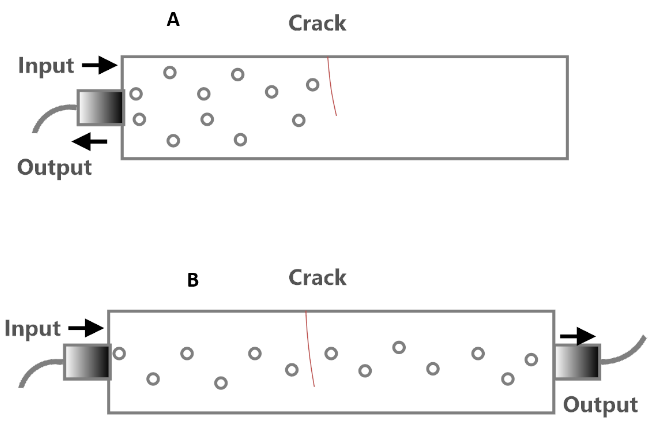

Figure 4.2: Pulse Echo (A) and Pitch-Catch Sensing Method (B)

The concept behind the technology is to measure the travel time of ultrasonic waves in a medium, and correlate them with the elastic properties and density of the material. The travel time of the ultrasonic waves reflects the internal condition of the test area (Schickert, 1984). In general, for a given path, the highest travel time is correlated with low quality concrete with more abnormalities and insufficiency, while the shorter travel time is correlated with high quality concrete with less abnormalities (Concu and Trulli, 2018). Once the ultrasonic wave propagates the tested area, it reflects the quality of the tested object. In concrete structures, it translates into longer propagation time (lower wave speeds) in poor quality concrete and lower propagation time (higher wave speeds) in good quality concrete.

There are three basic ways in which the transducers can be placed: direct, semi-direct, and indirect (see Figure 4.3). The UPV transducers must be in full contact with the concrete surface, otherwise, the air gap between the transducer and the concrete may result in measurement error (an incorrect measurement of the propagation time) (Turgut and Kucuk, 2006). The reason of incorrect measurement is that an insignificant amount of wave energy will be transmitted in inappropriate contact. Different couplers can be used to eliminate air space, ensuring good contact (for example, petroleum jelly, grease, liquid soap and kaolin-glycerol paste). It is recommended to make the coupling layer as thin as possible. Special attention should be paid to reinforcement bars in concrete, since the propagation speed of the wave in steel is much higher than in concrete.

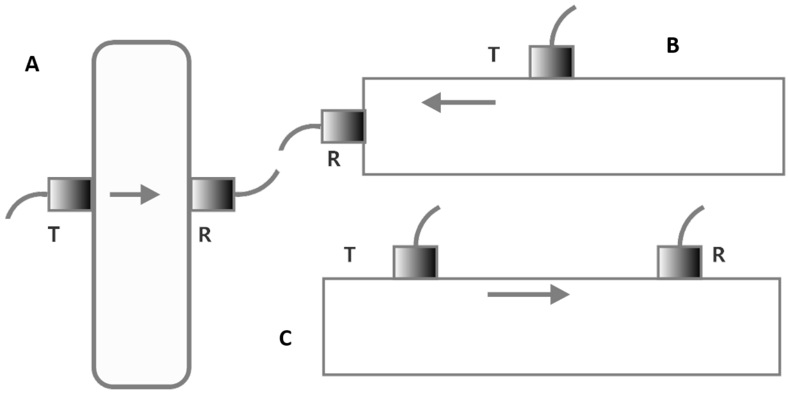

Figure 4.3: Pulse velocity configuration (A) Direct (B) Semi-direct (C) Indirect Method

A signal pulse generator and amplifier is used to produce an amplified electric wave, then it is converted to mechanical vibrations by a piezoelectric crystal transducer, and transmitted through the structure. Then, a reflected wave is received by the receiver and converted back to an electric wave which is called an echo (Brigante and Sumbatyan, 2013). In the ultrasonic inspection, the most commonly used modes are longitudinal and shear propagation waves. The UPV method (Brigante and Sumbatyan, 2013; Turgut and Kucuk, 2006) is a useful and versatile NDT method used in concrete structure inspection. Based on the velocity of propagation of ultrasound waves, it is possible to evaluate the different parameters of concrete (Lorenzi *et al.*, 2007). The UPV method can be used for similarity evaluation, locating the position of damage or depth inside both reinforced or masonry structures (Karaiskos *et al.*, 2015). However, several authors indicated the drawbacks of traditional UPV system. The first is the need of trained operator, which is sometime difficult in practice. Strong surface influence, affected by soft material and external environmental factors (changes in temperature, wind and others) undermine sensing accuracy. The transducers are subjected to accidents or impairment during practical field measurements (Gu *et al.*, 2006; Karaiskos *et al.*, 2016; Wolf *et al.*, 2015; Chakraborty and Katunin, 2019a). There are different manufacturer of commercial UPV systems, for example, 'Proceq' in Switzerland and 'RTUL' in India is a leading manufacturer of high quality UPV system for different applications. Figure 4.4 presents the 'Pundit' (Portable UPV system), that is an advanced UPV and pulse echo testing system.

Figure 4.4: Different models of UPV system (*Proceq products web-site*, 2019)

4.3.2 New ultrasonic transducer

In this thesis, a new ultrasonic transducer 'SO807' was used, designed by 'Acoustic Control Systems', a Russian company based in Moscow, cooperating exclusively with BAM. The main part of this sensor ('SO807') is a hollow piezo ceramic cylinder (see Figure 4.5). The primary benefit of this sensor is it can be used both as a transmitter and a receiver. Another benefit of this sensor is easy installation during construction, which helps investigate the inside of the concrete structure(Niederleithinger *et al.*, 2015).

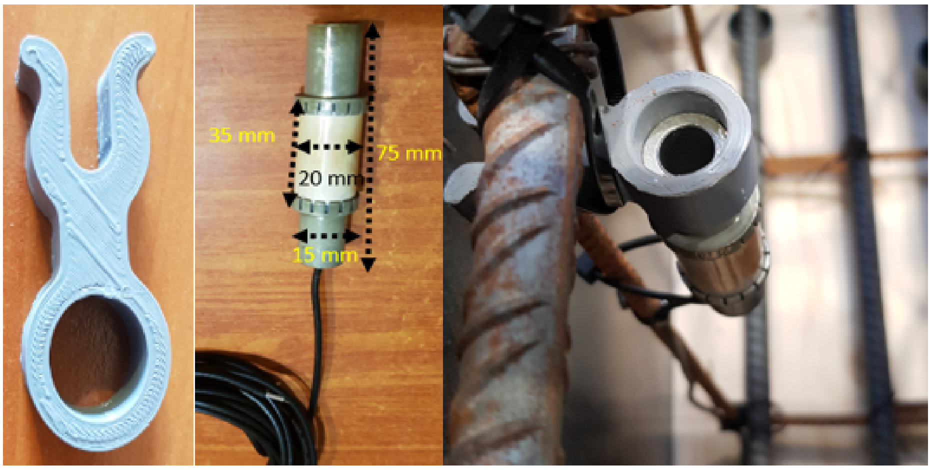

Figure 4.5: 'SO807' sensor installed on a plastic ring on the rebar

Figure 4.6 shows the amplitude spectrum of the 'SO807' sensor, which is representative of all the signals in duration and bandwidth. The first prominent frequency peak is at

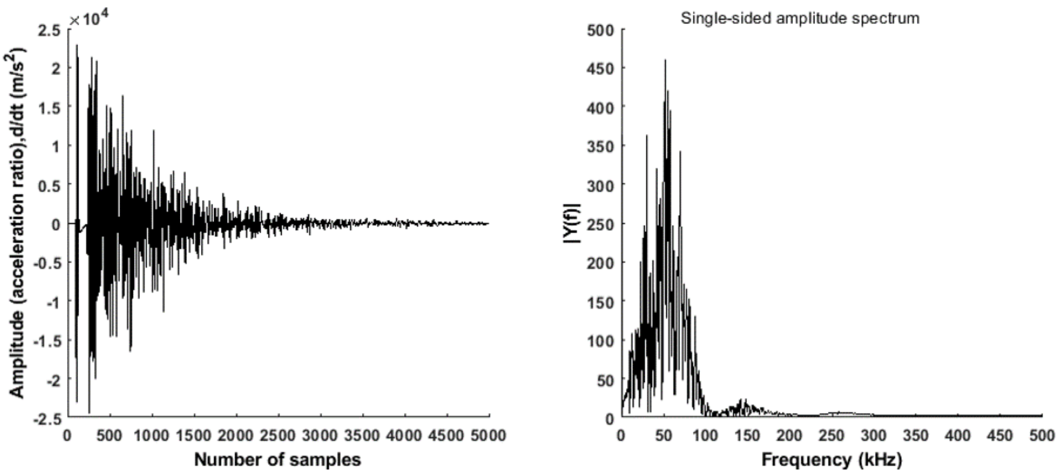

Figure 4.6: Diffuse ultrasonic signal and its spectrum

62 kHz and the second at 65 kHz, smaller peaks appear around 50 and 85 kHz. When the frequency is lower than 43 kHz or higher than 90 kHz, the amplitude is very low. In concrete, a frequency of 62 kHz relates to a wavelength which is at least double size of most aggregates. The recorded duration of 5 ms corresponds to about 20 m of travel for this mode, allowing many reflections to occur and resulting in a like diffuse wave. Therefore, the recorded duration is sufficient to acquire most of the reverberating energy. To ensure the sensors are stable and held in position during construction, different size parameters plastic parts are printed on a 3D printer (Figure 4.5). Using these plastic parts, 'SO807' can be easily installed on the rebar.

4.4 Conclusion

The long range inspection and long term monitoring of civil structures is a very important issue for structural integrity. Embedded ultrasonic active measurements can be a cost-effective and operator-friendly technique for damage/change detection systems in the infrastructure. This chapter will introduce the methodology used for the analysis of the ultrasound measurements and provide physical and mathematical background to these methods, as well as the behaviour of concrete structures under load. The example figures given in this chapter are,unless otherwise noted, based on a synthetic dataset.

In this chapter, the methodology used for propagation of the ultrasonic wave in concrete and physical mathematical approach behind these techniques is presented. The elastic ultrasonic waves behaviour through different loading also discussed. The authors has indicated the disadvantages of traditional ultrasonic inspection (such as the need for a trained operator, the influence of surface by soft material and external environmental effects, transducers impairment during practical field measurements). To overcome this problem, the novel ultrasonic transducers developed by BAM (Bundesanstalt für Materialforschung und -prüfung) have also discussed briefly. The main benefit of using this type of sensor is high sensitivity to large monitored areas of the structure with a limited number of sensors.

5. Feature extraction methods for early damage detection

As ultrasonic methods of concrete inspection, developed and evaluated in the laboratory, are being transferred to the field conditions, the influence of operational changes in a real structure is becoming of growing concern. To address this problem a major methodology must include features that are sensitive to operational changes and damage. Since it is hard to detect operational and environmental changes basing on a single feature, the approach generally taken is to develop features for a particular object and evaluate their operational changes. This chapter provides an overview of different feature extraction techniques. Then the feature extraction procedure for an ultrasonic signal is briefly discussed.

5.1 Feature extraction

The feature extraction process involves the extraction of load/crack sensitive features from the data collected during the data acquisition procedure to determine the presence of changes in the structure. The feature extraction process uses signal processing techniques to extract data, which involves data normalization, compression, and fusion. Data normalization minimizes the sensitivity to environmental variables such as temperature fluctuations. The data compression process reduces the dimensionality of the acquired data. Data fusion involves combining data from multiple transducers with the view of feature identification.

Wave scattering is a physics process that occurs when an induced wave is distressed by a change (damage) in the medium (Staszewski, 2000). Scattering is a complicated process that is dependent on the induced wave properties, the properties of elastic material, damage geometry and other factors. The objective of the feature extraction process is to identify relevance between non scattered (not perturbed by changes in the medium) and scattered (perturbed by changes in the medium) waveforms, and to then use these relationships to characterize load/crack in the structure. Relationships are established by extracting structural changes/damage sensitive features from time series sensor data through signal processing and then correlating with the level of changes in the medium (damage). Signal processing techniques include the time domain, the frequency domain, the time-frequency domain and physics based techniques (Qiao and Esmaeily, 2011).

5.1.1 Root mean square error

In the ultrasonic measurement, measured signals changes due to environmental or operational condition. These variables can be calculated using Root Mean Square Error (RMSE). This technique uses correlation between the variables. The SHM literature (Al-Adnani *et al.*, 2016; Bakhshizade and Reza, 2015; Malekjafarian *et al.*, 2019) highlights the fact that RMSE is an effective feature for damage detection tool. Therefore, it is considered to be a sensitive feature to tackle ultrasonic signal changes due to damage/change in civil engineering applications.

The RMSE is an estimator of the overall deviations between baseline ultrasonic signal $X(t)$ and measured signals $Y(t)$ at i-th time index from the structure. Here, signals are scaled and normalized, so that the resulting NMSE is not sensitive to absolute amplitude differences:

$$RMSE = \sqrt{\frac{\sum_{i=1}^{n}(Y(t-i) - X(t))^2}{n}}, \tag{5.1}$$

$$NMSE = \frac{[RMSE_{measured} - RMSE_{reference}]}{RMSE_{reference}}, \tag{5.2}$$

5.1.2 Normalized peak-to-peak amplitude

A research study (Moughty and Casas, 2017), evaluated a number of vibration features such as the maximum peak amplitude, minimum peak amplitude, standard deviation, and sum of squared differences between baseline acceleration and damaged acceleration. Li et al. (2019), investigates the peak to peak amplitude as a damage sensitive feature for ultrasonic wave propagation and the results was verified through acoustic emission. Casas and Rodrigues investigated vibration based criteria, and showed correlation between peak acceleration amplitude and the existence of damage for bridge structures (Casas and Rodrigues, 2015). The results from the previous research study shows that peak amplitude has strong damage sensitivity and the potential for damage localisation and quantification.

The peak-to-peak amplitudes can be defined as damage/change sensitive feature for diffuse ultrasonic signals. The feature extracted as a difference of the peak amplitude in each window template for various change levels normalized by the reference undamaged condition. This peak-to-peak amplitude can be written as:

$$P_a = \frac{[PA_{measured} - PA_{reference}]}{PA_{reference}}, \tag{5.3}$$

5.1.3 Window based cross-correlation

The basic idea of the window correlation-based measurement technique is to apply the local cross-correlation (Figure 5.1) to solve the correspondence problem. Window based cross correlation (WCC) has been commonly used in digital image processing for pattern recognition to evaluate the degree of similarity between reference template to image containing objects (Tsai and Lin, 2003). In object recognition or pattern matching applications, WCC is used to find reference template into correspondence image that contain similar object. The correlation coefficient is at maximum where reference template fully matches the corresponding image. For example, let $f(a,b)$ is an image that contain objects or parts of object and $h(a,b)$ is an template that has a region/part of similar object. To detect whether $f(x,y)$ contains a particular part or whether there is a full similarity of $h(a,b)$, WCC can be used. Thus, $h(a,b)$ can be slide in a pixel-by-pixel basis from left-to-right, top-to-bottom over $f(a,b)$ and correlating the overlapping regions of $h(a,b)$ in $f(a,b)$. If there is full or partial similarity, the correlation coefficient is maximum at the location where $h(a,b)$ finds a correspondence in $f(a,b)$ (Luo and Konofagou, 2010; Yang and Mueller, 2007; Chakraborty *et al.*, 2014).

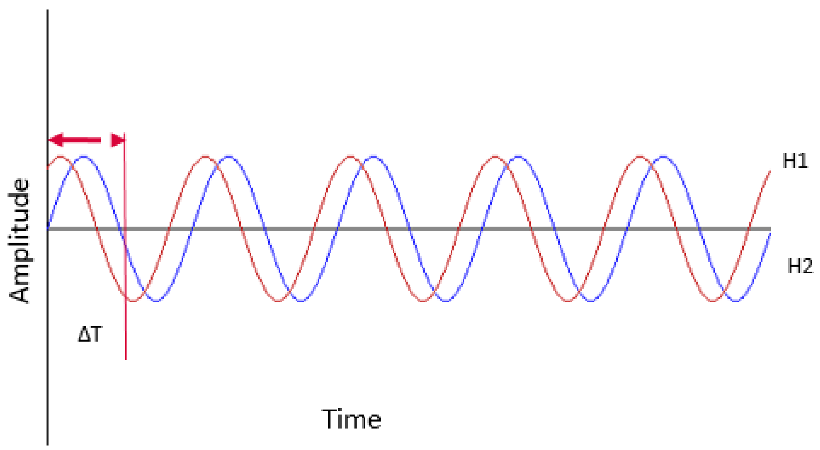

Figure 5.1: Graphic representation of normal cross-correlation

The main benefit of the window based cross correlation is that it is sensitive to small changes in the amplitude of illumination in the two compared images. One-dimensional window based cross-correlation technique can be used in order find specific patterns (changes in the medium) within a signal (Michaels, 2008). This technique is ideal, especially when dealing with many samples in a signal. In one-dimensional signal, window based correlation is used by considering a small window template from a baseline signal and the measured signal, then sliding it over the considered samples to find the similarities between these window. However, if the baseline signal window is properly matched with the measured signal window, then cross-correlation coefficient achieved maximum at zero lag. The representation of window based cross-correlation mechanism is shown in Figure 5.2, where W illustrate the window size and ΔW the sliding step. Figure 5.2 shows the window template from a baseline signal (red) contain a signal fragment to be matched within the measured signal (blue). The sliding mechanism can start at any sample within the signal, however in Figure 5.2 it starts at the origin. The general concept of sliding

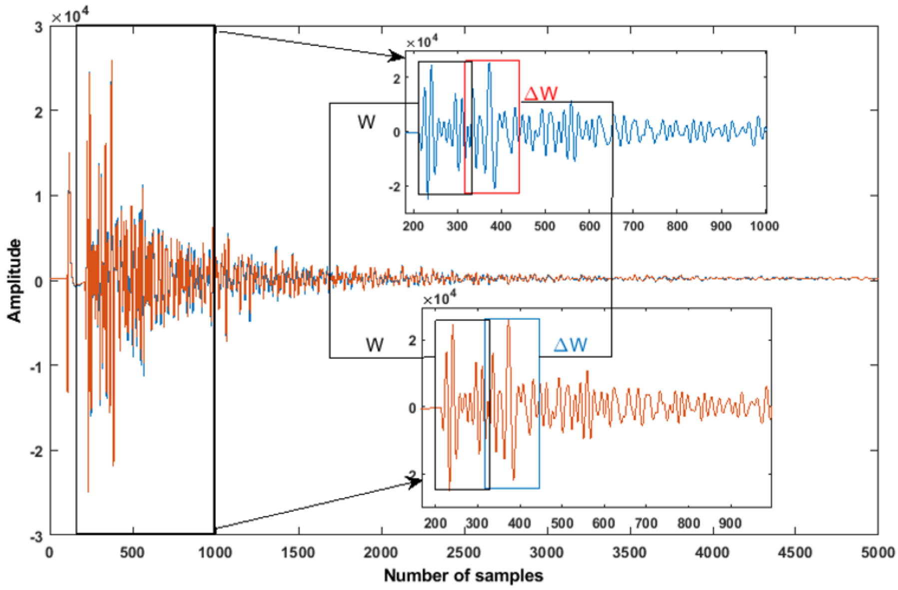

Figure 5.2: Graphical representation of window based cross-correlation

mechanism is to perform cross-correlation between the baseline window template and the measured window template covering a signal. The window template and the window over the comparison signal slides by ΔW remains stationary, while, updating the correlation values within the window frame. The window frame continuously sliding over the samples is shown in Figure 5.2.

One should remember, when performing the cross-correlation over the measured signal, both windows need to be of same length. Therefore, if the window has different length, then there is a good chance for window overlap between successive windows. However, in a two-dimensional object, it can be difficult because of the computational extensive, and a different method is required to eliminate redundant calculations (Poupinet *et al.*, 1996). On the other hand, in the case of a one-dimensional object, if the window size is properly selected, then redundant calculations can have a minimal effect to the computational speed. If $\Delta W \ll W$ then the sliding mechanism compute slowly as there are more samples to calculate, but correlation accuracy increases. If $\Delta W = W$, then the sliding mechanism is faster, but correlation accuracy can be decrease, since there is no overlapping, and part of the fragment of signal can be left behind.

A strongly reverberating signal, such as a diffuse ultrasonic signal can cover a larger area of complex structures which cannot be interpreted by guided waves (guided waves are suitable for steel, rods, etc.,). It is a combination of multiple paths and includes lots of other scattered waves, which arrive much later at the receiver. It is quite difficult to evaluate these arrivals (containing valuable information) separately (Figure 5.3).

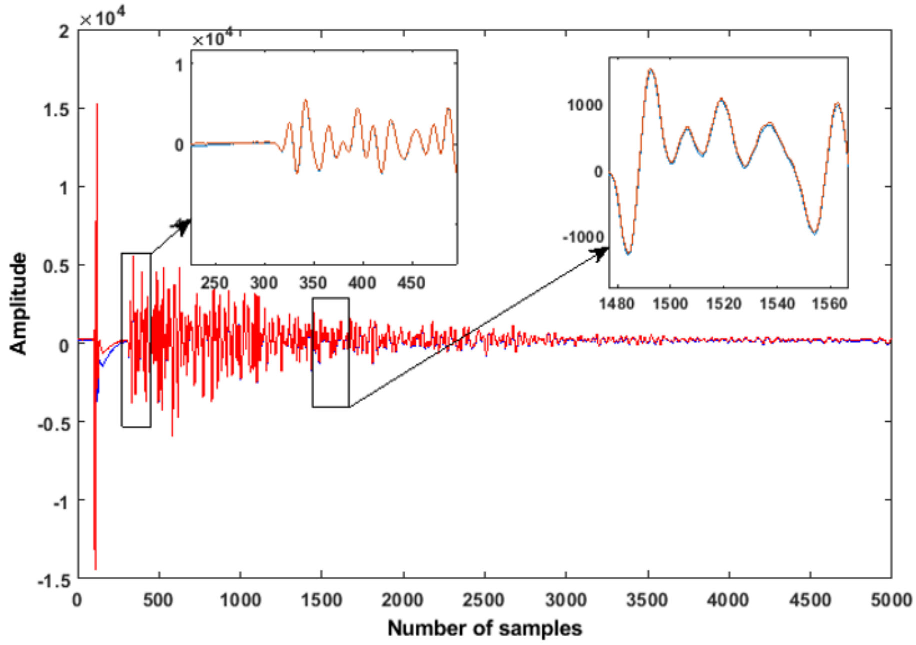

Figure 5.3: Reference Signal and signal under structural changes

The window based cross correlation is the basis to identify relevance between non scattered (not perturbed by changes in the medium) and scattered (perturbed by changes in the medium) waveforms in the window. It can be performed in the time domain (Zahiri-Azar and Salcudean, 2006). It is used to compute the degree of similarity of two signals in the window. The comparison of two signals $\sigma_{xx}(t)$ and $\sigma_{yy}(t)$ is done by computation in the time window, in the time window and later compute the mean of ρ_{xy}. The feature proposed here is the drop in the correlation coefficient to detect the changes in the structure from unity equation 5.5.

$$\rho_{xy} = \frac{\sigma_{xy}(t)}{\sqrt{\sigma_{xx}(t)\sigma_{yy}(t)}}, \tag{5.4}$$

$$D_{cc} = 1 - \rho_{xy}, \tag{5.5}$$

The flow chart of window based cross correlation is shown in Figure 5.4.

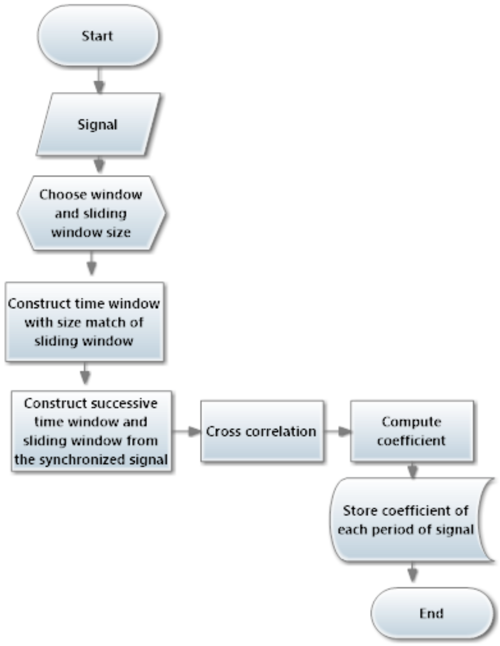

Figure 5.4: Flowchart of window based cross correlation

5.1.4 Autoregressive model

Linear time series models have been used in such a damage detection process which can be applied to a wide range of structures and associated damage scenarios, including cracking in concrete columns (Roach, 2007),(Hoon *et al.*, 2019), loose connections in a bolted metallic frame structure (Allen *et al.*, 2002), or damage to insulation on wiring (Clark, 2008). However, the linear nature of such a modelling approach limits the scope of application and the ability to accurately assess the condition of systems that exhibit nonlinearity in their undamaged state. The AR model may be used as a changes/damage feature extractor for the ultrasonic inspection. This AR model approach consists of using the parameters estimated from the baseline conditions, and calculating the response data obtained from the structure. This AR model can be written as:

$$\epsilon(t) = x(t) - \sum_{i=1}^{n} \alpha_i \bar{x}(t-i) + e_m, \tag{5.6}$$

where $x(t)$ is the measured signal at discrete time index t, and $\bar{x}$ is the predicted signal value. e_m is a noise that follows a normal distribution with zero mean and variance σ^2, and is independent of the past time series $\bar{x}$. The coefficients of the AR model parameter α_i, can be estimated using Akaike's information criterion (AIC) or RMSE (Figueiredo *et al.*, 2010). To estimate the correct AR model parameter, it is necessary to know the physical mechanisms underlying the system. RMSE can be a good choice to compute optimal model parameter from elastic properties of concrete, as it is easy to compute and more generally, minimizing RMSE finds an approximation for the conditional prospective value of the next observation. In this studies, RMSE is used to find an optimum model order:

$$RMSE(\alpha) = \frac{1}{n}\sqrt{\epsilon(t)}, \tag{5.7}$$

RMSE is a real value, which indicates how different the value is from the estimated parameter. The RMSE can be used as change detection feature for ultrasonic measurements, where the coefficient of RMSE can be realized between baseline to measured signals differences. However, the estimation of the AR model order can be realized by minimizing the RMSE value using equation (5.10). The average of RMSE values can be used to characterize model performance in the validation period as well as to compare the outputs to a perfect match between predictions and the measured signal. An example of ultrasonic signals presented in Figures 5.5a and 5.5b shows the effect of high-order (25th order) and low-order (8th order) models in resemble the signal.

The blue line curve represents the real signal $x(t)$, which is chosen as the reference signal, and the red line curve represents the predicted signal $\bar{x}$ for the high model order in Figure 5.5a, and low model order in Figure 5.5a, respectively. In Figure 5.7, the first plot indicates that the real signal and low model order estimated signal are less correlated, while the high peak in the second plot indicates that model is highly correlated to the signal.

$$RMSE = \sqrt{\frac{\sum_{i=1}^{n} x_{measured,i} - x_{model,i}}{n}}, \tag{5.8}$$

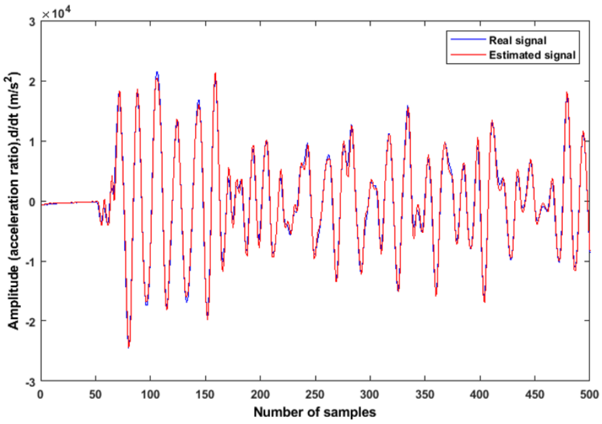

(a) Low model order

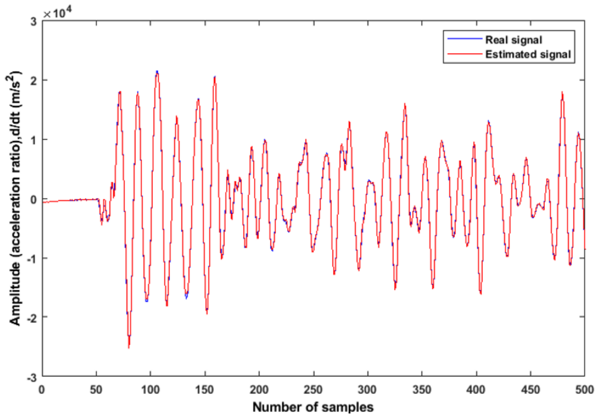

(b) High model order

Figure 5.5: Low and high model order for estimated AR model

The flow chart of modelling stage of AR algorithm is shown in Figure 5.6.

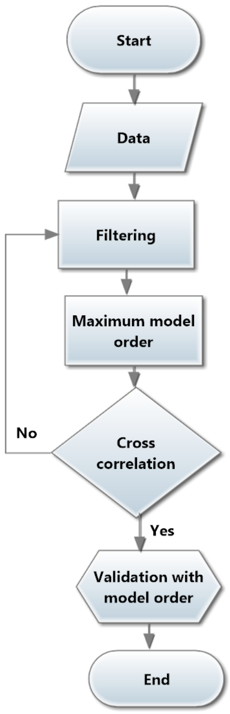

Figure 5.6: Flowchart of modelling stage of AR algorithm

AR models work especially well when modelling the feedback of linear, time-invariant systems. AR method delivers the best linear fit to the measured signal if the operational changes are nonlinear, but there is uncertainty when the system is suppressing other inputs then there is no guarantee that this model can exactly compute the responses.

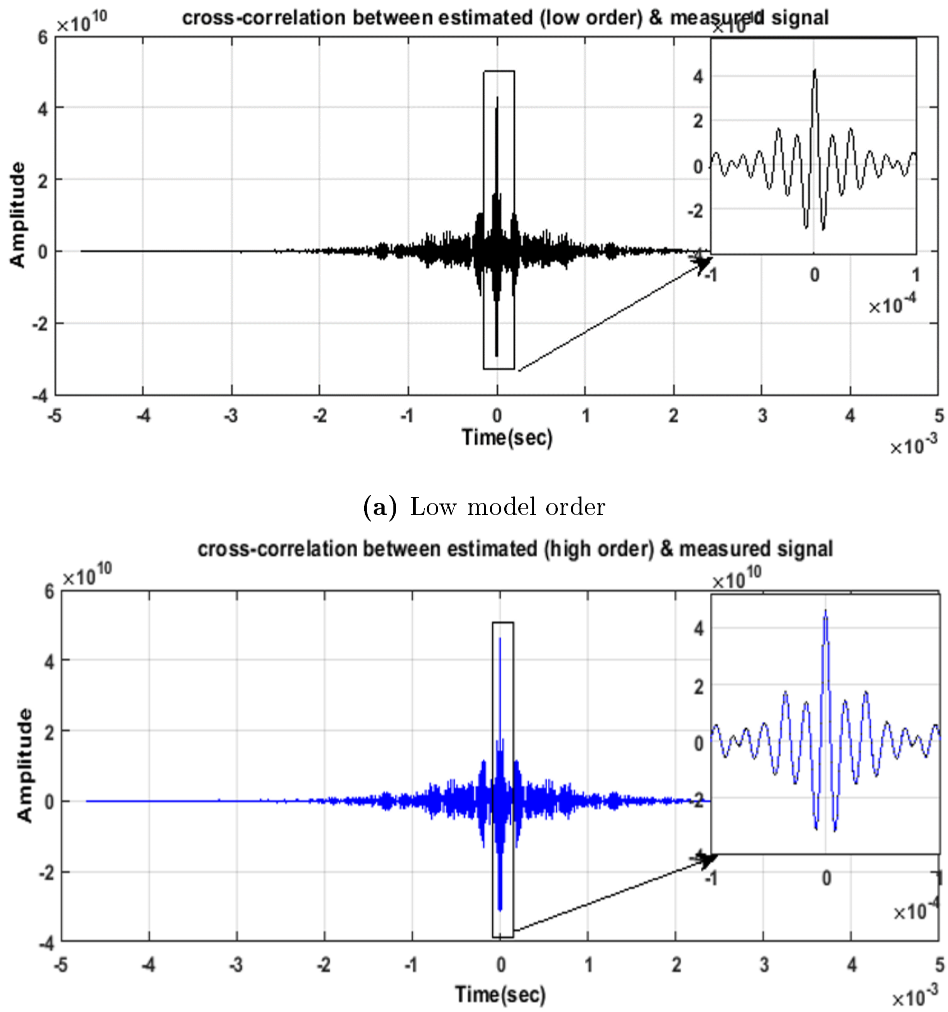

(a) Low model order

(b) High model order

Figure 5.7: Cross-correlation of real signal $x(t)$ to the estimated signal $\bar{x}(t)$

5.1.5 Short-time Fourier transform

The ultrasonic signals in concrete are non-stationary, which indicate the Fourier transform is not suitable. In order to overcome the problem with detecting the non-linear frequency components on time, the Short Time Fourier Transform (STFT) was designed to analyze the signal in a time-frequency domain. In the STFT method, the duration of a signal is divided into small time windows, therefore fast Fourier transform can be applied to each window. This small windowing method help to compress the time interval where the structural changes or damage is located.

The authors of (Yu and Giurgiutiu, 2005), proposed an advanced signal processing technique for structural damage detection. Different methods were used for the time-frequency analysis. Zak at al. (2017), investigated the application of STFT method to detect local damage in bearing. The results shows that STFT method is efficient in detecting local damage using vibration signals.

The research studies shows that, STFT is capable of providing information about signal behaviour by performing a time-frequency analysis, on the basis of which it is possible to determine the time instants at which specific harmonics are present in the signal, as well as the power spectrum analysis.

$$STFT_c = \sqrt{\frac{\sum_{j=1}^{n}(STFT_{e,j} - STFT_{e,1})^2}{\sum_{j=1}^{n}(STFT_{e,1})^2}}, \tag{5.9}$$

where the matrix element $STFT_c$ represents the STFT-based index of changes associated with the time histories of each pair of the sensors. The STFT index of changes value demonstrates the energy attenuation ratio due to the changes in the structure. The greater value of this index is due to operational effect and the energy attenuation is related to crack (Lu *et al.*, 2017). The disadvantage of STFT is its small frequency resolution, however, low frequency can be hardly represented with small window. Once one can select a particular time window, then this window is also the same for all frequency blocks. The STFT contain time information as well, but it is not as efficient as wavelet transform.

5.1.6 Continuous wavelet transform

Continuous wavelet transform (CWT) is an effective signal processing approach, used to detect changes/cracks in many applications due to the very high sensitivity to even tiny disturbances in the time-domain signal. The CWT algorithm is described by the following integral equation:

$$CWT(a,\tau) = \frac{1}{\sqrt{a}} \int x(t)\gamma\frac{t-\tau}{a}\mathrm{dt}, \tag{5.10}$$

where a is the detail of the mother wavelet and τ is the approximation of the mother wavelet with respect to the measured signal. It is important to note, that the CWT has no solid limitation to the type of wavelet function, i.e. these functions could be almost arbitrary.

It can extract features which can be related to changes/damage in the structure. WT is an estimator used to quantify the energy diffusion value from acquired signal. The CWT is applied to develop a time-frequency scalogram of a signal showing proper time and frequency localization. Wavelet analysis is effective, due to its capability to analyze the non-stationary signals at different frequencies simultaneously (Katunin, 2015b).

In each signal subset x_j can be written as:

$$x_{j,i} = [x_{j,1}, x_{j,2}, \ldots, x_{j,i}], \tag{5.11}$$

where $x_{j,i}$ is a each block of to CWT definition. A CWT-based change matrix is developed to evaluate the changes in the structure and crack propagation. The main procedures to compute the change index matrix is the following:

$$CWT_e = \sum_{i=1}^{i=n} x_{j,i}{}^2, \tag{5.12}$$

$$CWT_c = \sqrt{\frac{\sum_{j=1}^{n}(CWT_{e,j} - CWT_{e,1})^2}{\sum_{j=1}^{n}(CWT_{e,1})^2}}, \tag{5.13}$$

where the matrix element CWT_c represents the CWT-based index of changes associated with the time histories of each pair of the sensors. $CWT_{e,1}$ represents the CWT coefficient based on initial signal and $CWT_{e,j}$ represents CWT coefficient based on measured signal with time histories. Bump wavelet is used as a mother wavelet in this study since it is the most sensitive to time-domain signals (Vialatte *et al.*, 2009). The CWT index of changes value demonstrates the energy attenuation ratio due to the changes in the structure. The greater value of this index is due to the operational effect and the energy attenuation is related to the crack (Lu *et al.*, 2017).

5.2 Conclusion

The presented study was aimed at evaluating parameters obtained from ultrasonic measurement techniques in order to detect early cracking behaviour in RC structures. Different signal processing techniques used in different applications have been discussed. Since signals acquired from the mentioned novel ultrasonic sensors are the raw signals, their additional processing is needed. In this chapter, the fundamentals of feature extraction procedures based on diffuse ultrasonic waves have been presented, allowing the implementation of the techniques in damage/change detection in concrete structures. The strength of the current study was the use of the technique of obtaining multiple features from the same signals, collected in a laboratory and real environment, to predict the relative changes in the structure. To the best of our knowledge, this is the first study that used multiple features from the same signal for the purpose of change/damage detection in concrete, using different signal processing and machine learning algorithms.

6. Experimental validation

6.1 Background

The damage in reinforced concrete (RC) structures can be induced either by the dynamic or static load. The technologies available today have difficulty in detecting slowly progressive, locally limited damage, especially in hard-to-reach areas in the superstructure. Therefore, the four-point bending test on the benchmark RC structure was used as a test of the quality and sensitivity of the embedded sensors in the lab. It allowed assessing whether any cracking and propagation that occurs with the embedded sensors can be detected. Various methods are used for the analysis of the ultrasonic signals. By determining a feature from the ultrasonic signals, the changes in the whole structure are evaluated.The structural degradation of the RC benchmark structure was tested using various non-destructive testing methods to obtain a comprehensive decision about the structural condition.

The second structure on which the statistical SHM framework was tested, a reference structure called a BLEIB structure. The goal of the experiment was to measure changes in concrete during static and dynamic loading in the field condition.

The third structure was the Gliwice bridge. The main scope of this research was to develop an embedded monitoring system which could be applied to durability assessment of bridges. The system must interface and integrate the original practice principally based on traditional sensors and combine the response of several diffuse ultrasonic sensors, installed on the structure to monitor the progress of changes, damage using improved realistic degradation models.

This chapter provides an experimental validation of sensitivity of the embedded sensors presented in this thesis. Section 6.2 details the design of a new data acquisition system and limitations of this system. Section 6.3 describes the benchmark reinforced concrete structure and analysis of the destructive experiments. The reference reinforced concrete real structure in Germany, field test, data collection and analysis of the results and discussion of the experiments detailed in section 6.4. Finally, an experiment in the real structure (bridge assessment) is discussed in section 6.5.

6.2 Data acquisition system and preliminary experiment

6.2.1 Test object to analyse the limitations of data acquisition system

The goal of this measurement is to acquire ultrasonic signals to verify the developed new data acquisition system that relates ultrasonic feature with ADC resolution (Chakraborty. *et al.*, 20-2). For this purpose, a $20 \times 20 \times 100$ cm reinforced concrete beam has been cast in the NeoStrain lab for various tests of the embedded ultrasonic sensors, presented in Figure 6.1.

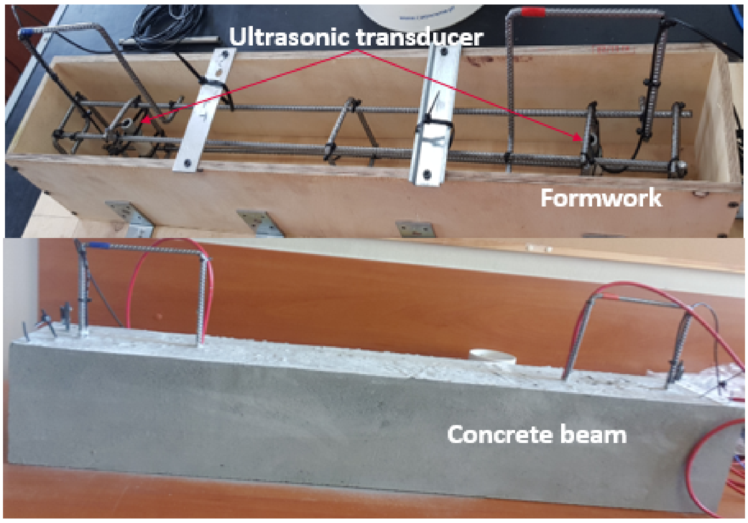

Figure 6.1: Concrete beam and sensor position

Rebar and formwork were manufactured for this meter size beam. Two ultrasonic sensors have been embedded in the beam during casting. A load step was applied in one cycle up to a maximum load of 1 kN.

6.2.2 Data acquisition system

The novel ultrasonic sensor was developed to overcome the limitation of traditional system and monitor certain areas of the structure. Therefore, it was important to design specific hardware and software to control different parameters and to find the relation between parameters and detection capability (Chakraborty *et al.*, 2019b). For this reason, the author designed a primary data acquisition system for this novel sensors (see Figure 6.2).

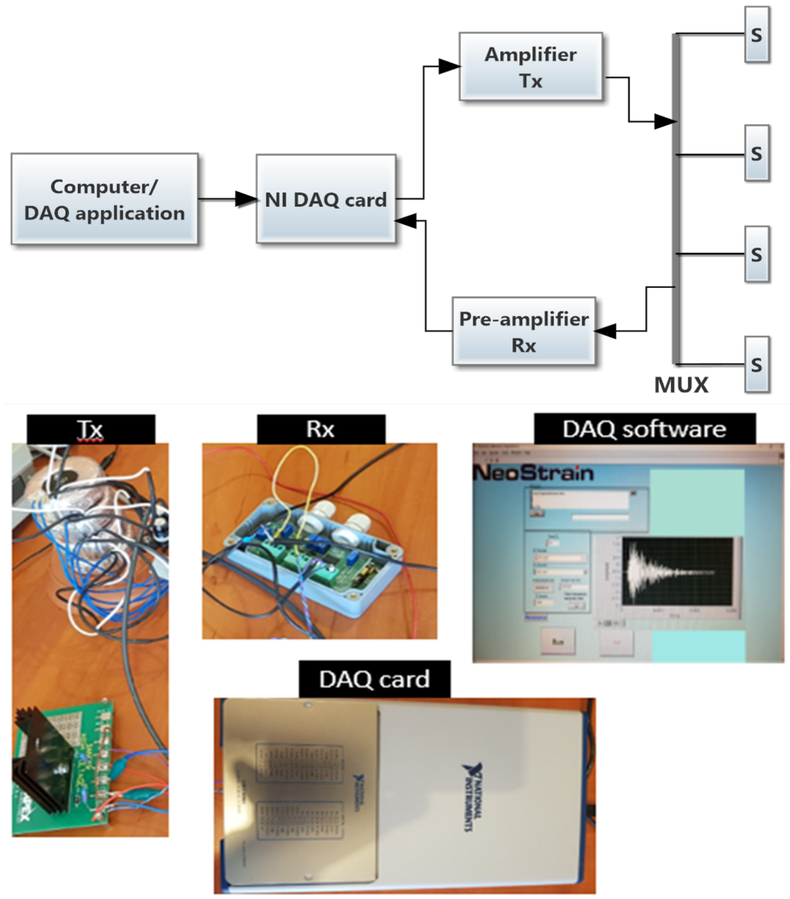

Figure 6.2: Data acquisition block diagram and components of the ultrasonic system

As 'SO807' can work as a transmitter and receiver at the same time, it can measure n couples of sensors ((n+1): number of sensors). The multiplexer can be connected to a local computer via an Ethernet cable and a DAQ which is connected to the local computer via a USB cable (for automatic switching between sensors). The measurement system (Figure 6.2) consists of a PC (application), a digital to analog converter (National Instruments® 6361 DAQ) with a resolution of 16 bits and an amplifier and pre-amplifier, to which ultrasonic sensors, can be connected via multiplexer. There is the 1st power amplifier (Tx), which amplifies the sine wave for the transmitter from $5V$ to $150V$ Figure 6.4. The pre-amplifier (Rx) is to receive the analog signal if the amplitude is too low (Figure 6.3).

For ultrasonic transmission, a signal (62 kHz) was generated from a National Instruments® 6361 DAQ card. A power amplifier ($+/-80V$) was designed to amplify the signal as shown in Figure 6.4. The two stage low noise pre-amplifier module connected with the sensor was designed to receive the signal properly as indicated in Figure 6.3. As presented in Figure 6.4, the power amplifier and pre-amplifier (Figure 6.3) was designed using an amplifier IC (Capineri *et al.*, 2018). The author designed the amplifier circuit using high

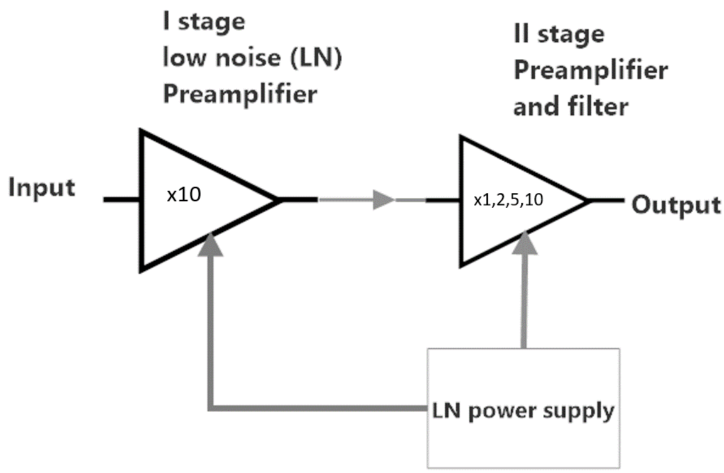

Figure 6.3: Schematic of the two stage low noise pre-amplifier

voltage power operational APEX® amplifiers. This low quiescent current MOSFET operational amplifier circuit with asymmetrical voltage supply is shown in Figure 6.4. The circuit can operate from supplies ranging over +/- 150 V. The current configuration has an amplification of about 19 dB in a band between 1 Hz and 100 kHz. A printed circuit board with an amplifier was designed for this purpose.

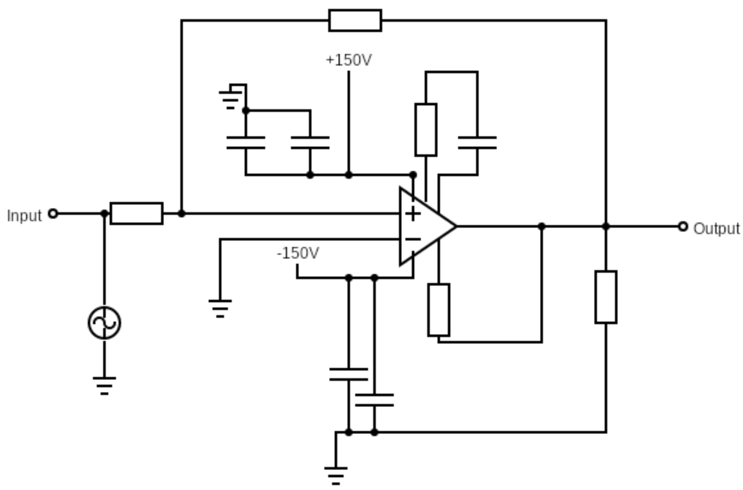

Figure 6.4: Ultrasonic transmission amplifier schematic

The author developed a LabVIEW® interface program (name 'NeoStrain@US') to control the set-up and drive the cards. 'NeoStrain@US' is an new application written in LabVIEW to acquire the ultrasonic signal, see Figure 6.5. This application can be installed on any computer with Microsoft Windows operating system. However, the configuration can be modified to measure the selected sensors or change the measurement parameters, such as time interval, sampling rate, etc. The information such as waveform, current sensors being measured during the test shown on the software interface. With this system it is possible to work in pulse-echo and transmission mode. All the parameters can be defined independently for each active channels. The main menu of NeoStrain@US application is presented in Figure 6.5. The ultrasonic signal can be generated through analog output (AO) channel of DAQ system, while such parameters as frequency, transmitting voltage and number of cycles can be introduced. In the receiving mode, several parameters can be also selected for analog input (AI), for example, filters range, number of channels, number of samples etc. The signals were digitalized using the Nyquist criteria, there was an option of selecting the number of samples, the sampling frequency, etc. The acquired signals can be stored and read by the majority of commercial software for post-processing purposes. The ultrasonic signals can be presented in time and frequency domains.

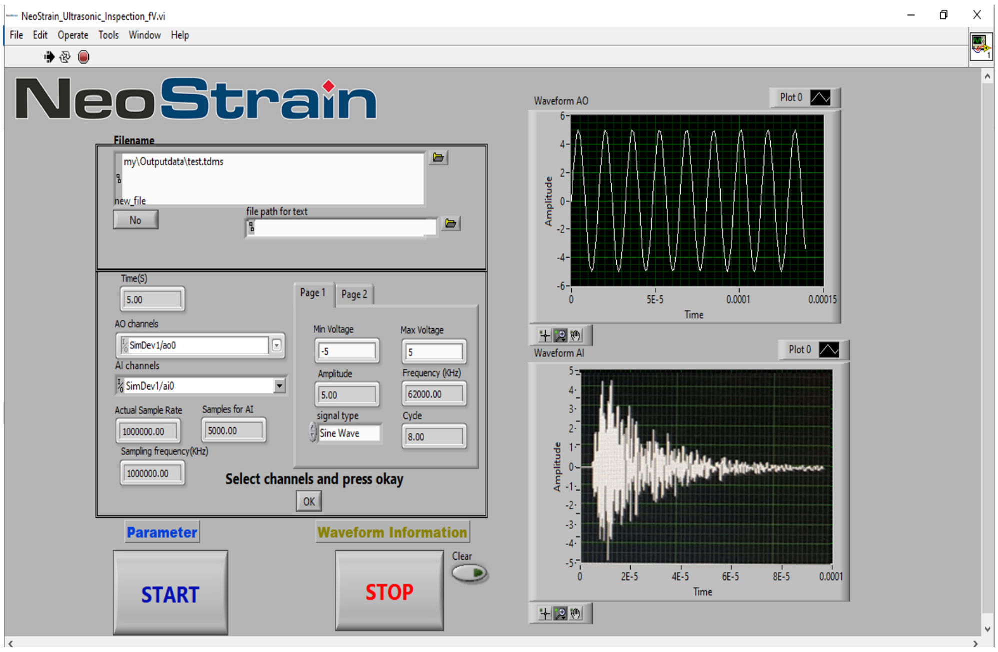

Figure 6.5: Main menu of LabVIEW application for ultrasonic inspection

6.2.3 Test procedure

The test duration was 45 minutes. The new data acquisition system was used for successive pulse trans-mission to sensor 1 (Tx), while other waves passing through the structure were registered by the ultrasonic sensor 2 (Rx) receiver and stored in the computer hard drive. The static test was performed to locate changes in the structure. For the purpose of the static test, a load of 1 kN was applied in the middle of the beam at 19 minutes to 24 minutes to classify the load from environmental changes in the beam. Figure 6.6 shows the overview of an ultrasonic propagation system configuration on a meter size concrete beam. There are four main parts: the DAQ system, power amplifier, pre-amplifier, embedded sensors, and the application system. The embedded sensors, installed within the concrete structure, are incorporated with the power amplifier and pre-amplifier to allow the ultrasonic propagation system to inspect large area of the structure. In addition, the ultrasonic inspection system is controlled by the computer to perform the wave propagation process on the desired inspection area (Song *et al.*, 6-9). In the ultrasonic sensor (Tx), the corresponding ultrasonic wave is generated and recorded by ultrasonic receiver (Rx), then digitized in the DAQ board and stored at the local SHM system via the USB communication (Chong *et al.*, 2014). The 5 ms signal duration corresponds to about 20 m of travel in case of this mode. This signal acquisition process will stop when the predefined period is reached. Lastly, the two-dimensional spatial ultrasonic signals are further processed (post-processed) for damage/change evaluation purpose.

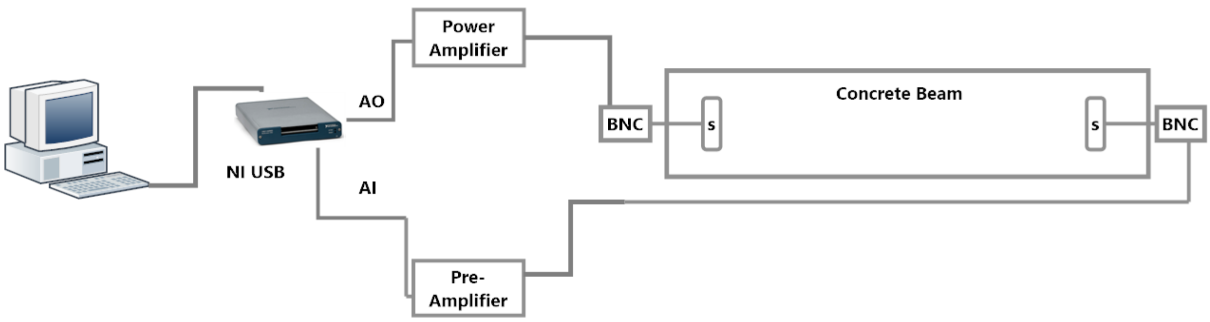

Figure 6.6: Overview of the ultrasonic propagation system configuration

6.2.4 Detection

In order to illustrate the detection of changes in the meter size beam structure, a feature is computed from the time-domain signals collected from this beam by one pair of ultrasonic sensors during the experiment.

A simple but valuable tool to measure the changes, is calculating the autoregressive (AR) model coefficient between a predicted signal from the initial measurement and all consecutive measurement under different operational effects (Chakraborty and Katunin, 2019a).

Acquiring good quality and compatible data is very important for long term monitoring. It is the first parameter the author wants to single out, therefore, the optimal setting for acquiring a good quality signal for this application was investigated first. Selecting optimal settings for specific signal seems hypothetical, so it is better to understand what requirements the acquired signal needs some in order to acquire it efficiently. As it is well known, the resolution, especially the sampling rate, has an effect on an acquired signal when digitalized. If the sampling rate is too low, then acquired signal can be distorted and information (feature) will be lost. Nevertheless, if it (the sampling rate) is high, then signal may contain high level of noise. In addition, higher sampling rate increases data size and, in consequence, significant storage resource is required, more power and processing time. The optimal setting for acquisition equipment is, therefore, important for data management. To validate this approach, the signal was recorded from a pair of ultrasonic sensor with 14 bits of precision at a 2 MHz and 1 MHz sampling frequency.

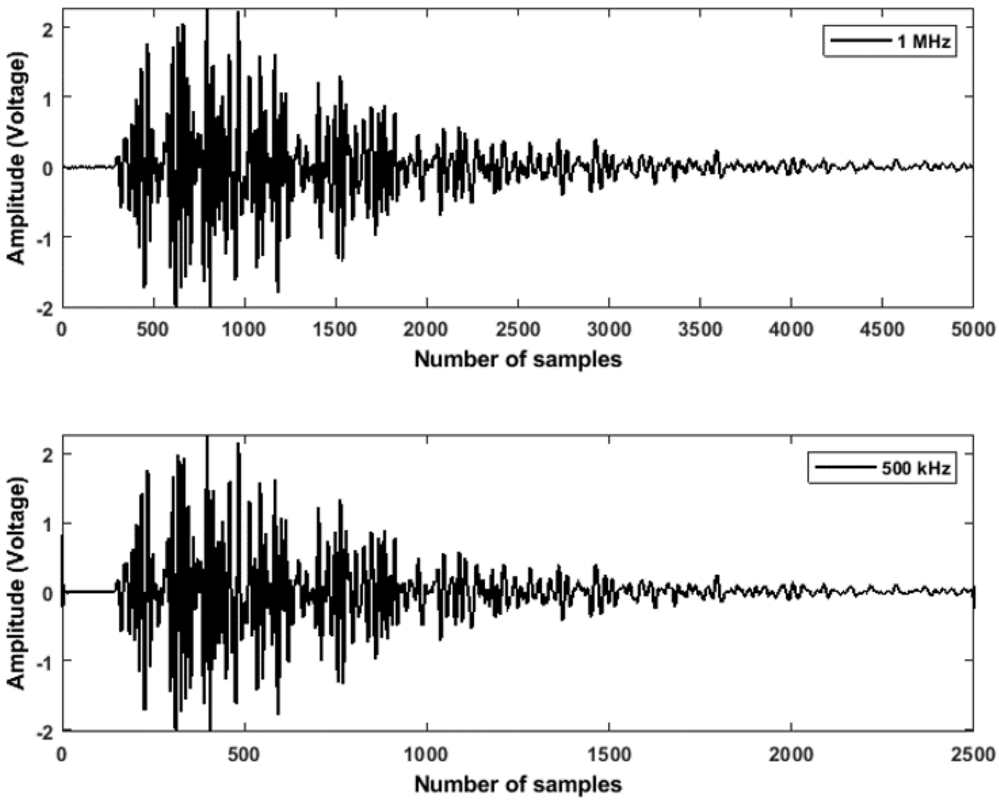

Figure 6.7: Signal at given sampling frequency

In post processing, the sample rate was reduced (see Figure 6.7) and the effect on AR coefficient result (Figures 6.8 (A),(B),(C)) was investigated for given sensor pair. The AR coefficient increase up to a maximum value when the static load is applied in middle of the beam (t = 21 minutes). The AR coefficient can separate the load from the environmental effect, see Figure 6.8. During the load test, the value of the maximum changes corresponded to the coefficient, which is relatively small since the applied load was negligible compared to the strength of the beam. Moreover, it was found that, the signal sample rate of 1 MHz was suitable for this SHM application but in certain situations one can the sampling frequency can be tuned so that it approaches the Nyquist frequency, provided that enough frequency components remain present in the sampled signal. When the sampling frequency is too low,however, the classification fails, as is the case for a sample frequency of 300 kHz. When sampling frequency is close (and under) the Nyquist frequency, the resolution seems to be of influence (500 kHz), see Figure 6.8 (C).

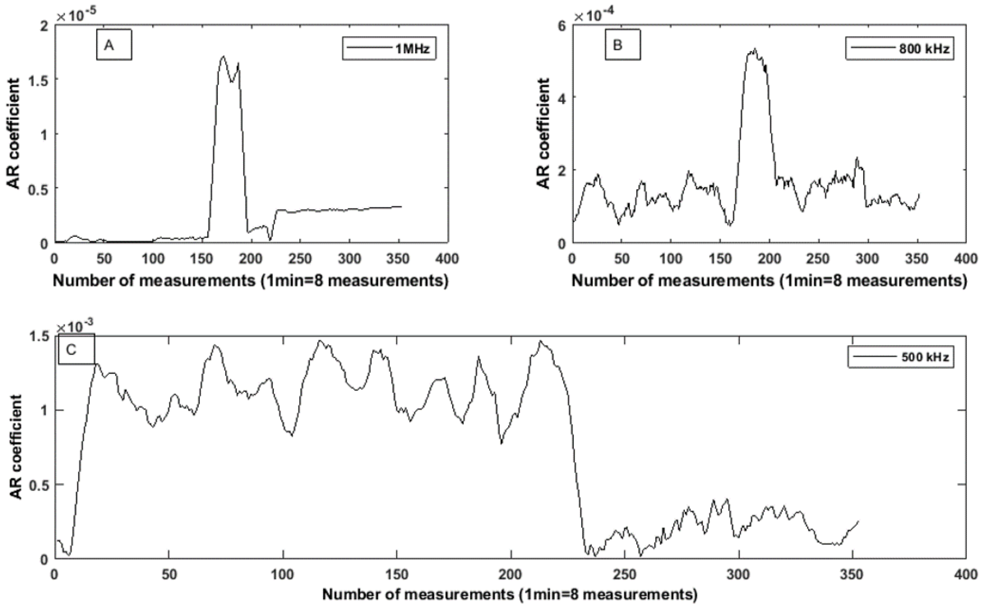

Figure 6.8: Feature based change detection for a given sample frequency

6.3 Destructive laboratory test

6.3.1 Test specimen

The reinforced concrete (RC) beam was cast as a specimen for the following induced cracks propagation. Figure 6.9 shows the test specimen, i.e. the RC beam that has the following dimensions: 2.9×0.4×0.2 m (length×height×width). The primary reinforcement of the 10 mm diameter consists of three lower bars in the tensile zone and two bars in the corners of the compression zone. Transverse reinforcement consists of two-legged stirrups with a diameter of 6 mm arranged in the support zone at a spacing of 150 mm. The beam was made of C25/30class concrete with compressive strength F_{cd} = 27.57 MPa. The capacity of the beam was calculated according to Eurocode 2 (Eurocode, 2005). The calculation results were used to determine the beam maximum breaking force.

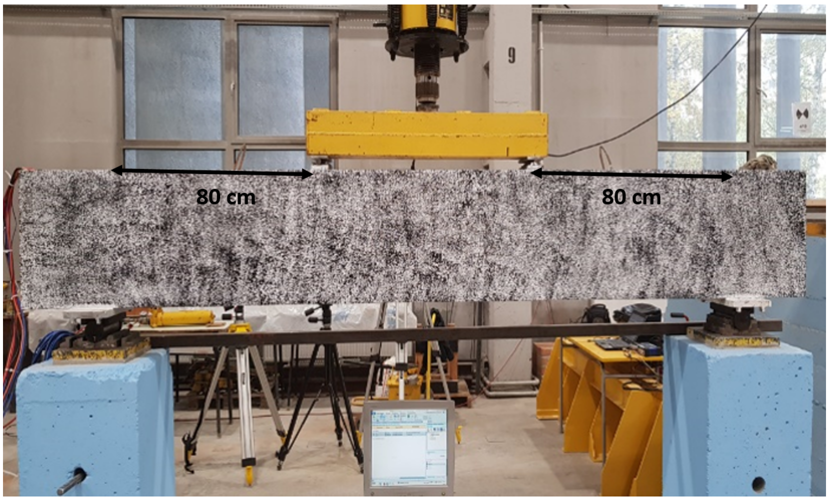

Figure 6.9: Measuring stand and beam load position

The reinforcement skeleton together with attached sensors was placed inside the formwork while maintaining the appropriate buffer cover. During laying, the concrete was properly compacted using vibrators (Figure. 6.10).

Figure 6.10: Vibration during pouring the concrete and collecting of specimens

To evaluate the actual class of concrete and its mechanical properties, during the concreting, 12 additional specimens were manufactured in the form of cylinders with a diameter of 150 mm and a height of 300 mm following Eurocode (Eurocode, 2005). Both the beam and specimens were seasoned in similar conditions for 28 days. During the period of concrete hardening and seasoning, the measurements began. The recorded signal from the internal sensors was sampled at interval of 5 minutes. In this way, the influence of concrete bonding temperature and rheological phenomena, such as shrinkage and creep of concrete, was assessed. Specimens were destroyed after 7, 14 and 28 days, which allowed to evaluate the increase in strength over time and determine the actual class of concrete with its compressive strength and modulus of elasticity. During compression and destruction of the concrete specimens after the mentioned duration of the casting works, the $\sigma - \varepsilon$ curve and the elastic modulus were determined. The exemplary view of the $\sigma - \varepsilon$ curve and the resulting destroyed specimen are presented in Figure 6.11.

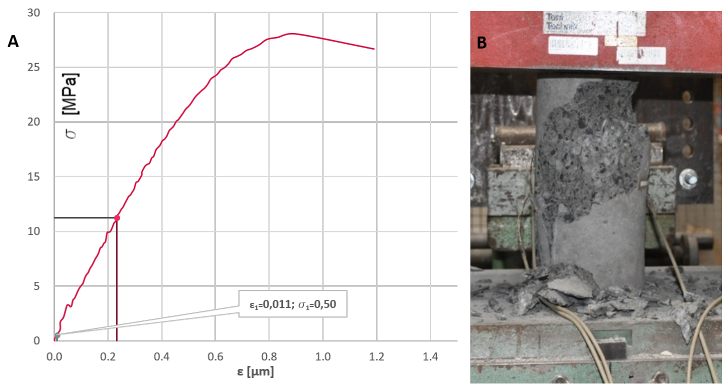

Figure 6.11: The σ - ϵ curve (A), and the view of the destroyed specimen after compression testing (B)

6.3.2 Experimental setup

During the preparation of the benchmark RC beam, the sensors were concreted. The location of concreted sensors together with reinforcement is shown in Figure 6.12. Four ultrasonic sensors (red box) were attached on four vertical stirrups. The position of ultrasonic sensors are shown in Figure 6.13.

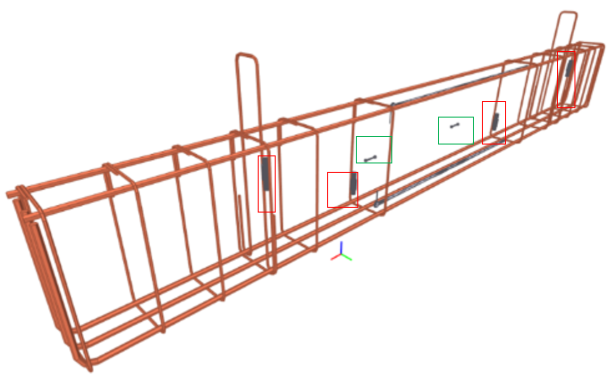

Figure 6.12: 3D view of the beam reinforcement with sensors location

The beam was also equipped with two vibrating wire strain gauge Ace Instrument® - model 1220 (green box) sensors, and two rebar stress Ace Instrument® - model 1260

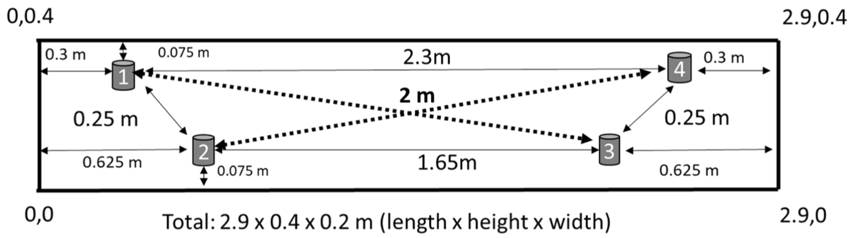

Figure 6.13: Ultrasonic sensor position

(attached to the top and bottom of the rebar) meters were embedded inside the concrete (Figure 6.12). External linear variable differential transducer (LVDT) displacement sensor PLETRON® - model PSX 100 and two strain gauges were used to monitor deflection. DIC device was used to measure deflections, crack propagation and width.

6.3.3 Data acquisition system and loading schedule

After placing the beam on the measuring stand, the acquisition system and power supply were connected for initial readings. In the middle of the beam specimen, an external LVDT sensor was installed to measure the deflection, and strain gauges were glued to the upper and lower surfaces of the beam. The front wall of the beam was painted with markers that allowed measuring the deformation using the DIC method. In the middle, the hydraulic jack and a load cell ZR DIORA® - model 25 set to transfer two-point force (see Figure 6.9) were mounted. Then, the whole system was tested, and the control data recording was performed.

The loading machine is controlled by an analog controller. Since the main goal of the test was to evaluate cracks evolution and damage level with the increasing load using ultrasonic techniques, it was decided to measure also the force. The loading rate was fixed at the beginning at 1 kN/min till 108 kN and then was increased to 5kN/min (Figure 6.14), which introduced appropriate stress/strain state in the tested specimen.

In order to visualize the strain distribution, the preliminary numerical FE calculations were performed basing on the material properties resulted from the quasi-static compression tests. For the purpose of examination of strain distribution the static non-linear analysis was defined in Midas FEA, and the Newton-Raphson iteration procedure was used for FE calculations (Chakraborty *et al.*, 2019). The resulting strain distribution of the tested structure is presented in Figure 6.15. The force and the LVDT outputs were recorded on a computer using National Instruments® DAQ card data logger system, respectively HBM® - model QuantumX MX1615B card for the displacement and GOM Correlate for the DIC measurement.

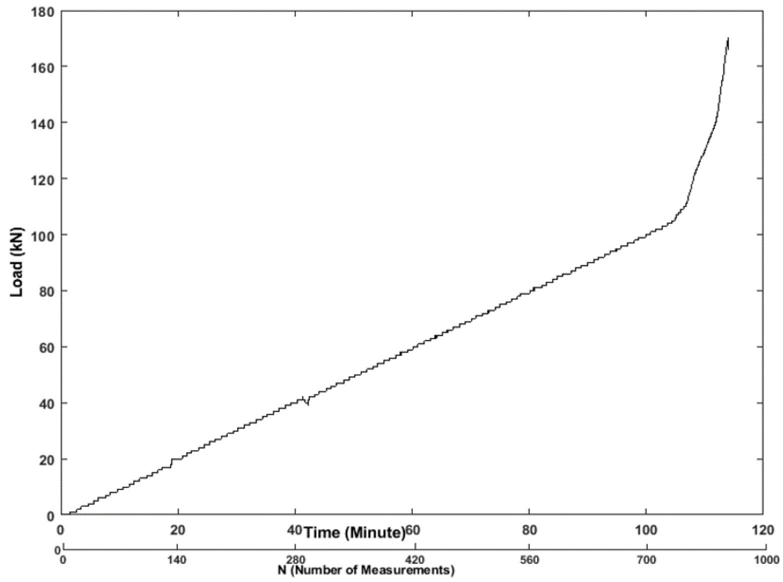

Figure 6.14: Loading schedule vs number of ultrasonic measurements

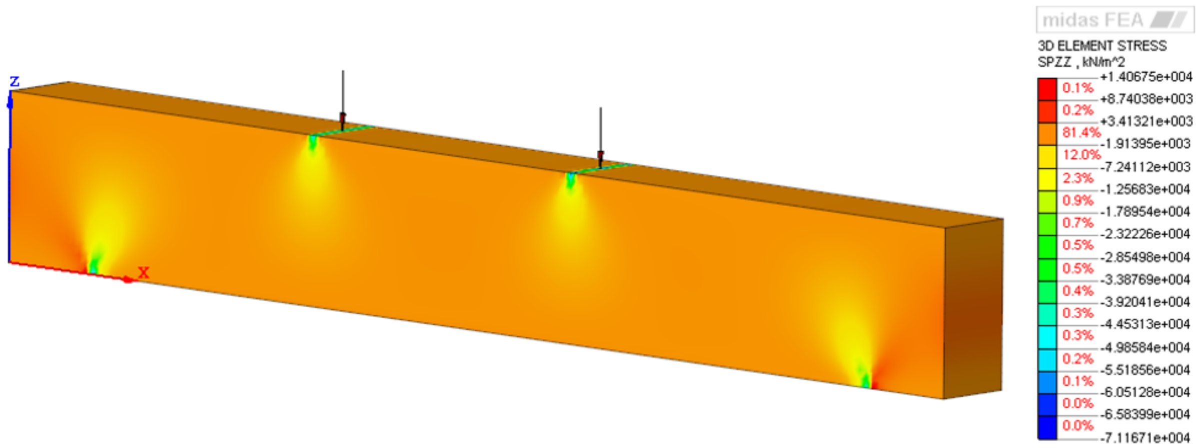

Figure 6.15: The strain distribution (Midas)

The data was collected by connecting the computer directly to the Campbell® data logger for embedded traditional sensors and customized data acquisition system for ultrasonic sensors (see section 6.2). The data logger had 8 channels (see Figure 6.16).

Data acquisition from vibrating wire strain gauges was made automatically in every 200 ms and stored in the computer hard disk drive. Regarding ultrasonic measurements, the data acquisition system contains multi-channel data acquisition module which was connected with the amplifier and the pre-amplifier to amplify the input, and output then the signals were filtered (see Figure 6.2). In the laptop, custom software was installed to configure and control the measurement system and store the signals (see details in section 6.2.2). The acquisition of the ultrasonic signal was made seven times a minute and stored in the laptop. The center frequency of the measured ultrasonic signal was around 60 kHz,

Figure 6.16: Campbell Scientific data logger

as regards proper resolutions for acquired signals, a sampling frequency of 1 MHz was used. The recorded duration was 5 ms for each measurements, allowing many reflections to occur and resulting in a like diffuse wave. The basic signal processing (band pass filter and data normalization) was used to remove noise and DC offset from the acquired signals.

Recently, DIC has been developed as a stable and reliable tool for fracture or damage measurements. DIC detects the smallest deformations caused by stress on the surface of the examined object. This pattern was used firstly as a reference. Later, after the application of loading, it was used as a pattern for comparison of similarities and determination of crack locations. The surface deformation of the benchmark RC beam was reflected by the shifts between pixels within these areas. To analyse this shifting different correlation algorithms can be used. This technique can measure deformations in the range of micrometers depending on the camera used, and its distance to the surface of the beam. In the performed experiments an ARAMIS® SRX DIC camera with a resolution of 4096×3068 pixels and GOM correlate system was used. The frame rate during testing was of 0.25 Hz.

The basic idea of evaluating the bending stiffness of the RC beam under increasing in time vertical load is a deflection measurement used as a performance indicator (PI). The typical changes of beam bending stiffness during loading (see Figure 6.17a) are illustrated in Figure 6.17. The degradation phase can be divided into four stages: (I) Un-cracked, (II) Cracks forming, (III) Stabilized cracks and, finally, (IV) Failure stage. Failure is typically yielding of steel reinforcement or crushing of concrete (see Figure 6.17b). During the test, the load was slowly and proportionally increased over time using a hydraulic jack compression machine. Simultaneously with the measurement of the load force, the responses from all sensors and measuring devices were registered.

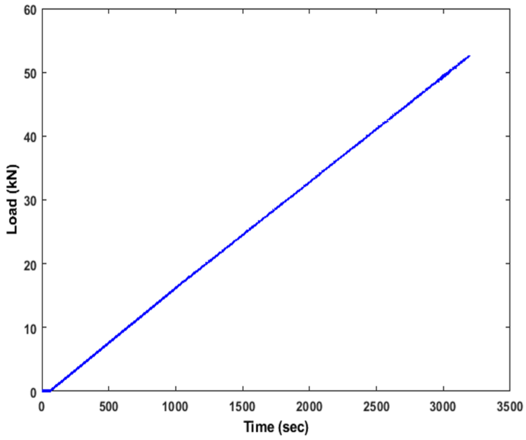

(a) General scheme of loading vs time

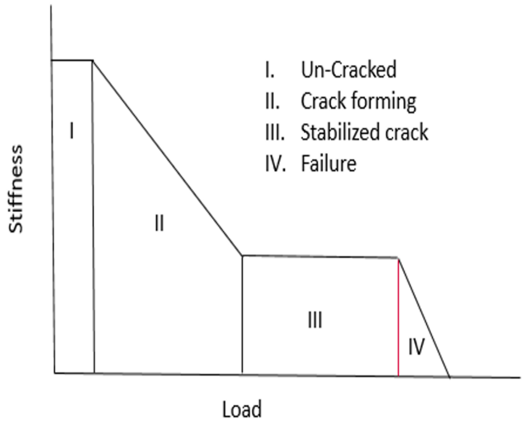

(b) Bending stiffness where four phases are shown

Figure 6.17: Generalized bending stiffness development where four phases are shown

The first step was to compute the features (see chapter 5) based on data acquires from ultrasonic sensor pairs. In step 2, the features were compared with other types of installed sensors in terms of propagation of cracks.

6.3.4 Test results and discussion

To represent the effectiveness of the features mentioned in chapter 5.1, all the features were computed from the time-domain signals collected from three pairs of ultrasonic sensors on the benchmark RC structure during the experiment depicted in Figure 6.9. It is important to mention, those raw signals were preprocessed (cross-talk was removed, basic digital filtering was performed, signal normalization and general baseline subtraction to minimize the temperature effect). In this study, one pair of ultrasonic sensors was analysed to investigate the cracks regardless of the location of the structure. The ultrasonic sensors pair located at the top was chosen to investigate the maximum area of the benchmark structure (distance of 2.3 m). The interpretation of all the features explicitly incorporated a comparison to a reference signal, and if a certain amount of changes in amplitude was not present, the phase and frequency of the signal were compared to the reference signal, and the condition of the structure was stated as being in good health (considering all the effects details in chapter 4 section 4.2).

Figure 6.18 shows the exemplary plot for the features of the time-domain signal, i.e., peak to peak amplitude. The normalized error graphs were derived as a difference between the peak amplitude in each fixed-length time window (when the beam was subjected to external stress) and the reference of the undamaged state. Higher deviations were caused

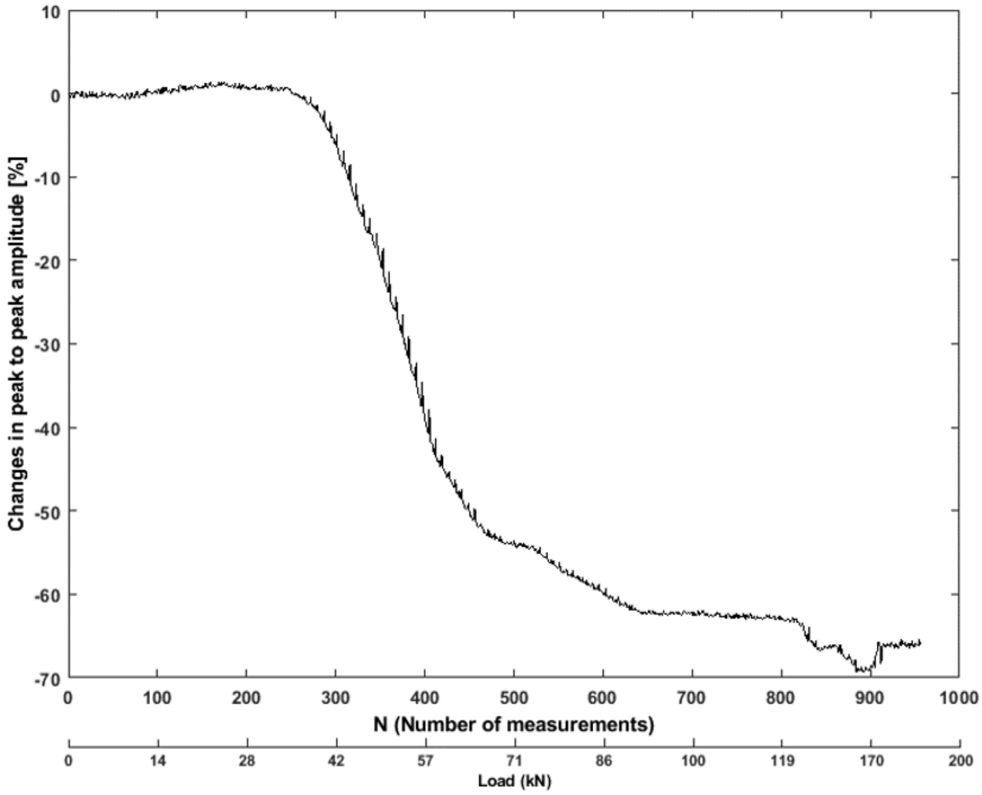

Figure 6.18: Values of Peak to peak amplitude feature from ultrasonic pair S01R04 time histories

whenever the amplitude of time signals dropped with the external load increases and the progressive stage of damage (cracking). From Figure 6.18, it can be observed that the peak to peak amplitude changes as the stress level varies due to tension region (bottom) and compression region of the beam (top). The changes in the peak to peak amplitude stay within the range of 0–1.9 %, when 0-35 kN (N = 242 ultrasonic measurements, which is equal to 35 kN) load is applied. When the applied stress increases, there is an obvious drop in peak amplitude, as the signal begins to attenuate with less energy and amplitude decrease, which indicates the crack opening. The changes had an increasing trend when 35-90 kN load was applied, due to forming multiple cracks opening and propagation along the beam. However, when the load between 90-160 kN was applied, the changes remained stable at the brittle-ductile transition stage. Although the beam deformation was indeed large, there were not enough new cracks in the specimen to obstruct the ultrasonic wave propagation. The reason for this stable propagation was that the reinforcement of the tested specimen carried the highest stress under such loading conditions.

The decorrelation coefficient was obtained in the normalized form, and it can be defined as the changes in the RC benchmark structure. The initial increase of this coefficient is originated from the bending of the benchmark specimen under increasing load, because it effects on the ultrasonic wave path. With the bending tensile force was 42 kN, the coefficient (see Figure 6.19, values increased by 0.27, compared to the reference state (before the start of the experiment), and sudden drop to 0.23 took place, which is indicative of the development of micro-cracks in the structure. When the applied stress became more significant. When the applied stress gets more significant (as a result from a bending

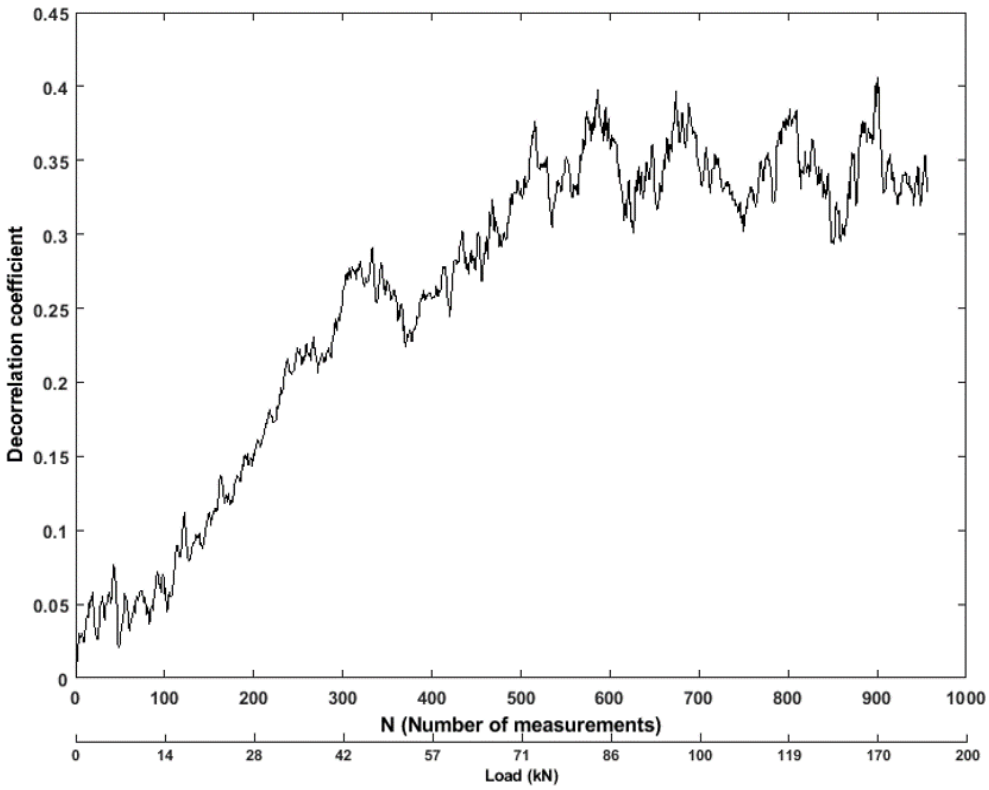

Figure 6.19: Values of decorrelation coefficient feature from ultrasonic pair S01R04 time histories.

tensile force between 42 kN to 160 kN), and the phases of the signals shifted by more than 90°, which was caused by the propagation of the crack, whereby the decorrelation coefficient increased to 0.4. The decorrelation coefficient provides an appropriate value to make judgements about the rate of changes in measured signal comparing to the reference signal through the correlation analysis detect a particular relationship between the two signals. It is evident that the signal analysis based on the decorrelation coefficient is more sensitive. Due to its sensitivity for small changes, D_{cc} can give misleading information about the signals changes due to environmental effect.

Figure 6.20 indicates that increment of the level of nonlinearities (cracking) in the beam subjected to external stress, and simultaneously, the amplitude of the AR parameters (increasing the residual error) tends to decrease. The AR parameters were evaluated by

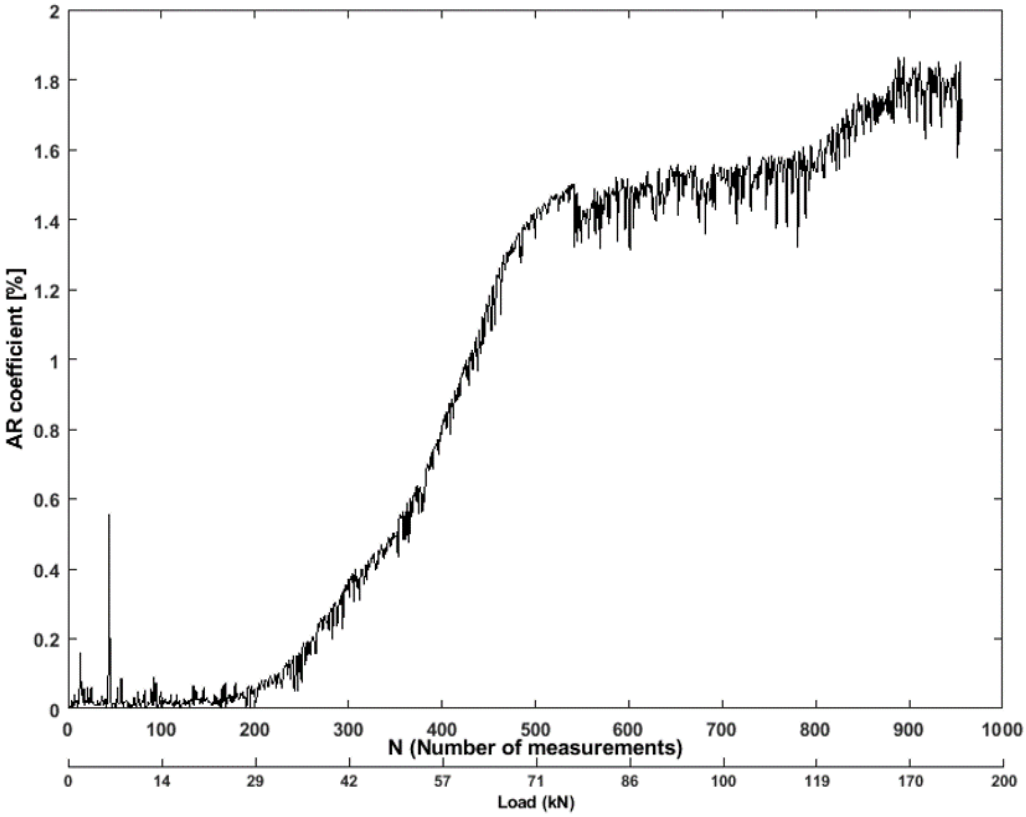

Figure 6.20: Values of AR residual error feature from ultrasonic pair S01R04 time histories

fitting the AR model (for more details see section 5.1.4) to a baseline signal from one sensor pair (top) before the start of the experiment using the RMSE technique (see (Chakraborty and Katunin, 2019a) for more details). If cracks are present in the structure, the residual errors may increase due to higher attenuation (decreasing the AR parameters amplitude), which is caused by the increased crack width under loading. It can be seen in Figure 6.20, that the residual error increases as the stress level increases in the beam. As a result of applying the bending tensile force between 36 kN to 160 kN, the rate of AR residual error increases up to 1.9 % due to energy attenuation, which indicates the opening and propagation of cracks.

The STFT, conventional as a spectrogram, corresponds to the energy distribution of a raw signal. It can define the amount of energy contained in the diffuse signal as a damage-sensitive feature. The initial increase of this coefficient is originated by the bending of the benchmark specimen under increasing load, related to the amount of energy released by the specimen. With a bending tensile force of 38 kN, the coefficient (Figure 6.21) increased by 0.14, compared to the reference undamaged state, and sudden drop to 0.002 took place, which indicated that the signal strength decreased due to development of microcracks in the structure. It could be observed that after the load of 115 kN was applied, the strength

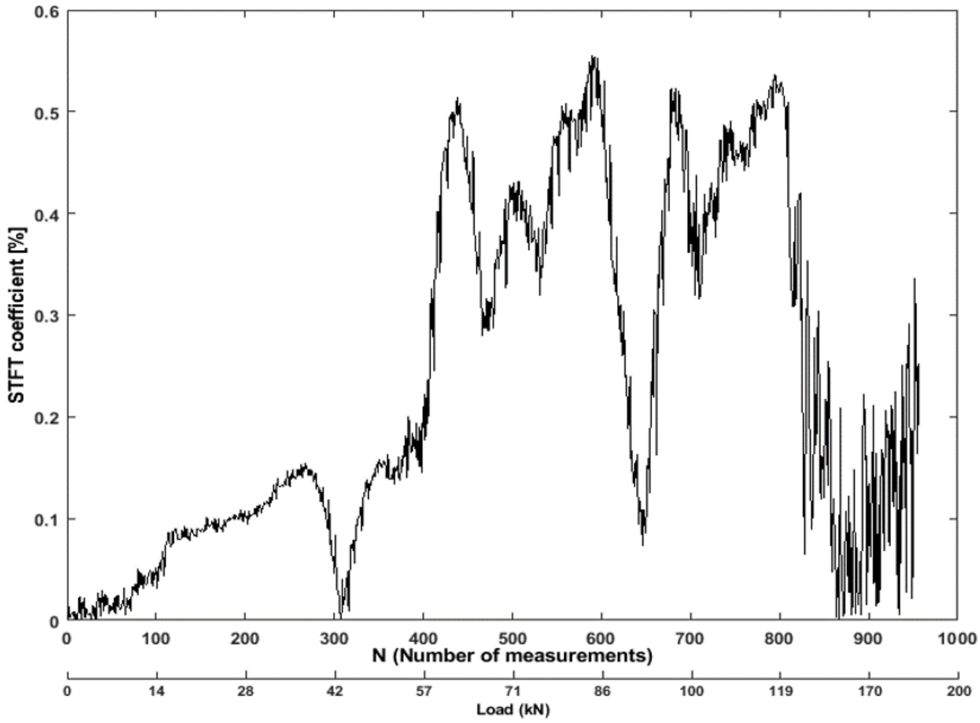

Figure 6.21: Values of STFT coefficient feature from ultrasonic pair S01R04 time histories

of the signal gradually decreased as multiple cracks started to propagate through the surface, until the last phase of the loading.

The plot for Continuous wavelet transform (CWT) is depicted in Figure 6.22. The energy of a signal is derived from the CWT from the raw signal time-series. The extracted feature from this time-frequency domain analysis is more useful than time domain only.

The energy vector is established by computing the energy of each branch (scalogram) to show the energy distribution towards the frequency bands. From the comparison of CWT coefficients between the changed/damaged state and reference undamaged state (as shown in Figure 6.22), a noticeable deviation can be found in different frequency bands. The proposed CWT energy coefficient is obtained by calculating the root-mean-square deviation in percentage between the energy vector of the health state and that of the damaged state. In Figure 6.22, it can be seen that the coefficient decreases as the bending tensile as the level increases between 36 kN to 48 kN in the beam, and then it dramatically increases as the load increases between 49 kN to 60 kN. This is because most of the cracks appear on the concrete surface parallel to the load application under compression. Ultrasonic wave propagation in such direction, therefore, may miss

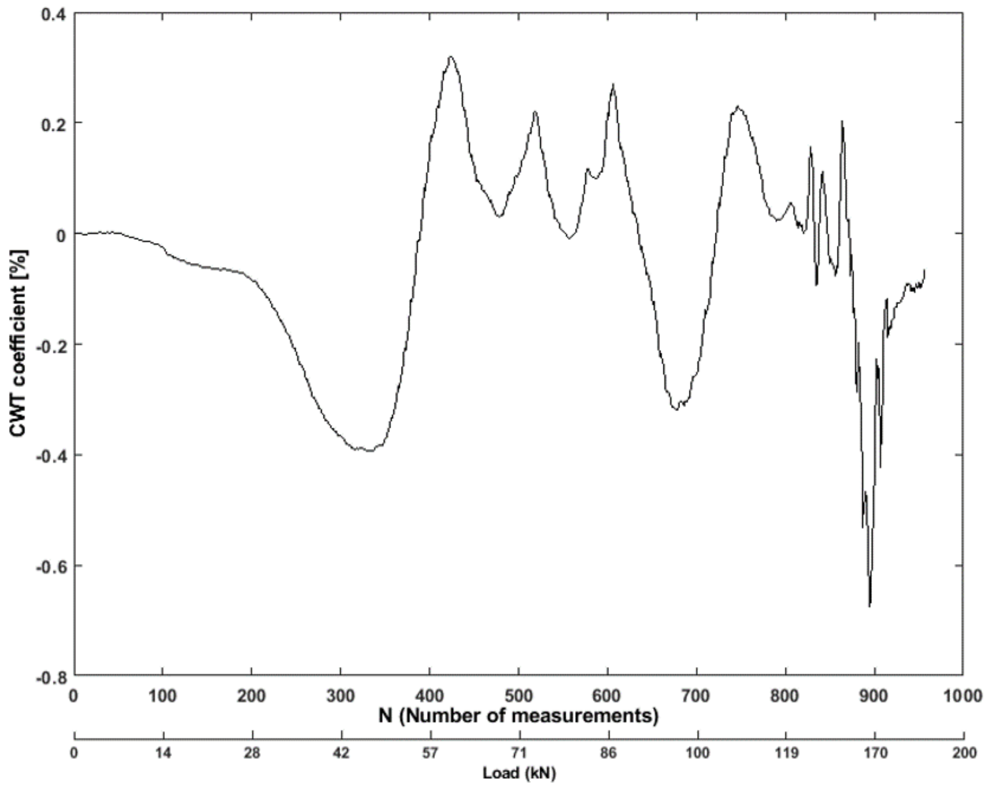

Figure 6.22: Values of CWT coefficient feature from ultrasonic pair S01R04 time histories

encountering cracks.There are no large values of the wavelet coefficients since the specimen has been destroyed by the horizontal splitting cracks that prevented the propagation of ultrasonic waves from sensor 1 to sensor 2 through concrete.

The crack opening displacement was measured by the vertical LVDT. A lack of symmetry in the loading or the shape of the beam can be observed. However, the variation of the crack width is proportional, meaning that one can suppose that the distribution of the crack opening displacement is linear all along the width of the beam. The measured load-displacement curve of the control beam is shown below in Figure 6.23, along with the load-displacement curve from DIC measurements which can be seen in Figure 6.26a. It can be seen that cracking occurred at approximately 42 kN.

The vibrating wire strain gauges embedded within the concrete structure (in the middle of the beam), register a steady increase in strain from 1 up to 1000 $\mu\varepsilon$, during loading (Figure 6.24). The increase is caused by the elastic bending of the beam. The growing strain in the bending tensile state from 43 $\mu\epsilon$ onwards, indicates an inelastic change as the surface cracks.

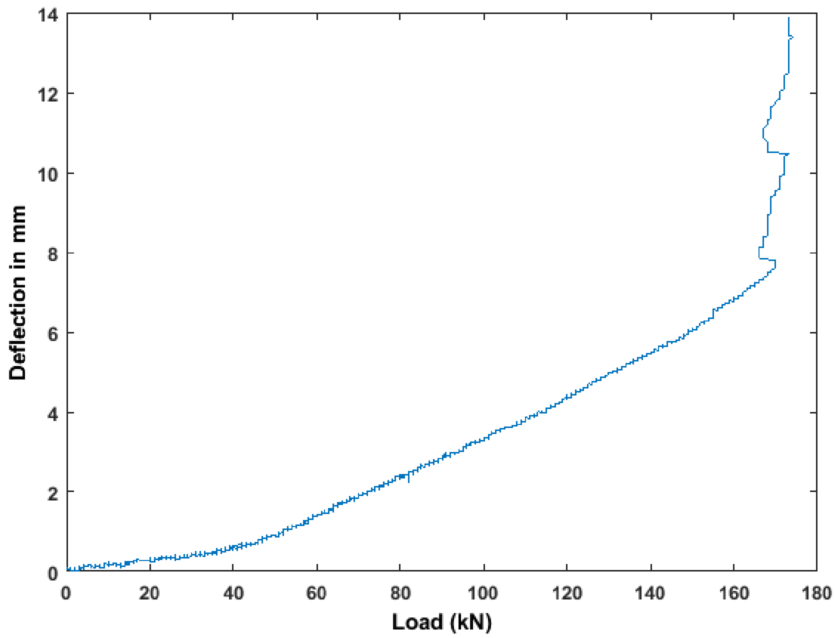

Figure 6.23: Deflection (LVDT) and load.

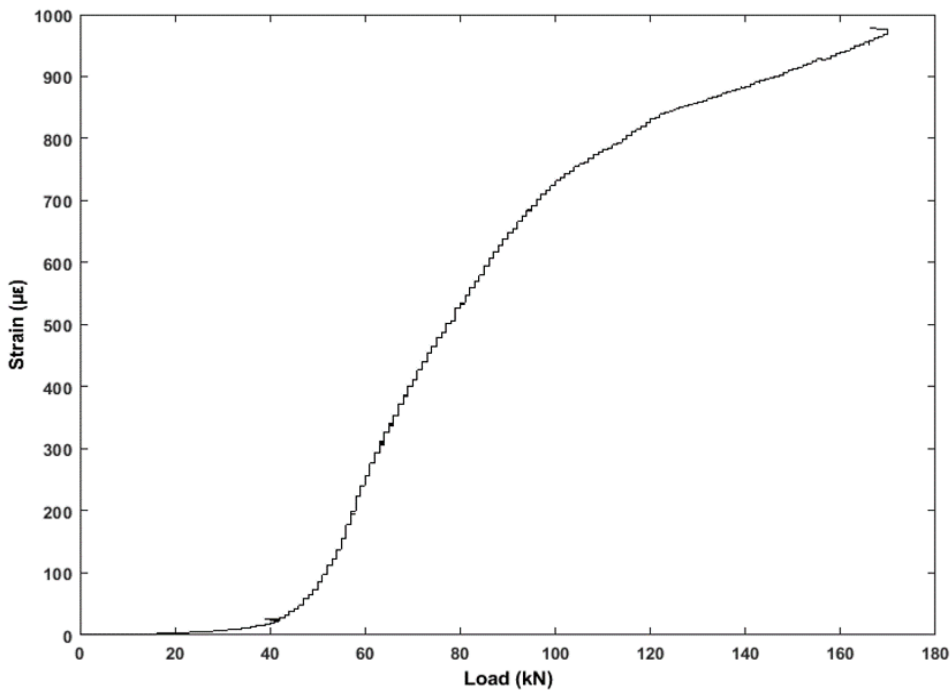

Figure 6.24: Strain (bottom vibrating wire) vs Load

Figure 6.25 indicates that, the rebar strain gauges embedded at the top rebar in the RC benchmark structure, register a steady increase in strain from 1 up to 272 $\mu\varepsilon$, during loading which is an indication of elastic changes.

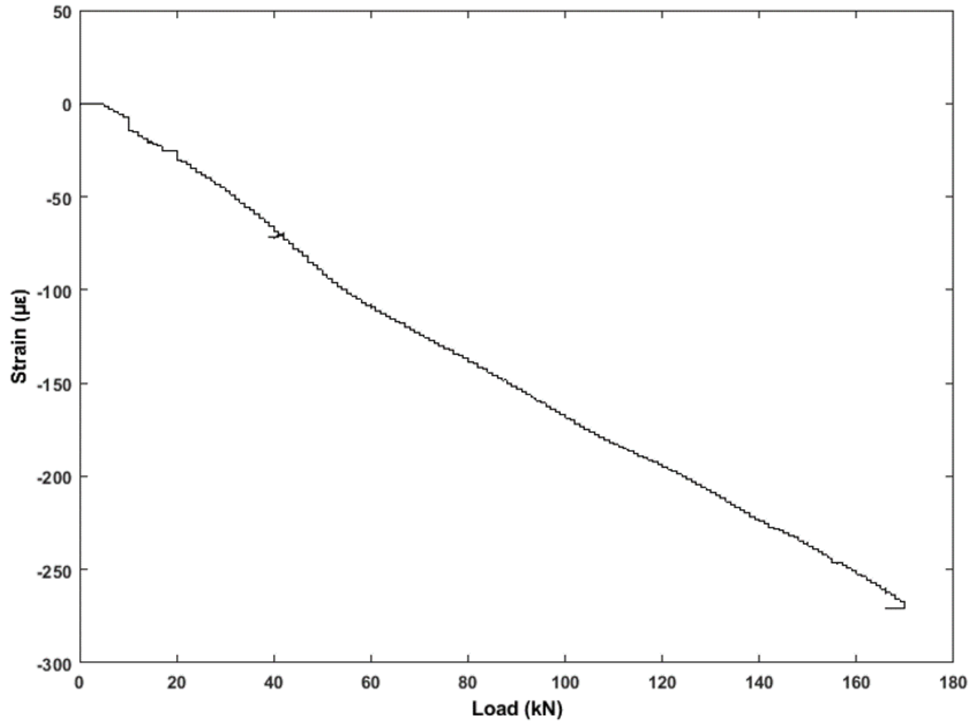

Figure 6.25: Strain (attached at the top rebar) vs Load

In order to investigate the ability of DIC to detect the degradation and characterization of the material, the data obtained from DIC frames were matched with corresponding force - deformation and beam depth - crack width profiles. The displacement of the benchmark RC beam at each load step was determined by locating each subset from the baseline image (pixel subset) in an image of the deformed test specimen through the use of the highest correlation to the reference subset. Figures 6.26a (A) and (B) show the state of cracks and strain fields at selected levels of load. These figures are essential for evaluation of the state of deformation and understanding the cracking behavior of the material, especially when specimen with different properties were compared. It can be observed in Figure 6.26a presenting the benchmark RC beam that the highest level of strain is observed at the first stages (0-50 kN) of loading, and distributed through the maximum moment region immediately after peak stress and strain localization became recognizable, represented by red colour. In the end, one small crack was observed at 40 kN. Then one major crack together with several other cracks (Figure 6.26a) was visible. The first signs of deformation were at bending tensile strength of 42 kN, which correlates with the results of embedded strain gauges and the displacement sensor. When the specimen surface was examined for cracks, these cracks were not visible by the naked eye. However, in DIC, the propagation of deformations upward in the direction of load entry was visible. At bending tensile strength of 52 kN, from this period, forming cracks became visible by naked eye. However, in the second stages (55-170 kN), DIC showed more cracks in the specimen, not visible by the naked eye (Figure 6.26b). At 80 kN, the cracks were started to be visible with the naked eye. Figure 6.26 shows the increasing propagation of the deformation in the direction of the load, which correlates well with all the sensors.

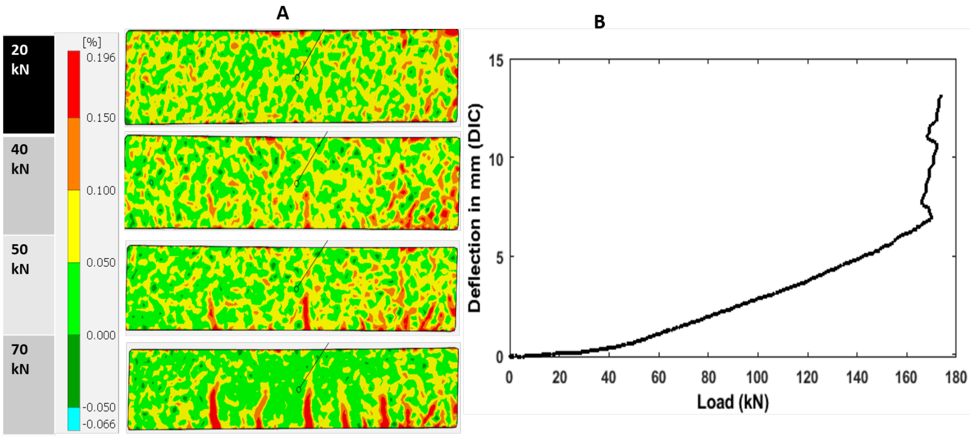

(a) 1st stages

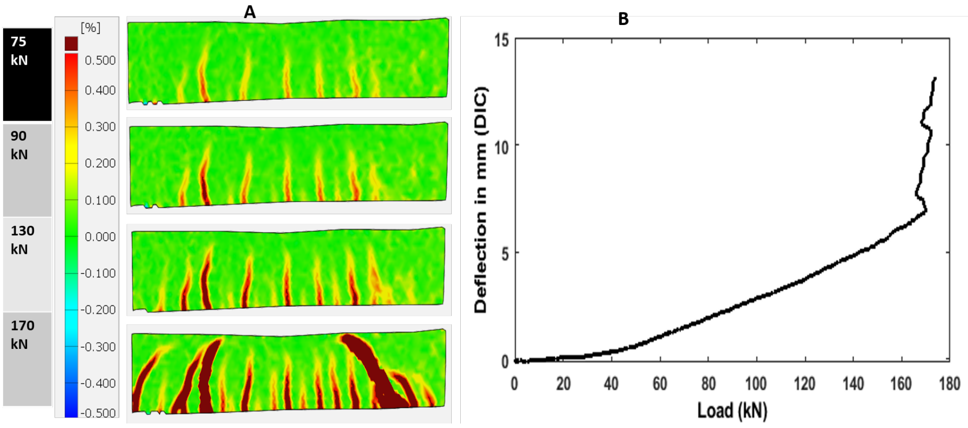

(b) 2nd stages

Figure 6.26: Crack images and strain fields for different load levels of specimen

6.3.5 Discussion

The ultrasonic sensors were located at the top and bottom and within the concrete element subjected to a tensile force. The post-processing of the signals in time and frequency domains as well as by the CWT was a base for early crack detection algorithm developed in this study. The characteristics of each stage are described below:

- At the beginning of the test, all the features of the test specimen were weak, displaying minimal changes (energy release). At this stage, the specimen was under a confining pressure and axial loading stress applied to the top (N=*240*). The specimen was experiencing elastic deformation.

- The sudden decrease of change/damage index of all the features could be observed before the appearance of the first vertical cracks observed by DIC.
- In the second stage, the rate of changes in all the features remained at a high level. Due to the rapid expansion of internal cracks in the concrete, the reinforced concrete displayed a large deformation. The changes in the ultrasonic features were extremely intensive. The rate of the structural changes reached its peak (energy was released from multiple cracks). This can be used as a parameter for final decision about structural condition.
- As it can be noticed after the post processing of the data, all the sensors detected the crack properly and with a very high sensitivity. This is because the cracks appear in the middle of the tested beam where most of the sensors were located.

6.4 Full scale experiment

6.4.1 Reference real structure

First-class infrastructure is an inevitable factor for economic growth. Bridges have a key position in this infrastructure system. Its functional failure or collapse has significant economic and financial consequences. For this reason, it is important to regularly monitor the current bridge condition, and derive estimates about the remaining service life. This ensures a safe and economically sensible use of existing structures. In view of the above, BAM developed a structure shown in Figure 6.27 called BLEIB structure (Shared object for INFRASTAR project) at Horstwalde (Berlin, Germany) to perform experimental studies of ultrasound inspection for the detection of operational changes or cracks in the real structure. The structure is 25 m long with three supports, and 5 cross sections (Figure 6.29). The load cell was installed on the front bridge side (fixed anchor) on the tendons during their initial installation and was supplemented by a spherical cap and steel plates. In the BLEIB structure, a control crack was developed to produce certain limited damage in one of the spans. Therefore, most of the cracks became visible between sensors no. 12–14, marked with a marker pen in Figure 6.28. After the test, when the structure was reloaded again, all cracks were closed.

Figure 6.27: BLEIB Structure at Horstwalde, Berlin

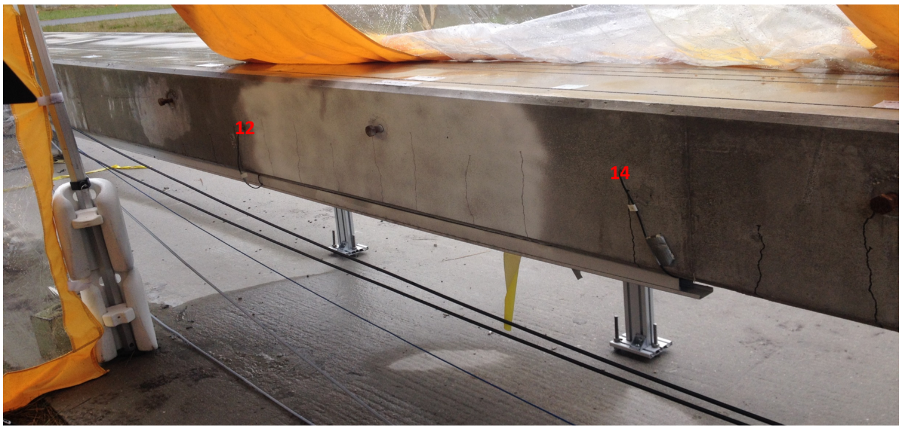

Figure 6.28: Location of the cracks (between S12S14) at the BLEIB structure

6.4.2 Experimental setup

Fourteen ultrasonic sensors were embedded in the structure during construction. They become vertically mounted on the stirrup reinforcement. They are controlled by an external BAM data acquisition system. The data acquisition system conducts a transmission pulse successively to each of the sensors, pass through the structure are registered by ultrasonic sensor receivers and stored in the local system, e.g. sensor pair 1 and 2, where sensor 1 sends the pulse and sensor 2 receives the response, respectively. The set-up is divided into sections as shown in Figure 6.29 and Table 6.1. Parameters are derived from the ultrasonic signals (e.g. Ultrasonic velocity changes), from which one can draw conclusions about the temporal change of the elastic parameters or (micro) cracking in the influence area of changes. Two kinds of test were performed to locate changes in the structure, static and dynamic tests equipment is shown in Figure 6.30.

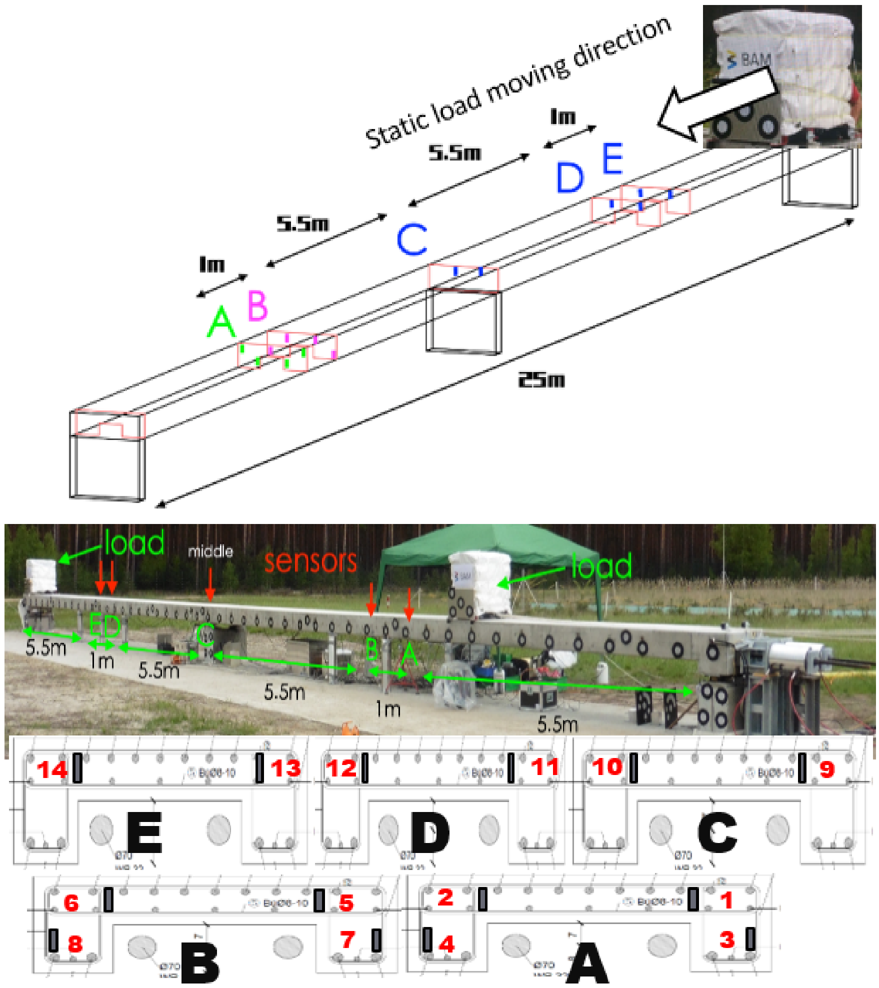

Figure 6.29: A scheme of sensor positioning at the BLIEB structure, and its view with main dimensions and loading

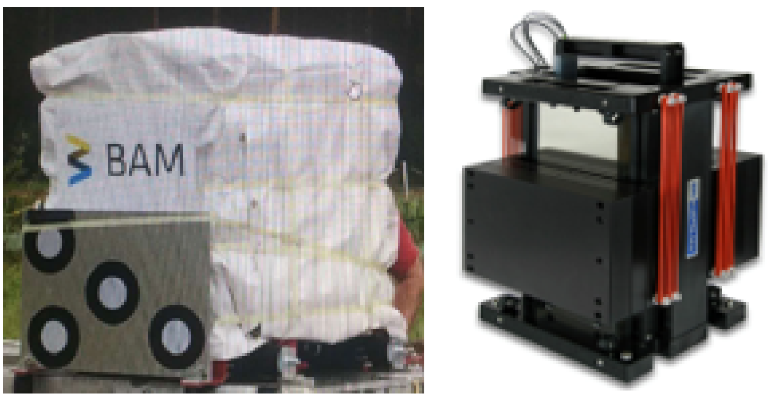

Figure 6.30: 4 tons load for the static test, and the shaker for the dynamic test

Tab. 6.1: Sensor positions

Section	Sensor Number
A	Sensor 1 , 2; Sensor 3 , 4
B	Sensor 5 , 6; Sensor 7 , 8
C	Sensor 9 , 10
D	Sensor 11 , 12
E	Sensor 13 , 14

Tab. 6.2: US measurement parameters

Parameter	Value
Signal Shape	Sine
Sampling frequency	1MHz
Center frequency	60 KHz
Signal duration	5 ms
Measurement Interval	1 min

6.4.3 Data acquisition

For this experiment new data acquisition from BAM was used. Fourteen embedded ultrasonic sensors were used for active monitoring, and controlled by the external BAM data acquisition system. This data acquisition system controlled active monitoring using transmission pulse, acquired signal, and duration of successive repetitive pulses sent to the selected sensors. The Keithley® 2700 multiplexer was connected to a PC with the Ethernet cable to switch the sensors combination and the 'Digital-Analog' converter which is connected to the PC with a USB cable to digitalized the signals. A simplified block diagram is shown in Figure 6.2. Dealing with a real structure, one should be careful to acquire a good quality and compatible signal, as it can influence the long-term monitoring detectability. Therefore, optimal sampling frequency is needed for acquiring good quality and compatible data (as describe in section 6.2.2). For this purpose, the National Instruments® 6361 data acquisition card was used to record signals from all 14 arrays with 14 bits of precision at 1 MHz sampling frequency. All the parameters are summarized in Table 6.2.

6.4.4 Methodology

In order to illustrate the detection of changes in the reference real structure due to quasi-static load states and dynamic load states in the presence of environmental effects, all the features discussed in chapter 5, were computed from the time-domain signals collected from the BLEIB structure by three pairs of ultrasonic sensors during the experiment depicted in Figure 6.27. The features were obtained from the decorrelation coefficient D_{cc}, the α_i coefficients of the AR model, the (CWT_{cc}) coefficients, peak-to-peak amplitudes coefficients, and the RMSE coefficient.

6.4.5 Test results and discussion

The interpretation of all the features explicitly incorporates comparison to a reference signal, and if there are no changes from the reference signal, the condition of the structure is stated as operationally unaffected. In order to illustrate the changes in the structure, two different kinds of tests were performed. In the dynamic test, shaker (0.3 kN) was placed near the S05E06 sensor position (see Figure 6.29) in the structure. It was used to apply random excitation between 2 Hz to 60 Hz for the first 15 minutes ($12:08 \le t \le 12:24$) of the structure measurement time period. Then, quasi-static load was applied from the right top side of the structure (Figure 6.29). During the static test, the quasi-static load of 39.85 kN was moved ($12:55 \le t \le 14:00$) in various steps (after each step there was one minute break before the next move was initiated) from the edge of the cross section E to the end of cross section A of the structure. The time and position of quasi-static loads are shown in Figure 6.31. To distinguish between the unchanged/no load and changed/load/crack states, the values of an effective feature should be separated according to these two states. The proposed features are compared within the three sensor pairs located on different cross-sections (A,C and E) illustrated in Figure 6.29.

It can be observed that all the features perform fairly well in their ability to separate the quasi-static and dynamic loads states in the presence of noises (see Figures 6.32-6.34). The applied loads, even within very small moves (e.g., after the shaker was removed and quasi-static load was placed on the edge of cross-section E ($t = 12:37$), had a clear influence on the ultrasonic signals. The influence of dynamic load was much smaller (varying between 0.05 to 0.17), compared to the quasi-static load. Obviously, all the features could be used to detect the dynamic influence in the structure ($t = 12:08 - 12:24$). The changes in coefficients could be observed due to tension and compression regions of the structure, as presented in Figure 6.32 based on all the feature values, when the quasi-static load moved to the tension region, all the features coefficients (e.g. P_a

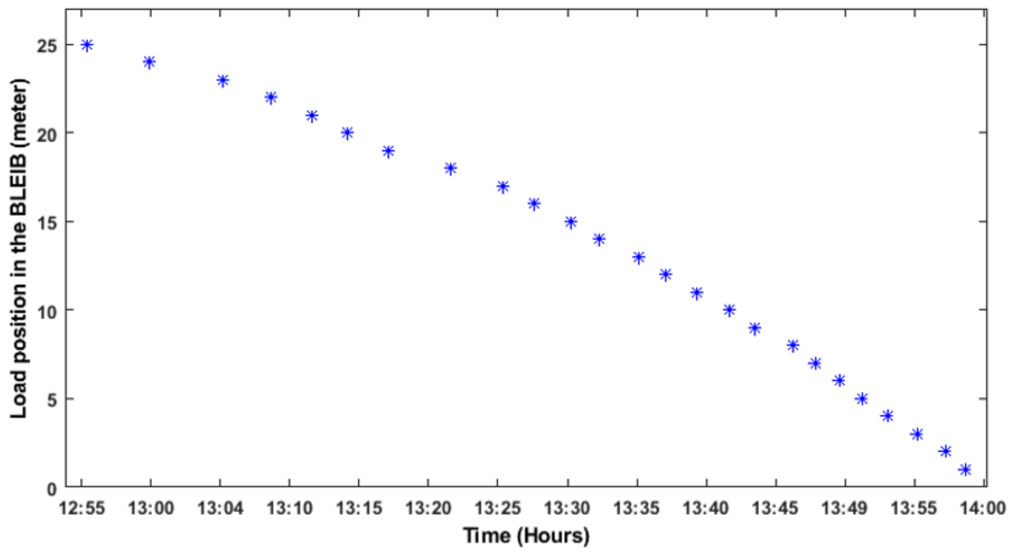

Figure 6.31: Position of quasi-static load as a function of time

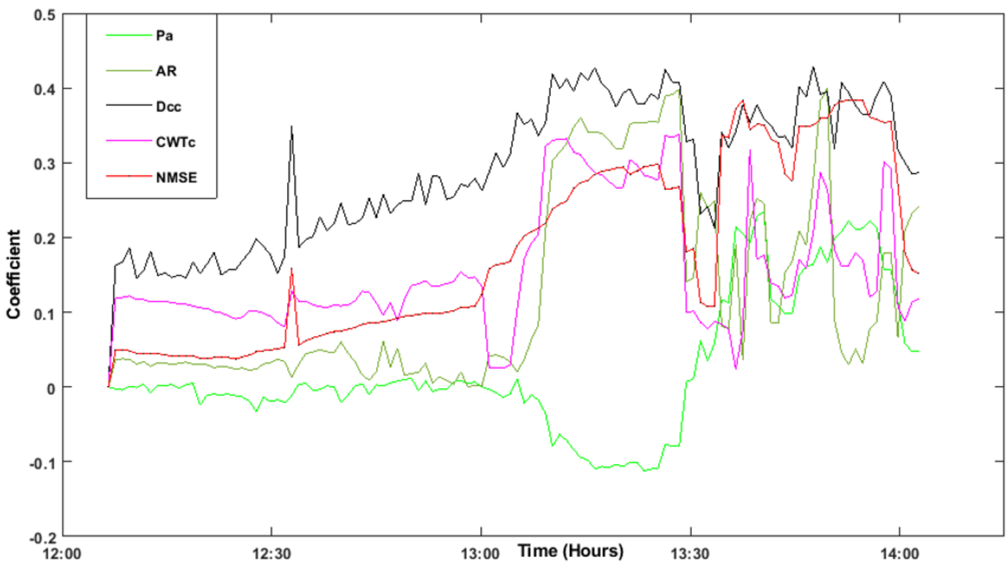

Figure 6.32: Values of the all features from ultrasonic pair S02R06 time histories in Cross-section A

feature) changed due to compression in the sensor pair S09R10 located in the middle of the structure (Figure 6.33). The average strength of the signal was recovered only partly after a pause at the middle of the structure, probably due to a lack of operational effects during these periods. The plots show that the resulting coefficients from all the features are correlated, because it is still possible to distinguish the dynamic and quasi-static changes in the structure. The coefficients increased up to a maximum value when the quasi-static load was applied on the top sensors in cross-sections A, C and E ($t = 13:13; 13:32; 13:54$), which is comparable (quasi-static load position 19, 12 and 6 meters on the structure) with

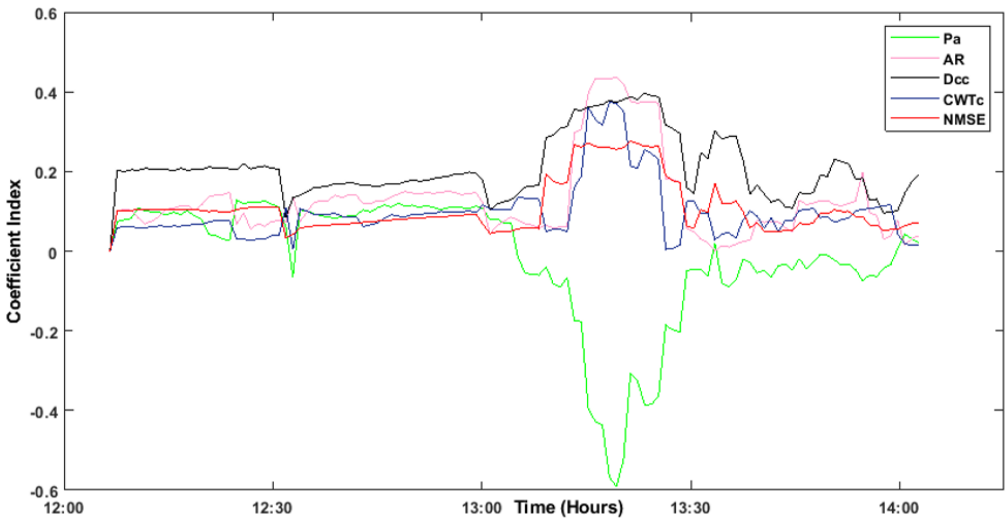

Figure 6.33: Values of the all features from ultrasonic pair S09R10 time histories in Cross-section C

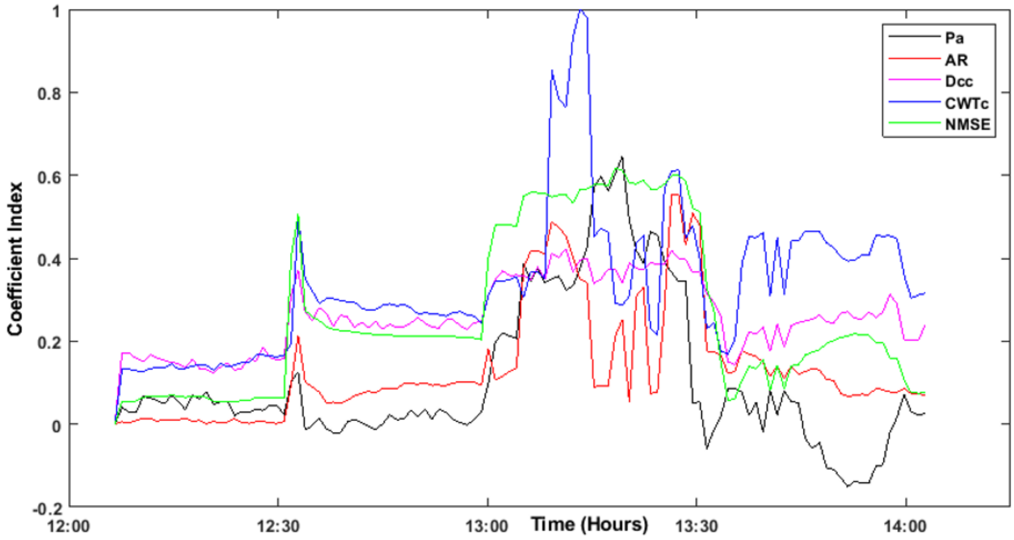

Figure 6.34: Values of the all features from ultrasonic pair S12R14 time histories in Cross-section E

Figure 6.32. In the presented features one can observe three characteristic periods:

1. Even load is passing through the sensor pairs in different cross sections ($t = 13 : 13; 13 : 32; 13 : 54$);
2. Short pause;
3. When the quasi-static load is far from sensor pair positions 11-14. However, for any given feature, its performance (ability to detect and distinguish the two states – quasi-static and dynamic loading) varies for different sensor pairs and cross-sections.

The coefficients increased up to the highest value in cross-section E, compared to other cross-sections, when the quasi-static load was passing through sensor pair S12R14 (the highest coefficient may be an indicator of the opening of cracks). Moreover, from Figure 6.32, one can see the values increases and sudden degradation ($t = 13:15 - 13:25$) in the $\boldsymbol{CWT_c}$ and AR feature values due to energy attenuation which is indicate the cracks opening.

Various features extracted from diffuse ultrasonic signals prove their ability for damage/change detection due to different operational effects. The embedded ultrasonic sensors are sensitive enough to detect and localize the change/damage in the real structure. The obtained experimental results show that all features computed from ultrasonic signals have a capability of detecting quasi static and dynamic load states from environmental effects, as well as detecting damage (crack opening), but their performances were different for different cross-sections, that can be verified looking at the ROC curves.

6.5 Real bridge in-situ experiment

The objective of the field test was to demonstrate the sensitivity of the proposed features to monitor internal changes in tensile and compressive stresses in a real structure. The excellent test object which allowed us to demonstrate the sensitivity features was the bridge in Gliwice (Poland) with embedded ultrasonic sensors. The Gliwice bridge over the Kłodnica river has great importance in the daily life of the local population since the bridge provides communication in the highly urbanized Upper Silesia region (Chakraborty *et al.*, 2019a).

The bridge is located along the Katowice - Gliwice route within Silesian Central Motorway (see Figure 6.35). It was built to overcome an obstacle, which was the Kłodnica river with its floodplain. The location of the bridge is illustrated in Figure 6.35a. It consists of twelve-span continuous beams made of prestressed concrete supported by two girders and the total length of the bridge is 552 m (Figure 6.35c). There are two steel pot bearings on each support. The 36 - metrelong span at the south-east end of the bridge (Figure 6.35b) was selected as a research object.

6.5.1 Measuring system

The sensors were installed in the cross-section at the south-east end of the bridge during construction work in 2015. The location of sensors is marked in red and green in Figure 6.36. The middle part of the girder was chosen to be monitored, as the biggest stress

(a) Location of Gliwice bridge

(b) Monitored bridge span at southeast end

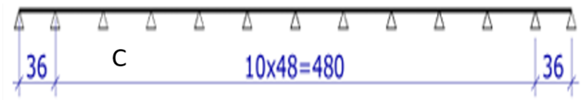

(c) Quasi-static scheme of the bridge

Figure 6.35: Gliwice bridge

changes are encountered there. There are four groups of measurement systems to determine the changes in the superstructure. In the first group, new ultrasonic sensors were mounted in the middle of the span over a length of 4 meters. Each of the eight ultrasonic sensors can work as a transmitter and a receiver.

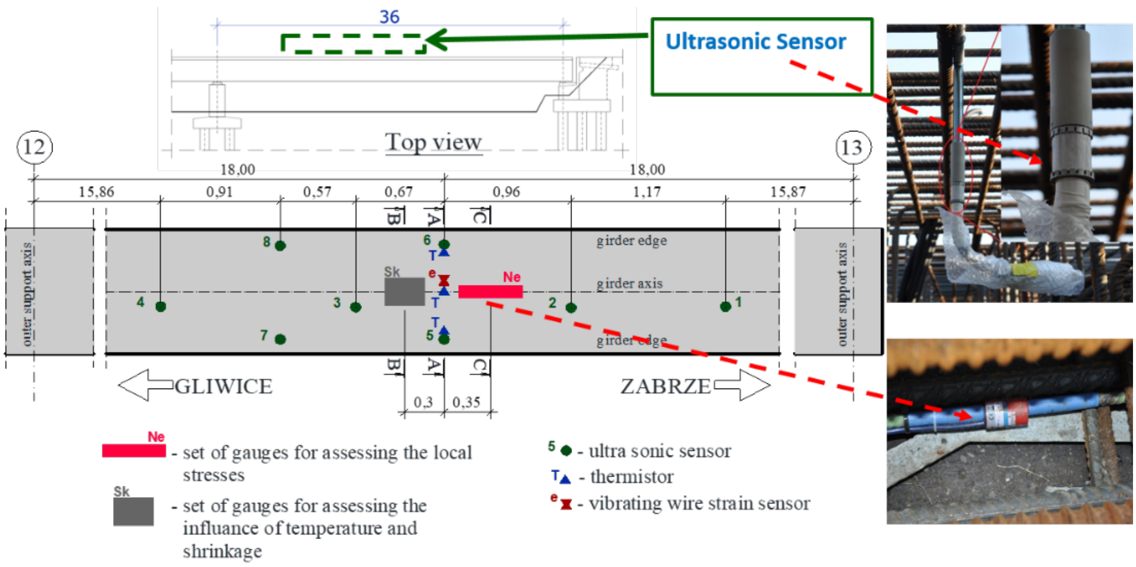

Figure 6.36: Arrangement of ultrasonic sensors and strain gauges in the girder

Three Geokon® 4202 sensors were installed in each of the bearing pads. Their purpose is to measure the forces transmitted by the bearing to the concrete of the sub-bearing blow, so they are used to determine the correct operation of the bearing. Six Tascas® thermistors and three Geokon® 4911 sensors were installed in cross-section A (see Figure 6.36). The second group, located in the B-B cross-section (see Figure 6.36), consists of three Geokon® 4202 sensors. The third group, located in the C-C cross-section (see Figure 6.36), consists of three Geokon® 4200 and one Geokon® 4370 sensors. The aim of installing the sensors in these three mentioned cross-sections was to recognize changes and compare them with the ultrasonic sensor zone.

6.5.2 Load test and Data acquisition system

The time for the load test was chosen during the night to reduce the influence of the daily traffic. One 382.66 kN truck (5 axial's - the values and direction of loading are depicted above the arrows in Figure 6.37) was used as a load during the test (Figure 6.37). The truck was passing the bridge slowly (10 km/h) and stopped at the southeast end of the bridge near the zone of ultrasonic sensors location (see Figure 6.36). This static load took 8 min in the first round and 15 min in the second round. During the examination, the position of trucks was marked according to the zone with ultrasonic sensors. The measurement instruments were placed, and initial readings were made. In this studies, the selected strain gauges (section C-C) and one pair of ultrasonic (S01R02) sensors were chosen and acquired signals were processed to determine the changes and measure strains in girder.

Figure 6.37: Truck (5 axial) used for load test

The data was collected by connecting the computer directly to the Campbell Scientific® data logger and customized data acquisition system for ultrasonic sensors. The data logger has 8 channels (6.16). The acquisition devices were placed in the box near to bridge, where every 200 ms data was acquired from vibrating wire strain gauges and stored in the local hard disk drive in the same box. For ultrasonic measurement, the same set up was used (more details can be found in section 6.2.2). However, the acquisition of the ultrasonic signal was made two times a minute and stored in the laptop. The features were obtained from the decorrelation coefficients D_{cc}, the AR coefficients of the autoregressive model, the coefficients of CWT, coefficients of STFT).

6.5.3 Analysis and results

In order to evaluate the performance and overall response of the integrated system in strain monitoring set of data was recorded. The strain gauges simultaneously measured the distortions related to the passage of traffic and mass of truck (load), but also the variations of thermal curvature. In reality, it is difficult to compensate slightly thermal expansion when the temperature increases or decreases sharply. The thermal curvature in the bridge direction is very small, especially as sensors installed inside the girder. Specifically, the thermal curvature mostly changes within 1°C, which requires a longer period. However, the load test lasted one hour, which had less effect on the area of vibrating wire-gauge strain time histories. Through the experiment calibration, it was found that the strains varied 2 $\mu\varepsilon$/°C. Fortunately, it was easy to dissociate the deformations related to the temperature or the traffic-induced distortions, due to the fact that the effects of traffic occurred at frequencies much higher than temperature variations. Figures 6.38a and 6.38b show the realization of the strain time series monitored at vibrating wire strain gauges during the tests performed in 2018. An overall trend is observed in the strain values, which is mainly caused by the mass of the truck. The results obtained showed that the recorded data clearly indicated the strain levels developed due to tension and compression of the live traffic and mass of the truck (load). Figure 6.38c shows the percentage of the changes in strain due to traffic load and mass of the truck load used for the load test.

The ultrasonic features derived from the combination are presented in Figures 6.39. The variation of the velocity of the S01R02 combinations corresponds well to the mass of the truck. The higher the mass, the higher the velocity (propagation in elastic material, see details in chapter 4 section 4.2.2). The degradation in correlation coefficient (see Figure 6.39a, AR coefficient (see Figure 6.39b) and CWT(see Figure 6.39c) could separate the load from the live traffic. The correlation coefficient and CWT increased up to the

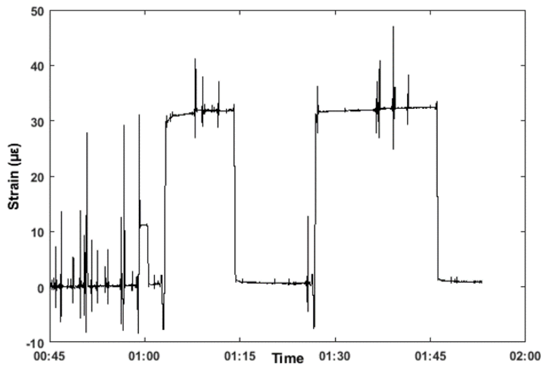

(a) Strain changes due to mass of the truck (bottom)

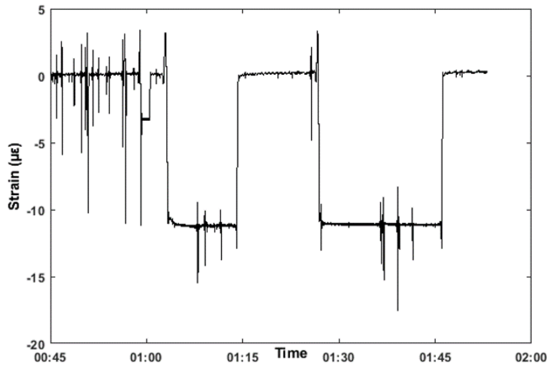

(b) Strain changes due to mass of the truck (top)

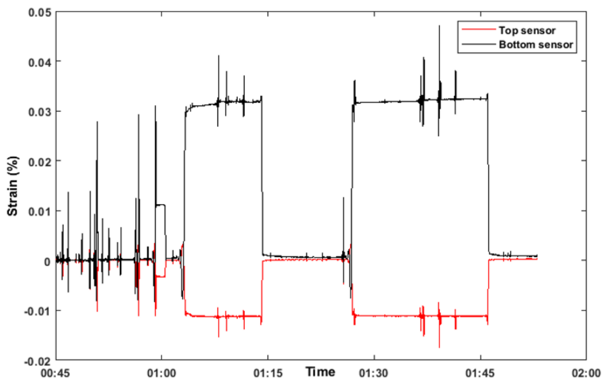

(c) Percentage of the total changes

Figure 6.38: Strain changes measured by vibrating wire strain gauges

maximum value when the static load was applied for 15 minutes (the second round) on the top of the sensor pair S01 and R02 (time 1:30 $< t <$ 1:43). The velocity changes varied significantly although they still follow the same trend as the traditional strain gauges. However, STFT features values in Figure 6.39d gave us misleading information and it was difficult to separate the load from the traffic. Since, in the real structure, acquired signals are very complex, in some cases features extracted using advanced signal processing technique also gives misleading information due to different effects (e.g. noises) in the real structure. However, it can be sensitive enough to detect environmental related changes in the structure, therefore extracting more features could be beneficial. During these load tests, the value of the maximum velocity changes corresponding to coefficient (D_{cc}, AR) was 0.03 and CWT 0.01, which is still relatively small and comparable with percentage of strain measured by vibrating wire strain gauges (see Figure 6.38). Normally, the opening or appear of cracks in the vicinity of the sensors causes unusual behaviour in coefficients. Since the Gliwice bridge is five-year-old, from our technical point of view it is in a fine condition.

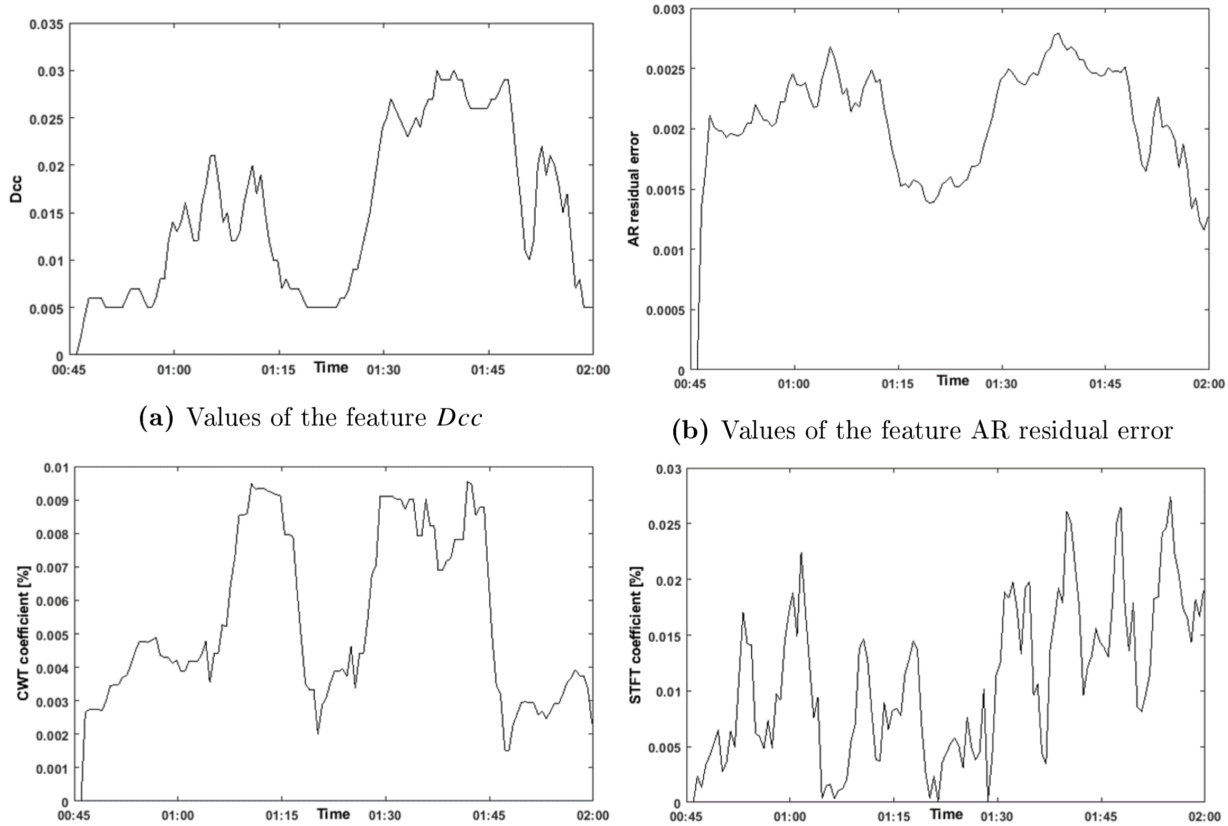

(a) Values of the feature *Dcc*

(b) Values of the feature AR residual error

(c) Values of the CWT feature

(d) Values of the STFT feature

Figure 6.39: Values of the feature (coefficient) from sensor pair (S01R02)

6.5.4 Discussion

The above studies show that applied embedded sensors together with proposed features can detect the changes in real concrete structures as well as traditional strain gauge sensors. An integrated monitoring system was analysed in the real structure, including traditional gauges and novel ultrasonic measurements. The health condition of the bridge could be assessed from the correlation coefficient and AR coefficient features. Degradation in correlation coefficient and AR residual error appears to be potential changes/damage-sensitive features (ultrasonic measurements). The origin of changes in the structure seems to induce variations in correlation coefficient and AR parameter related to the level of changes in the structure. Load changes can be detected and localized and, therefore, this feature can also be used to evaluate the severity of the damage. One can see the influence of a load of the truck (with lightweight traffic) on AR coefficient, and the correlation coefficient is negligible which indicates the good health condition of the bridge. The embedded ultrasonic sensors are very practical in the concrete structure, have shown to be valuable sensors for various tasks in long-term SHM for easy installation and high durability.

6.6 Conclusion

The study has concluded that ultrasonic measurements have the potential to be used as an alternative to more traditional sensors. They offer significant advantages over conventional measurement techniques providing full-held surface strain measurements, as well as are advantageous in determining crack opening and propagation. Most importantly, the ultrasonic feature can monitor even tiny strains/cracks during loading. Various features extracted from diffuse ultrasonic signals prove their capability for damage/change detection due to different operational effects. The embedded ultrasonic sensors are sensitive enough to detect and localize the change/damage in the real structure. The obtained experimental results show that all of the features computed from ultrasonic signals have a capability of discriminating different types of load and detect damage (crack opening, propagation). However, their performances are different for different kinds of structures, even in various cross-sections. Four of the features such as P_a, D_{cc}, achieved better performance as those determined by more simple methods.

7. Data fusion

7.1 Background

The idea behind data fusion is to combine information from multiple sensors to improve the overall performance of damage detection and quantification. Techniques for processing of synchronized information from various sensors located in the same area of the structure that does not show the same accuracy (have different uncertainties) are rarely used in SHM. Multi-Sensor fusion techniques seek to address these challenges. For a multi-sensor system, data fusion can be classified into three levels: signal-level, feature-level, and decision-level fusion (Liu and Wang, 2001). Signal-level fusion is called the lowest level fusion, which combines raw signals from multiple sensors, and produces new raw signals that are expected to be more informative. Feature-level fusion, called medium level fusion, involves calculating feature values (observables) extracted from the signal of an individual sensor or combining observables from different sensors, so that the most relevant ones are used to make decision. Then, a fusion of these features can be achieved through several techniques such as Fuzzy inference system. Decision-level fusion is called the ultimate-level fusion in this hierarchy. At these level, each sensor can provide an independent decision based on its own features, and the results from all of the features are then fused.

This chapter provides results of different levels of data fusion based on the experiment presented in chapter 6. Section 7.2 describes the information on fusion used as a basis of Decision-Making Strategy. The feature level fusion is detailed in section 7.3. Finally, signal level fusion is discussed in section 7.4.

7.2 Information fusion

7.2.1 Methodology

The idea behind the information fusion (Decision-level fusion) is to compare the information from multiple sensors to improve overall decision/localization (Liggins *et al.*, 2017). Decision-level fusion is less complex than another two types of fusion techniques, however, it requires more preprocessing to analyse data/signal to get individual decision from each sensors or pair of sensors. Then, results from each sensor are compared to get overall decision/localization.

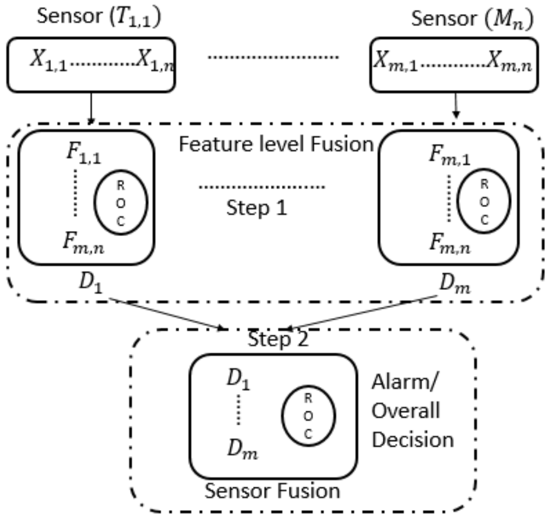

Figure 7.1: Two-step feature based sensor fusion model

The procedure of information fusion is illustrated in Figure 7.1. As a first step, the feature level of fusion is applied to a signal coming from multiple sensors. The general frame of data fusion is investigated, for example: $X_{1,1}, \ldots,$ where $X_{1,n}$ is the vector of data from one ultrasonic sensor pair T_{11}, (one emitter and one receiver) and $F_{1,1}$ is a feature value from one sensor pair. In step 1, feature level fusion represents the step of computing the features from all the sensors or sensors pair. In step 2, the decisions taken from ultrasonic sensor pair and outputs for other types of installed sensors, are fused using binary declaration in terms of operational changes (like presence/absence of load, presence/absence of crack/multiple cracks etc.).

In this section, a voting scheme at the decision level is used for information based fusion. The first step is to select a threshold for each feature from the pair of ultrasonic signals using a voting scheme. This threshold is used to discriminate between the undamaged and damaged states in the features. Generally, the weight of the value for undamaged state is lower than loading or damaged state. The next step is to use the receiver operating characteristic (ROC) to compare the features for overall decision (Metz, 2019). The ROC curve is a metric used for statistical evaluation of a feature, and can be used to visualize the overall decision (see Figure 7.2).

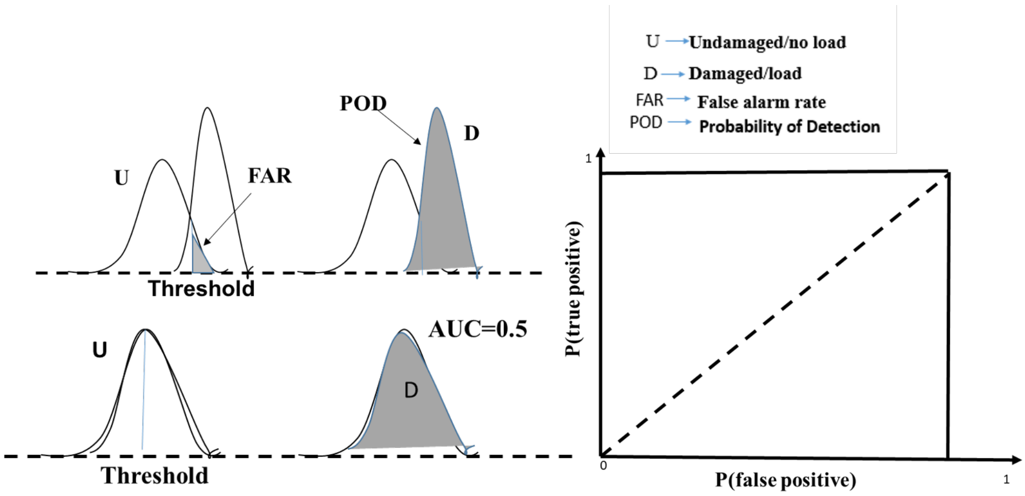

Figure 7.2: Illustration of ROC for a feature

In the voting scheme, an overall decision is made to differentiate between damage and undamaged class following the maximum value of the voting index (Njoku, 2014):

$$O_d = max(\sum_{n=1}^{N_n} W_n F_n), \tag{7.1}$$

where N_n is the length of the vector of features used to assess the n-th sensor; F_n is the feature value by the n-th sensors in relation to the different location; W_n represents the voting weight (the default: $W_n = 1$). The highest weighted average probability indicates a high possibility of the existence of damage.

7.2.2 Features comparison using ROC curve

In order to validate the feature-level fusion, five ultrasonic features were computed from the data collected on the benchmark RC specimen (see details in section 6.3). The decision and creditability of these features was analyzed using ROC curves. The threshold was defined from the voting scheme and swept over the range of the feature values, and the probability of detection (POD) is plotted versus the false alarm rate (FAR). POD or True Positive rate trying to asses a minimum number of observations of load or crack size that is correctly detected by specific NDT techniques. The FAR is defined as the number of false alarms or observations per the total number of load or crack exist but in reality no crack or load exists. A FAR is also known as the probability of false detection. The ROC curve is a perfect detector which measures the value area under the curve (AUC). The accurate classifier corresponds to the maximum AUC (maximum AUC = 1). Therefore, larger AUC values indicate better performance. In the next stage of the algorithm (see Figure 7.1), features from different sensors were analysed using a voting index threshold for ROC curves. In the end, the final decision was evaluated.

The proposed features from the ultrasonic signal were compared with the S01R04 sensor pair readings (location of the sensors can be seen in Figure 6.13) in Figure 7.3 via their ROC curves. It can be seen that all the features perform fairly well in their ability to detect crack opening and propagation as well as damage states in the presence of noise. The peak amplitude coefficient and AR coefficient performs better (AUC = $1, 0.989$) in classifying damage from the undamaged state based on the sensor pair S01R04 sensor pair readings of this structure. This result was not unexpected because features D_{cc} and CWT coefficient value's fluctuate suddenly, which miss-classified the damage state from undamaged sate. For the proposed features, the performance is similar for different threshold values. Hence, even though, there may be the best feature for a particular sensor pair and a specific threshold technique, so it may be suitable to use the information from all features from different sensors to reach better localization or detection of crack/changes. The output presented in Table 7.1 shows that the peak amplitude coefficient feature extracted from the ultrasonic signal perform better (AUC = 1) compared to all the NDT methods in this benchmark structure. It can be observed that the ultrasonic sensor detect the crack (damage) located between the pair of sensors earlier than other NDT methods of detection.

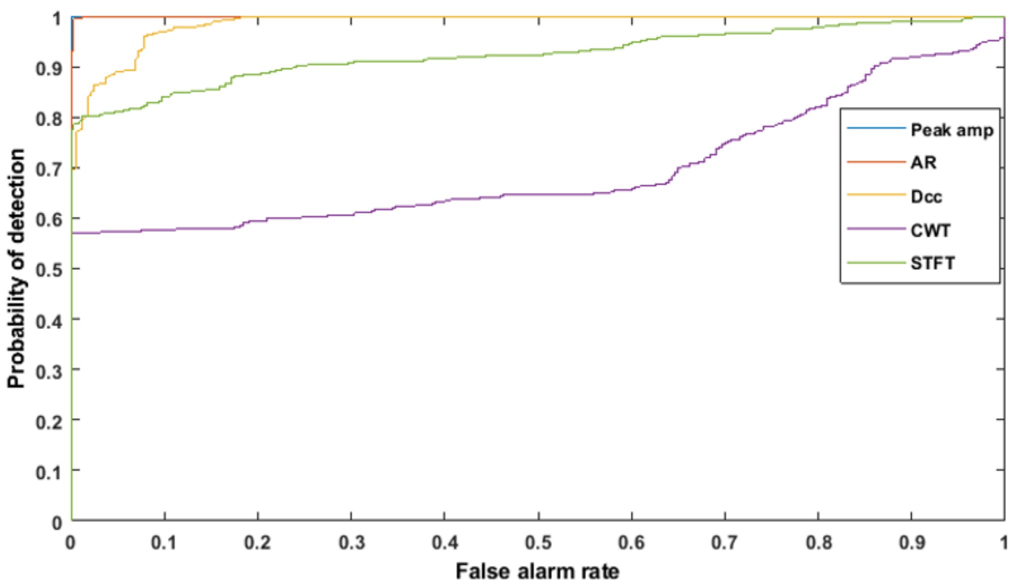

Figure 7.3: ROC curves for all the features in RC beam

Tab. 7.1: Overall results for different NDT techniques.

NDT Methods	AUC
Ultrasonic	1
LVDT	0.994
DIC (deflection)	0.992
Strain gauge	0.985

7.2.3 Crack opening displacement

The crack opening displacement (COD) of reference benchmark structure was determined using the DIC method. To determine the crack opening displacements (COD), the displacement fields were used (Barnby *et al.*, 2014). COD values were achieved by taking into consideration the discontinuity of two point (middle of the beam) by following the crack path (central crack), the transformation of the dissipated energy. The crack opening along the crack path was measured (anticipating the crack opening width vs depth line to zero). As peak to peak amplitude perform better (AUC= 1) than other ultrasonic features, it was presented as linking with COD. Figure 7.4 shows a comparison between the changes in peak to peak amplitude (absolute value) regarding the ultrasonic feature and those measured with DIC method. One can see that, COD was well matched with the ultrasonic feature.

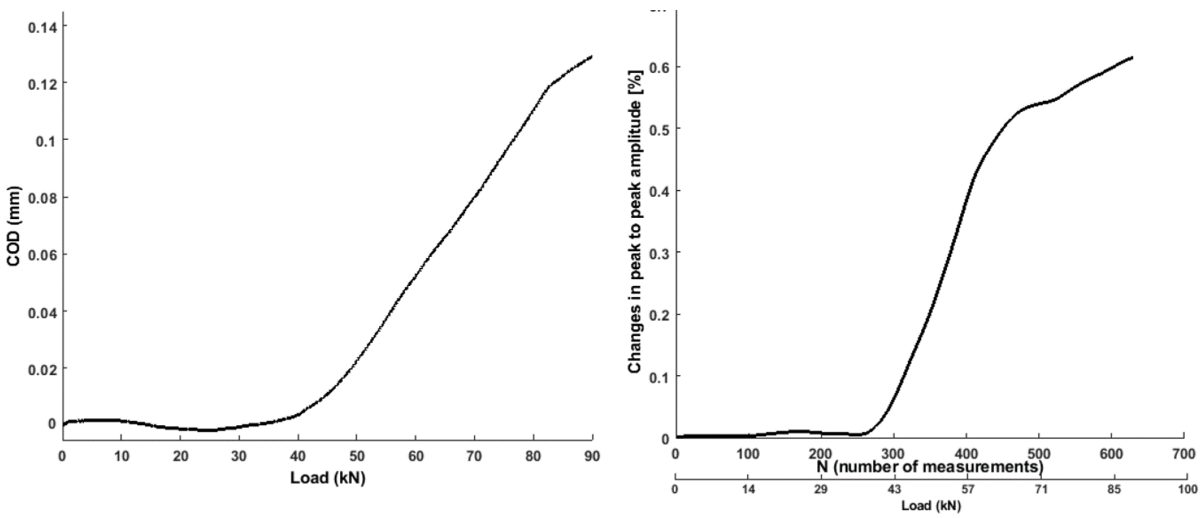

Figure 7.4: Load-COD vs load-changes in peak to peak amplitude response of a reference structure

7.2.4 Discussion

As Table 7.1 shows, all the sensors detected the crack properly and with a very high sensitivity. This is because the cracks appeared in the middle of the tested beam where most of the sensors were located. The declaration of the structural status ('damaged' and 'undamaged') was very important, therefore proposed information based on fusion using voting index provide more accurate results (e.g. AR feature provided misleading damage status when the beam was at the undamaged stage (N=50, after 7 kN)).

7.3 Feature level fusion

7.3.1 Fusion methodology

Feature-level fusion is also called as medium-level fusion, which involves calculating feature values from each sensor pair individually or comparing or combining the features from different sensors so that the most relevant ones to make a decision. Authors in this research field often propose different machine learning approaches for feature level fusion (Hossny *et al.*, 2008; Sharma and Davis, 2009; Stepinski *et al.*, 2013). Several research studies of sensor fusion is seen in SHM application where different parameters from different or same sensors at different resolution are combined to extract more useful information for the diagnosis of structure.

Osman et al. (2014), extracted multiple features from radiography, and ultrasonic data, and then classified to differentiate defects on the basis of alarms classification ratio. The authors (Bastien Masse, 2015), presented a comparison of multiple ultrasonic features for damage detection in aluminium specimen. Surface roughness was estimated using a Fuzzy inference system in (Barai *et al.*, 2015). The authors of (Aliustaoglu *et al.*, 2009), proposed a new fusion approach for tool wear condition-monitoring based on two-stage fuzzy logic scheme. These examples clearly indicate the potential of using fusion methodology for features extracted from multiple and different types of sensors to improve the quality of diagnostic information obtained from particular sensors. Moreover, the acquired signals need to be processed prior to the fusion, and feature-based processing may significantly reduce the amount of processed information and enhance damage detection capability.

In data fusion, early effort of using fuzzy rules for data fusion can be seen in (Solaiman *et al.*, 1999). In (Karlsson, 1998), the authors proposed new fuzzy logic operators for sensor-based classification. The research study (Chakraborty *et al.*, 2013) proposes a generalized decision scheme for power control and improves the performance of secondary user using Adaptive neuro fuzzy inference system (ANFIS). The authors of (Wang *et al.*, 2019), feasibility of different decisions in fusion for damage detection.

Fuzzy inference transforms the inputs using fuzzy rules to develop the outputs. The output inference translates the result of fuzzy inference into a suitable format required by the application environment. However, if the whole fuzzy system is considered as a feature network, the purpose is to adjust the variables of this feature network in a way that it correctly maps the system inputs to the desired feature outputs. The system uses a general structure described in Figure 7.9. Fuzzy inference system (FIS) is the first such system where decisions are based on testing all the rules and combined in some manner. The general goal of this fuzzy system is to combine the feature and improve the output. The role of the proposed method is to aggregate information obtained from two features to estimate in the best way the structural variable as a feedback for damage/change detection. Fuzzy aggregator, which define a membership functions of each feature F_n to beliefs of weight W_n on the proposition of rate of changes. We can have a combined membership function of degree of belief of change/damage occurrence through fuzzy conjunction. Then defuzzification value is combined with features by using the following equation:

$$f(F_n) = \frac{W_1 F_{n-1} + W_n F_n}{W_1 + W_n}, \tag{7.2}$$

where $f(F_n)$ is the fused fuzzy index, which is the degree of belief on the proposition of damage/change occurrence.

To verify our proposed methodology, feature level fusion was applied in third test object described in section 6.4. The results of different feature comparison in this test object were presented (details in section 6.4). However, to discriminate between the quasi-static load states from dynamic load states, the values of an effective feature should be separated for these two states. Feature values for operational state are assumed to be larger. Fisher Discriminant Ratio (Fdr) method (Wang *et al.*, 2011) can compare the feature's ability to separate this two states.The Fdr is given by the formula:

$$Fdr = \frac{(m_1 - m_0)^2}{s_1^2 + s_0^2}, \tag{7.3}$$

where m_1 and m_0 are the means, and s_1 and s_0 are the variances of the two classes (dynamic and quasi-static load, respectively). The Fdr is large for a specific feature if the classes have a large separation between the projected class in means combined with small variances.

Figures 7.5 and 7.6 show the Fdr for the all the features for different sensor pairs. It can be seen that feature D_{cc} and AR have the largest Fdr for sensor pair S12R14, and

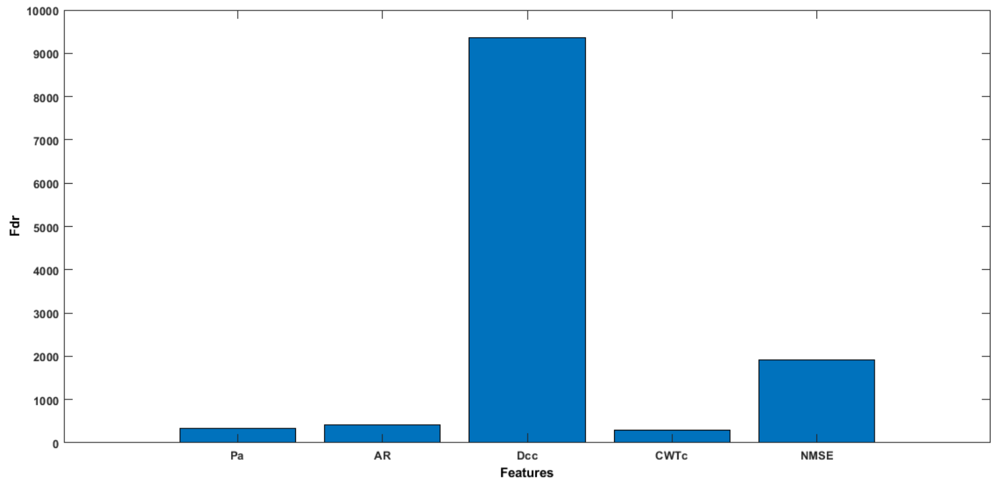

Figure 7.5: Values of Fdr for all the features from Cross-section A (S02R06)

D_{cc} and NMSE for sensor pair S02R06, and thus, it is most effective in separating the classes.

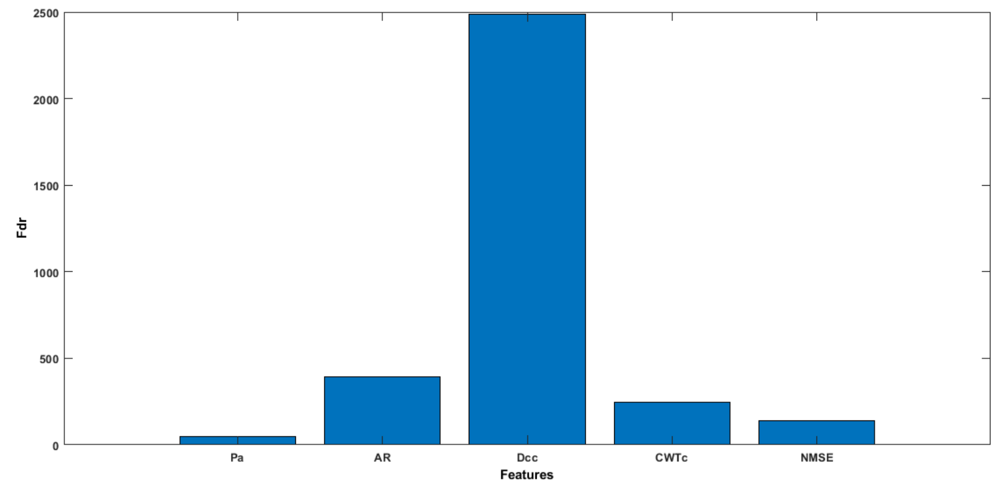

Figure 7.6: Values of Fdr for all the features from Cross-section E (S12R14)

The performance of these features is also analyzed using the ROC curve (for more information see (Fawcett, 2006)). For each of the features a predetermined threshold is swept over the range of the feature values of each of the sensor pairs (computed at several times in the experiment), and the probability of detection (True positive rate) is plotted versus the false alarm rate (FAR). A perfect detector, that calculates the features accuracy to classify the two states, measures the value area under the curve (AROC). The result can be comparable with the Fdr. All five proposed features are compared in Figures 7.7 and 7.8 via their ROC curves.

Tab. 7.2: Overall results for different features in Cross-section A

Features	AROC
Pa	0.650
AR	0.812
Dcc	0.922
CWTc	0.810
NMSE	0.978

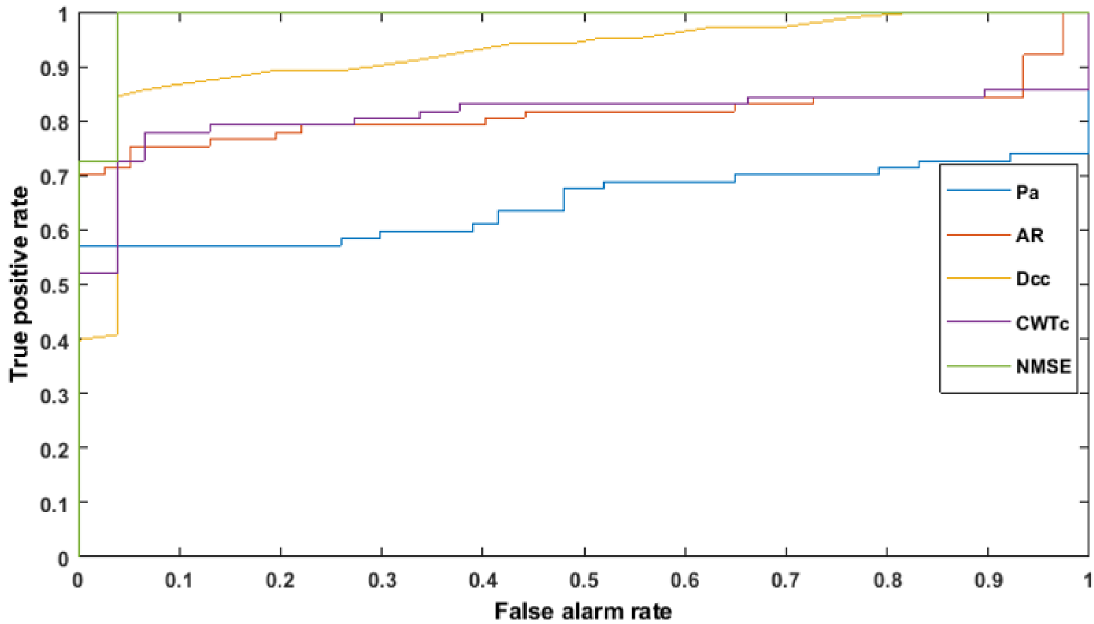

Figure 7.7: ROC curves for all the features in Cross-section A.

It can be seen that all features perform fairly well in their ability to separate the dynamic load (vibration) and quasi-static load states in the presence of noise, but no single feature is the best for both sensor pairs (see 7.2 and 7.3). The performance of the P_a feature is poor compare to other features, because P_a coefficient value is positive due to sensitivity to tension and negative for compression region of the structure, which miss-classify the two states. Sensor pair S12R14 has the poor performance in that the best Fdr. This result is not unexpected, because most of the cracks appeared around cross-section D and E, where sensors no. 11–14, were located, which is directly related to sensor pair S12R14, and its signals have a strong impact compared to signals from other pairs (see Figure 6.34).

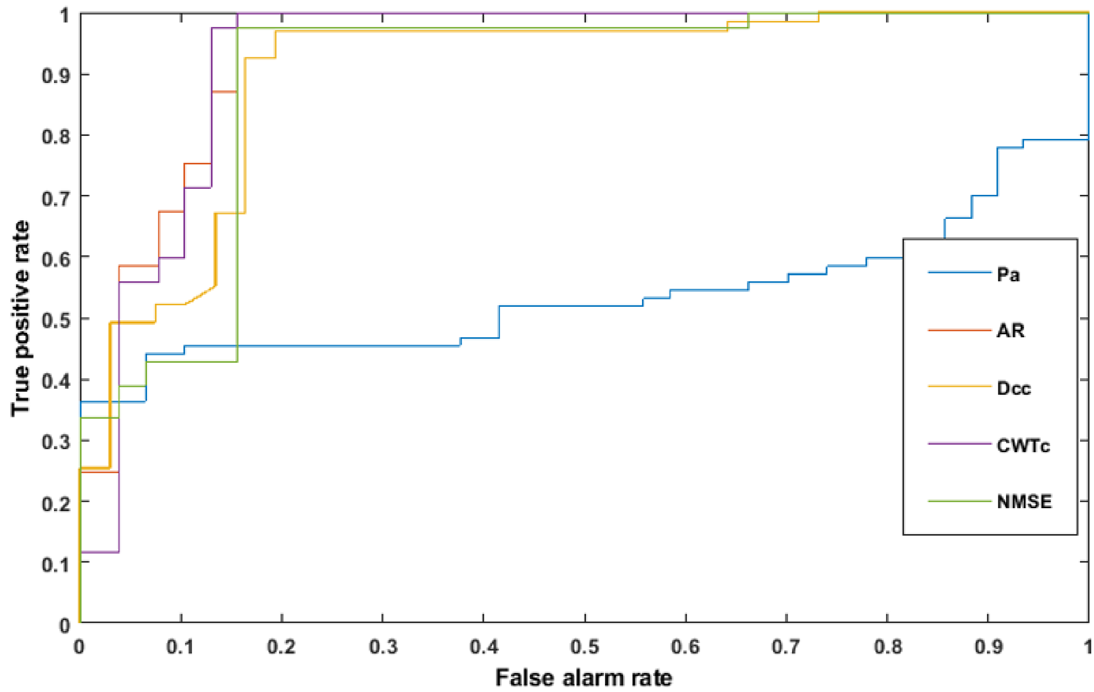

Figure 7.8: ROC curves for all the features in Cross-section E

Tab. 7.3: Overall results for different features in Cross-section E

Features	AROC
Pa	0.565
AR	0.936
Dcc	0.900
CWTc	0.9298
NMSE	0.893

7.3.2 Analysis of proposed methodology

As one can see in Tables 7.2 to 7.3, for the sensor pair S12R14 the AROC values are different in different cross-sections. Therefore, it is essential to fuse two best features describing the appearance of cracks in these cross-sections to obtain a valid detectability of these cracks. Two best features were chosen because features with less accuracy may add more uncertainty. Since the AR and D_{cc} features are the most sensitive for distinguishing between quasi-static and dynamic loading (see Figures 7.5 to 7.8) and small changes, they were selected for the fusion. Normally, the use of characteristics of these features can lead to better model for feature based fusion algorithms. The outcomes may be more robust if one can take the method benefits, considering feature characteristics.

Fuzzy logic was used to design an appropriate fusion method by translating two features as a linguistic variable to transfer as much information as possible from the features into the fused feature.

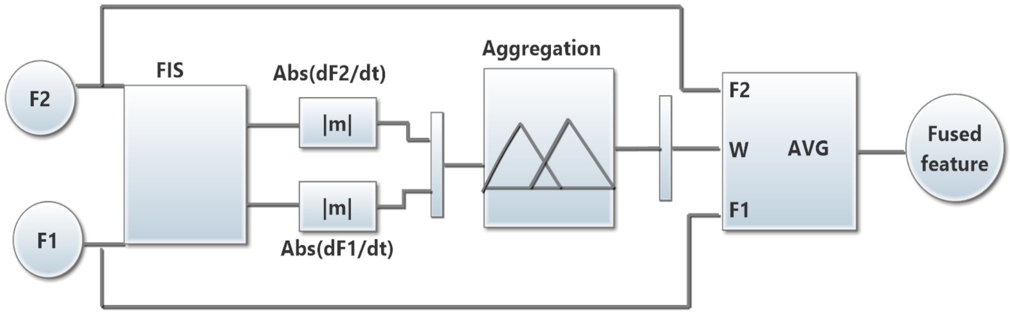

Figure 7.9: Fuzzy model

D_{cc} (F1) gives a proper value being the basis of judgement about the rate of changes in the measured signal thanks to the correlation analysis and direction of a particular relationship between the two signals. Due to its sensitivity to small changes, D_{cc} can provide misleading details about the signal's changes due to opening and closing of the cracks or the environmental effect, but its rate of changes when the values are measured by AR (F2) can provide some details about the reliability of D_{cc} in the circumstances of sudden changes (degradation) in the value of AR. If the weight of each feature is determined properly, then weighted average of F1 and F2 can give an appropriate estimation as a fused variable. With two best features in hand, the optimal change/damage index weight value of selected sensor pair can be obtained using a fuzzy system as displayed in Figure 7.9. The input membership functions presented in Figure 7.10 both for F1 and F2, are used to obtain the optimal index weight value of change/damage in the structure. Input and output membership functions consist of three levels, each level is represented by a fuzzy set with an assisting membership functions, low (L), middle (M), and high (H). In general, the membership function represents the distribution of the input or output values in a fuzzy system. The linear (triangular) membership function was adopted in this research, since it was beneficial considering processing speed and difficulties (Barua *et al.*, 2014). Based on the characteristics of the best features F1 and F2 of each sensor pair explained in the previous section, these inferences can be expressed as fuzzy rules, as in Table 7.4. The output of Table 7.4 represents the quality index of change/damage in the structure. The output surface graph of the two inputs is shown in Figure 7.11. From the surface graph one can tell how the inputs affect the output.

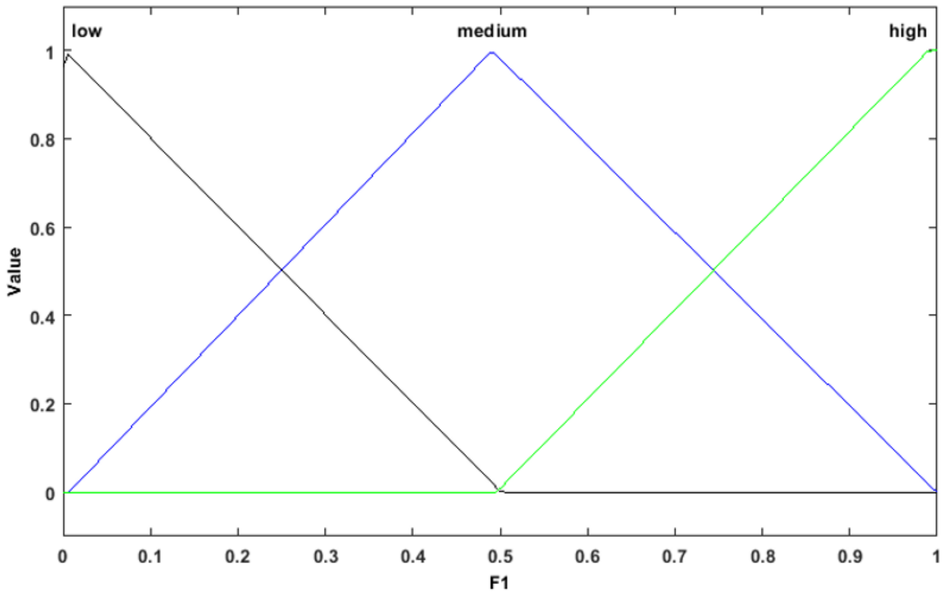

Figure 7.10: Membership Inputs 1 and 2

Tab. 7.4: Fuzzy rules tables for Feature 1 and Feature 2

F1	F2	output
Low	Low	Low
Low	Medium	Medium
Low	High	Medium
Medium	Low	Medium
Medium	Medium	Damage
Medium	High	Damage
High	Low	Medium
High	Medium	Damage
High	High	Damage

7.3.3 Results and discussion

FIS-based fusion strategy was applied for improving the performance of the damage/change index of the structure. The performance of a system can be observed by plotting the output of our fuzzy index model (Figure 7.12). This figure shows the response of the control system and also outputs of the fuzzy system designed for the sensor fusion. The proposed two features are fused for the sensor pair S12R14. It can be observed that fused features improved well in their ability to separate the quasi-static and dynamic loads states compared to a single feature, also compared via their ROC curves (Figure 7.13). This fusion

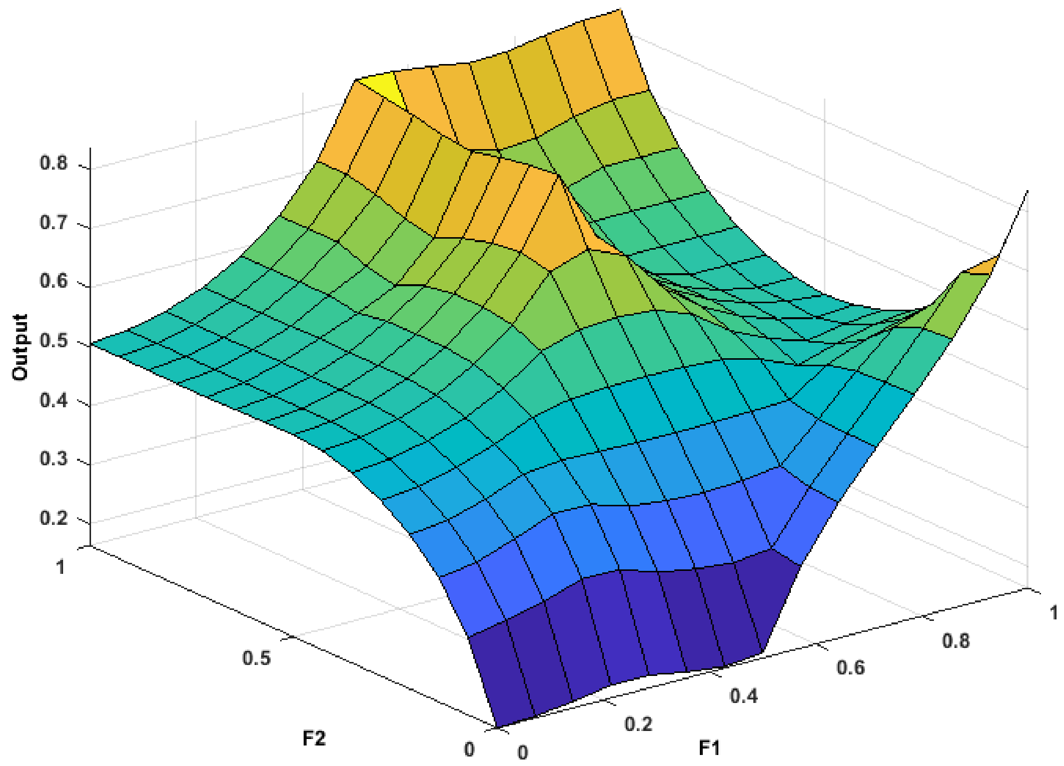

Figure 7.11: Fuzzy output surface.

strategy acquires 94% detection of the changes/damage with a FAR under 6%. Indeed, when the quasi-static load is applied (from the right top side of the structure see Figure 6.29) on top sensor pair ($t = 12:56-13:14$), the fuzzy index coefficients are increasing up to a maximum value. Sudden decrease of fuzzy index coefficients ($t = 13:15-13:23$ hour) may be an indicator of the opening of cracks ($t = 13:15$). From the Figures. 7.12 and 7.13, it was concluded that in fuzzy-based fusion the damage/change index performance was slightly better as compared to a single feature (see Table 7.5) at higher index values and indicating crack openings.

Tab. 7.5: Single feature versus fused feature in cross-section E

Feature	AROC
Dcc	0.900
AR	0.936
Fuzzy index (fused)	0.9398

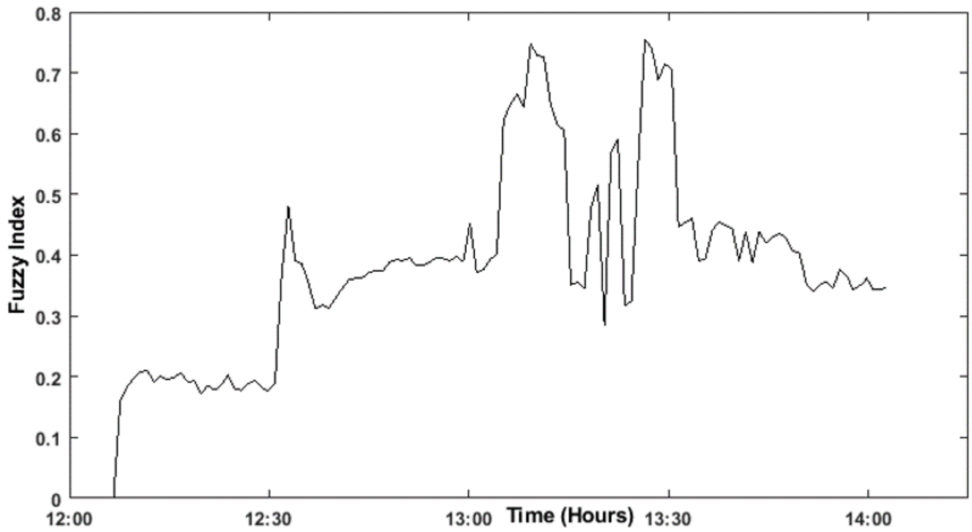

Figure 7.12: Values of the Fuzzy index coefficient in Cross-section E (S12R14)

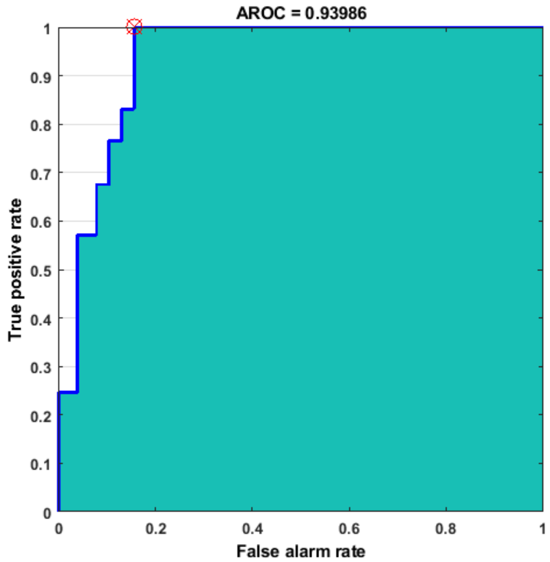

Figure 7.13: ROC curves for fused features in Cross-section E (S12R14)

7.3.4 Proposed fusion methodology applied to real structure

To demonstrate the sensitivity of the proposed fusion methodology, it was applied to monitor internal changes due to tensile and compressive stresses in the real structure, as illustrated in section 6.5. However, as one can see in Figures 6.39 and 6.38, the feature values differ in time compared to strain values measured by vibrating wire strain gauges. Therefore, it is worth to fuse these two features from two different sensors. Since the D_{cc} feature of the ultrasonic sensor is comparable with other considered features in detecting the mass of the truck (see Figure 6.39), selected to be fused with strain data.

FIS-based fusion strategy was used to the ultrasonic feature for improving the performance of change index of the structure. With these two features from different sensors, the optimal change/damage index weight value is obtained using a fuzzy system as displayed in Figure 7.14. It can be observed that the value of fused features increases up to 0.055. Clearly, they performed well in their ability to detect not only the mass of the truck but also missing traffic load at the same time (see Figure 6.35, e.g. strain gauge values at $t = 01:52$) compared to a single feature from these two different sensors. Therefore, the missing values problem was minimized using the data fusion technique. However, the value of the maximum influences the ultrasonic signals corresponding to the fuzzy index of 0.055, which is still relatively small and comparable with strain measured by vibrating wire strain gauges (see Figure 6.38). Normally, the opening or appearing of cracks in the neighbourhood of the sensors causes an unusual behaviour in fuzzy index values. Since the bridge in Gliwice is five years old, therefore the bridge is, as expected, in a good condition, which was evident from our results, too.

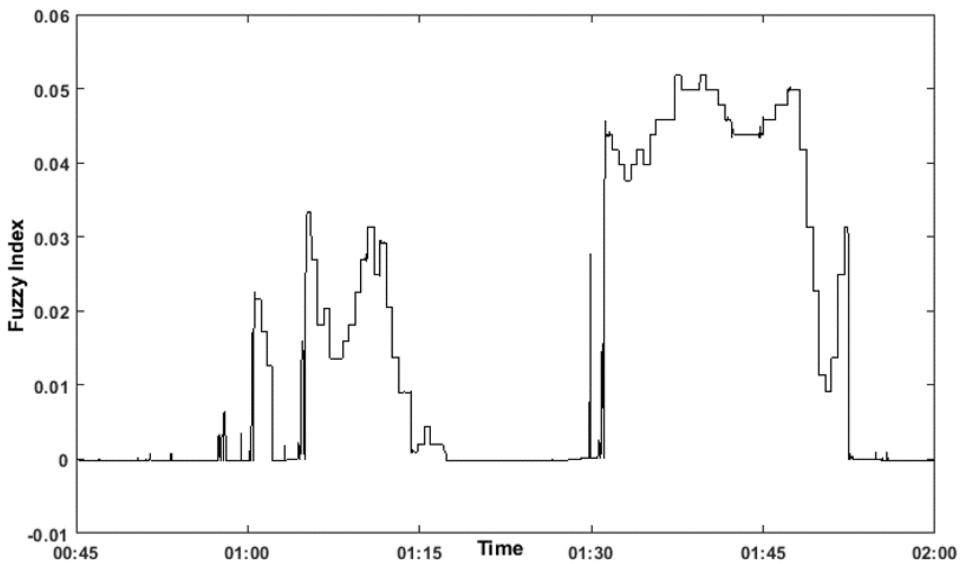

Figure 7.14: Fuzzy Index for load test

7.4 Signal level fusion

Signal-level fusion is called the lowest level fusion, which combines the raw signals from multiple sensors and, in consequence, the new raw signal, that is anticipated to be more informative.

A wide range of studies has already been reported on the application of embedded ultrasonic sensors to evaluate structural changes, before and after damage, in particular wave scattering from damage in the form of cracks (de Vera and Güemes, 1998; Niederleithinger *et al.*, 2015; Wolf *et al.*, 2015). The majority of these research works used more than two embedded sensors located in different geometric areas. Detection from the each pair of the sensors have been investigated. Yet the combination of the multiple pair of sensors located in same geometrical area remains a great challenge for this technique, despite the special interest in making such degradation detection since these decisions may lead to impressive results in crack detection. While employing multiple pairs of sensors and combining the two sets of signals, a fused representation is generated which illustrates different aspects of the object at once and thus offers clarified interpretability.

7.4.1 Fusion algorithm

Signal level fusion is one of the significant procedures to combine one dimensional signal and acquire meaningful features from the sensors located in different positions (geometrically). The idea behind the signal fusion comes from pixel level fusion. There are several research publications about combining two dimensional data to improve overall damage detection (Ni *et al.*, 2018; Gros *et al.*, 2000; Gros, 2001; Zapłotny *et al.*, 2017). The authors have shown that pixel level fusion have capability to extent damage detectability. However, there are different techniques which has been used in pixel level fusion, such as Simple average, Intensity and Saturation (HIS), Principal Component Analysis (PCA), Discrete Cosine Transform (DCT) and Discrete Wavelet Transform (DWT), etc. Some of their advantages and disadvantages are described below.

In HIS fusion method, the IHS space is converted from the Red, Green and Blue (RGB) space of the Multispectral image. The intensity factor I is replaced by the panchromatic image (PAN). Then, the reverse transform is applied to get RGB image as an output. HIS used the intensity part by reversing to RGB color of the fused image. However, saturation is dependent on luminance value (Choi, 2006).

The PCA method is a statistical method, which is mainly used to dimension reduction studies (Abdel-Qader *et al.*, 2006). In SHM, PCA has been used to distinguish between changes due to load/damage from environmental changes. PCA extract the information with highest influence and reduce redundant information, and in that way it increases the signal-to-noise ratio. In PCA, high and low frequency components are obtain separately by filtering and finally added together as a fused outcome. However, PCA results are not sensible, if the feature component do not follow the linear combination.

In DCT, sum of cosine functions of different frequencies is used to produce the fused image. DCT coefficients are obtained from different blocks, and then the average is used to get fused DCT coefficients. The limitation of DCT is the loss of time information (Alfalou *et al.*, 2011).

The DWT, provides a structure, where the analyzed input signals passed through a filter with different cut off frequency at different scales (Knitter-Piątkowska *et al.*, 2016). Hence, signals got converted to a frequency domain. The output came as a set of detail coefficients from the high pass filter and a set of approximation coefficients from the low pass filter. Using the fusion rule and inverse wavelet transform, a fused output was produced. The limitation of DWT is that, when the signal is shifted slightly, the amplitude of the wavelet coefficients changes significantly due to the lack of shift invariance.

There is a simple approach to overcome this problem, namely, application of the Non-Decimated Wavelet Transform (NDWT) (Unaldi and Asari, 2010). The NDWT is an un-decimated form of a conventional DWT based on Mallat,s multiresolution algorithm. It is performed by insertion zeros in the filter for up-sampling and suppressing the down-sampling step of the decimation algorithm (Figure 7.15). Its main advantage is translation-invariance with respect to DWT, since the main signal is not decimated, so the resolution can be maintained, also signal to noise ratio has increases (Ellmauthaler *et al.*, 2013). It makes this algorithm suitable for change detection, signal fusion, and feature extraction.

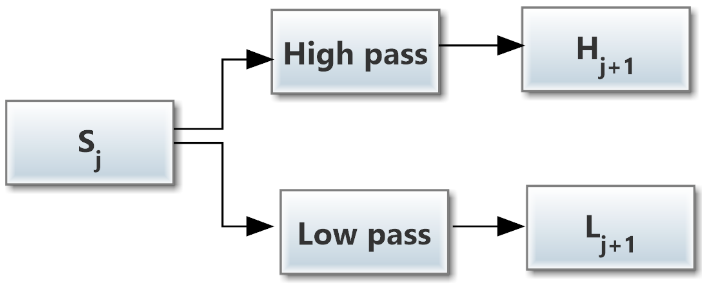

Figure 7.15: NDWT wavelet decomposition of a signal S_j

The NDWT decomposition uses the scaling function (low-pass filter) and the wavelet function (high pass filter) (Katunin, 2015a). These functions satisfy the two-scale relation:

$$2^{-\frac{1}{2}}\phi(\frac{t}{2}-k) = \sum_{n=-\infty}^{\infty} h(n-2k)\phi(t-n), \tag{7.4}$$

$$2^{-\frac{1}{2}}\psi(\frac{t}{2}-k) = \sum_{n=-\infty}^{\infty} g(n-2k)\phi(t-n), \tag{7.5}$$

where h_n and g_n are the impulse responses of low-pass and high-pass mirror filters. The jth level of decomposition is shown in Figure 7.15.The decomposition formulas of NDWT are as follows:

$$A_{j+1}[l] = \sum_{n=k} h[k]A_j[l + 2^j k], \tag{7.6}$$

$$D_{j+1}[l] = \sum_{n=k} g[k]A_j[l + 2^j k], \tag{7.7}$$

where $A_{j+1}[l]$ and $D_{j+1}[l]$ are the low frequency and high frequency components of the NDWT respectively. $h[k]$ and $g[k]$ are upsampled by 2^j when the j-level is processed, which results in a constant length of A_j and D_j. The inverse formulas of NDWT (INDWT) are as follow:

$$A_j[l] = \frac{1}{2}[(\sum_l (h'^j \times A_{j+1})[l] + g'^j \cdot D_{j+1})[l]]. \tag{7.8}$$

In general, using the NDWT method and fusion rules, the author trying to fused one dimensional signal coming from different pair of sensors. objective was to combine information from multiple signals (sensors) in order to create a new fused signal, which contained better information comparing to both signals (Chakraborty and Katunin, 2019b).

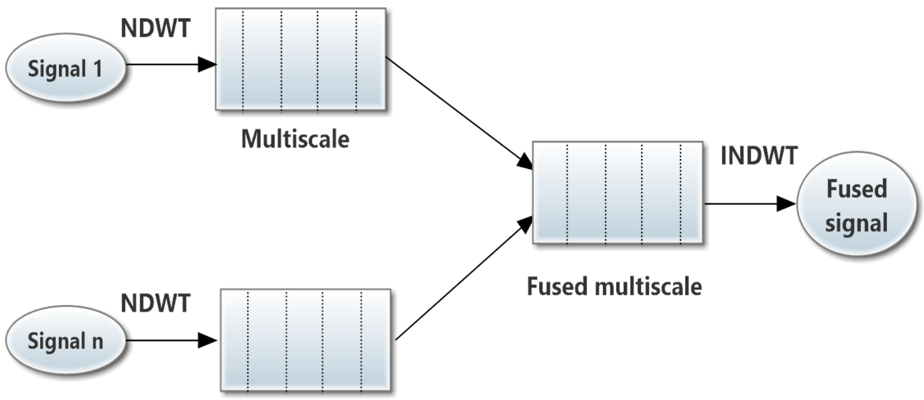

Figure 7.16: Generic fusion scheme

The fused signal has information from both signals which produces better information compared to the acquired signals. Combining information from multiple sources, and fusion rules play an important role, and it discussed in the next section. The block diagrams of general signal level fusion scheme is shown in Figure 7.16.

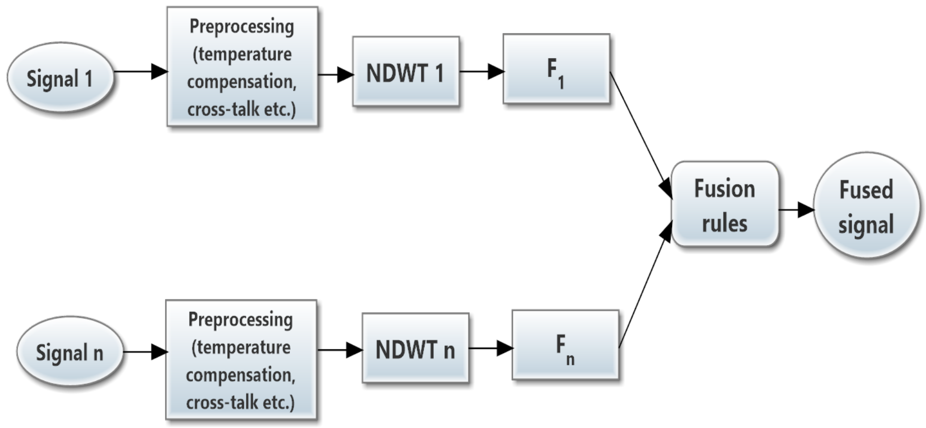

Figure 7.17: Procedure of signal based fusion

7.4.2 Fusion rules

As summarized in Figure 7.17, the signal processing approach consists of three steps.

Figure 7.17 illustrates the proposed methodology for signal level fusion, which is composed of three stages, namely, pre-processing, NDWT, feature extraction, and feature fusion. Pre-processing stage is divided into two steps, that is, removing the temperature effect, cross talk and normalization. In the first step, temperature effect was removed from input signals with the help of baseline subtraction. In the second stage, normalization of the signal in a proper way is performed in order to align the signal for fusion.

The process of feature extraction is shown in Figure 7.17. The preprocessed signal is firstly decomposed into different sub bands using NDWT as shown in subsection 7.4.1. The types of wavelet and its order have crucial influence on the effectiveness and accuracy of change/damage detection during the analysis. However, there are no strict rules for selection of wavelets for damage or change detection in SHM. In the previous studies, it was shown that low order wavelet gave the best results (Katunin, 2014). Therefore, low order biorthogonal wavelet was selected to extract features from the signals. With the level L and wavelet selected appropriately, based on NDWT coefficients sets, $A_j[l]$, $D_j[l]$, the principal features at different scales were extracted. Therefore, the characteristics of changes (damage) in both geometric locations in the material were preserved and transformed into NDWT domain. Let the two ultrasonic signals from two pairs of sensors be F_1 and F_2, and F is the fused signal. Simple fusion rules were applied to these coefficients.

Fusion rule plays a vital role in signal level fusion algorithms. Fusion rule is the main processing step that determines the formation of fused multiscale representation from source signals. Most of information (changes, damage) content can be available in low-frequency and high-frequency coefficients, hence the average with baseline modulated fusion rule has been used for fused multiscale representation. Here, F_2 is less influenced by cracks and influenced from noise, therefore, baseline is modulated with signals from F_2 to get optimal fusion output. To compute weighted-averaging fusion rules (7.9) and (7.10) was used.

$$A_j[l] = (A_j[l]F_1 + ((1 - A_j[l]F_m) \cdot A_j[l]F_2))/2, \tag{7.9}$$

$$D_j[l] = (D_j[l]F_1 + ((1 - D_j[l]F_m) \cdot D_j[l]F_2))/2, \tag{7.10}$$

where F_1 represents the signal from sensor pair 1, F_2 represents the signal from the sensor pair 2, and F_m represents the undamaged condition baseline signal. Based on (7.8), the inverse NDWT was performed to reconstruct the fused signal from the combined new feature set $A_j[l]$, $D_j[l]$.

7.4.3 Test results and discussion

The fusion methodology was tested on the structure used for destructive test, as it is easy to verify from the other NDT methods used during this test. The examples of the ultrasonic signals acquired from sensors pair S01R03 (see sensor position in Figure 6.13) are shown in Figure 7.18. It can be seen that at the initial stage, no significant differences were visible in the measured time signals (e.g. for the interval of 0 - 10kN). Then, the amplitude started to decrease with the increase of the external loading.

However, it is difficult to conclude damage/change detection from these raw signals, therefore, it is useful to extract features using signal processing method for the signals registered from sensor pairs..

The interpretation of measured signals in the frequency domain was performed by the Continuous wavelet transform (CWT). This transform was used since CWT is an effective signal processing approach, used to detect changes/cracks in many applications due to very high sensitivity to even tiny disturbances in the time domain signal. However, the CWT feature is sensitive to high energy, in particular case of the multiple cracks initiated between signal path, in consequence, false alarm for crack detection sounded (See Figure 7.3). One of the methods to improve the feature accuracy is to used signal based fusion technique. As the sensors were installed at the top and bottom of the benchmark structure (see Figure 6.13), the influence due to changes in the structure could differ. For this reason, the author analyzed signals from two sensor pairs located across from each other (at the same distance), and then combined the signals using the proposed fusion techniques to compare the improvement.

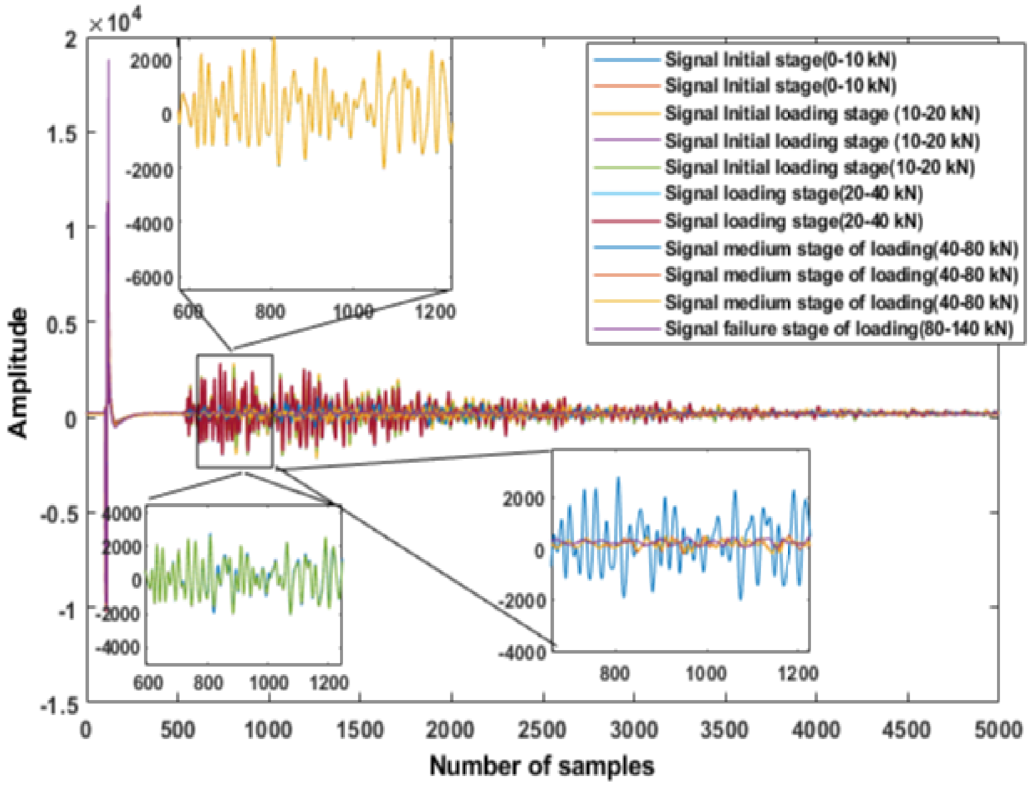

Figure 7.18: Ultrasonic signals from sensor pair 01–03 for different load levels

A CWT-based change matrix was developed to evaluate the changes in the structure and propagation of cracks (details in section 5.1.6). Figures 7.19 and 7.20 shows the CWT coefficient values of the signals registered at sensor pairs S01R03, and S02R04 (see sensor position in Figure 6.13), for the benchmark RC structure. The information about the energy of a signal is derived from the CWT transform and from consecutive measurements of propagating ultrasonic waves. The features extracted from ultrasonic signals analysed in the time-frequency domain is more meaningful than time domain analysis alone. An energy vector was introduced by evaluating the energy of each time interval from the resulting scalogram to show the energy diffusion towards the frequency bands. The first energy coefficient index corresponded to the first stages of wave travelling in the benchmark structure, which was 0.20% with respect to unloaded state of the tested structure. The first wave packet can be clearly seen for signal numbers from $N = 1$ to 30 kN (see Figure 7.19). The results indicate that the coefficients fluctuating as the tensile level increased between 36 kN to 48 kN in the beam, and then it ultimately decreases as the load increased between 49 kN to 60 kN. This is because most of the cracks appeared in the normal direction to the concrete surface. In the second stage, loading schedule between 80 kN to 120 kN, the coefficient was steady, it was obvious as no new cracks appear. The ultrasonic wave propagates in such a direction, nonetheless, that it may miss the cracks. The wavelet coefficients are low in general, since the benchmark structure has been destroyed by the horizontal splitting cracks that discontinued the propagation of ultrasonic waves through the concrete.

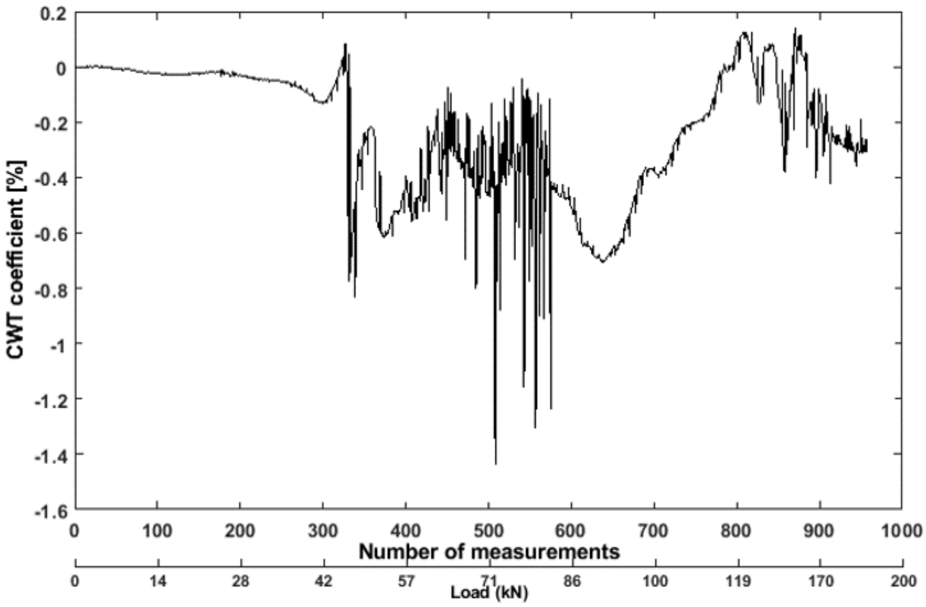

Figure 7.19: Values of CWT coefficient feature from ultrasonic pair S01R03 time histories

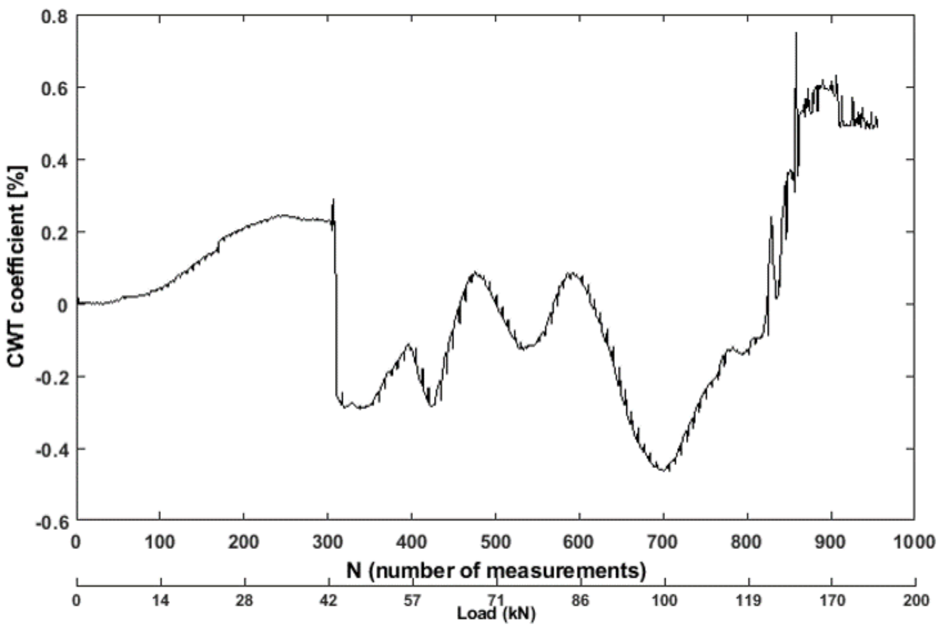

Figure 7.20: Ultrasonic signals from sensor pair S02R04 for different load levels

The result shoed that CWT detected cracks earlier than other features, but the coefficient of this feature fluctuated due to sensitivity to high energy, and in some cases fail

Tab. 7.6: Evaluation of fusion results by SNR.

Signal	S01R03	S02R04	Fused
SNR	-6.8	-7.85	-6.5

to detect damage as compared to undamaged states (Berriman *et al.*, 2006; Chakraborty *et al.*, 2019). Therefore, it could be beneficial to use proposed signal level fusion technique to improve damage detection.

The 1-D ultrasonic signals from both pairs of sensors attached in the benchmark RC structure were processed using the proposed fusion algorithm (see section 7.4.2). The example of the fused ultrasonic signal is shown in Figure 7.21.

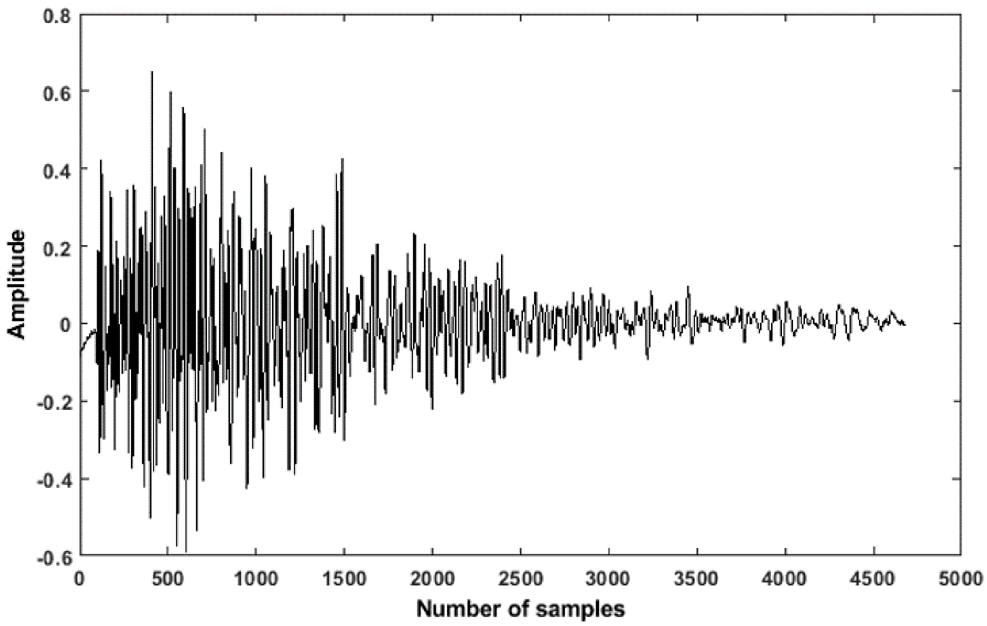

Figure 7.21: Exemplary ultrasonic signal after fusion

To evaluate the SNR for a fused signal, the following formula was used.

$$SNR = \frac{P_s}{P_N} \tag{7.11}$$

The results of fusion clearly show (see Table 7.6) that the fused signal reveals less noise influence than the signals from both pairs of sensors before the application of fusion procedure. One should remember, here this study considering diffuse signal which is a strong reflection dependent on the particles of material.

To evaluate the fused signal, the CWT features were extracted from the fused signal time histories. Figure 7.22, it can be observed that the coefficient decreased as the bending as the level in the beam increased between 30 kN to 40 kN in the beam. The coefficient was fluctuating due to energy attenuation, which was indicating microcracks. The coefficient was much steadier compared to results from both pairs of the sensors, which prevented the growing false alarm rate. As seen in Figure 7.22, the fused signals based on averaging rules enhanced the damage detection to some extent.

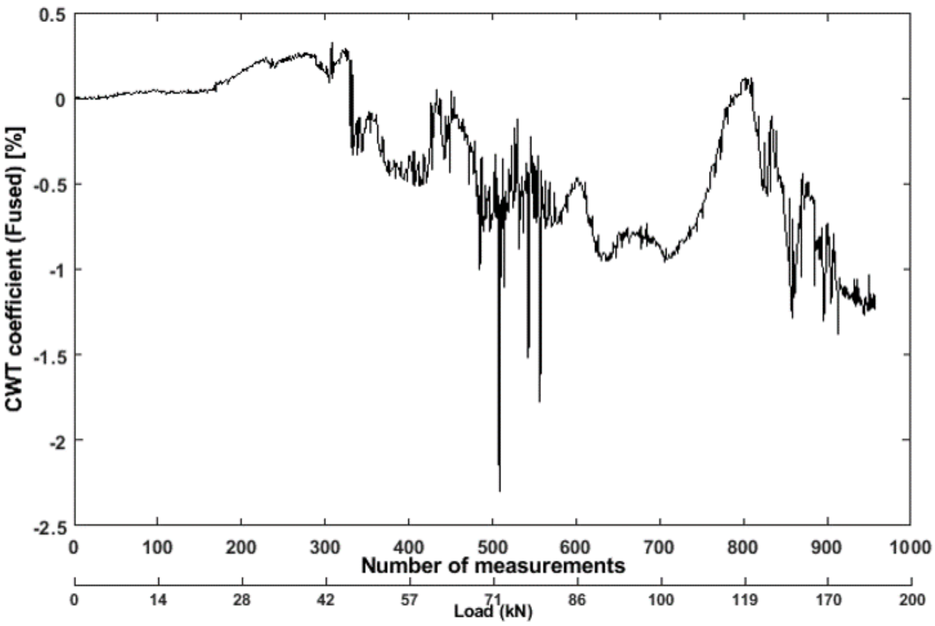

Figure 7.22: Values of CWT coefficient feature from fused ultrasonic signal time histories

The performance of these features is analyzed also using ROC curve (as details in section 7.2.2). The CWT features from the ultrasonic signals (for both pairs) are compared with the fused signal in Figure 7.23 via their ROC curves. The results indicate that all the features represent well in their capability to detect crack opening and propagation as well as several states in the appearance of noise. However, after using the proposed fusion algorithm, the coefficient performs better (AUC= 0.979, see Figure 7.23) to classify damage from the undamaged state in this benchmark structure. Since the most of the cracks appeared in middle part of the beam and few in the side, so this result is not unexpected from the sensor pair S01-R03, because signals affect strongly comparing to the signals recorded in the top pair (S02R04). After averaging the NDWT coefficients of ultrasonic signals by the baseline signal set, the crack information was highlighted more obviously than the other two pairs.

This result can be verified using another NDT technique (DIC) applied during the test (See Figure 6.26a).

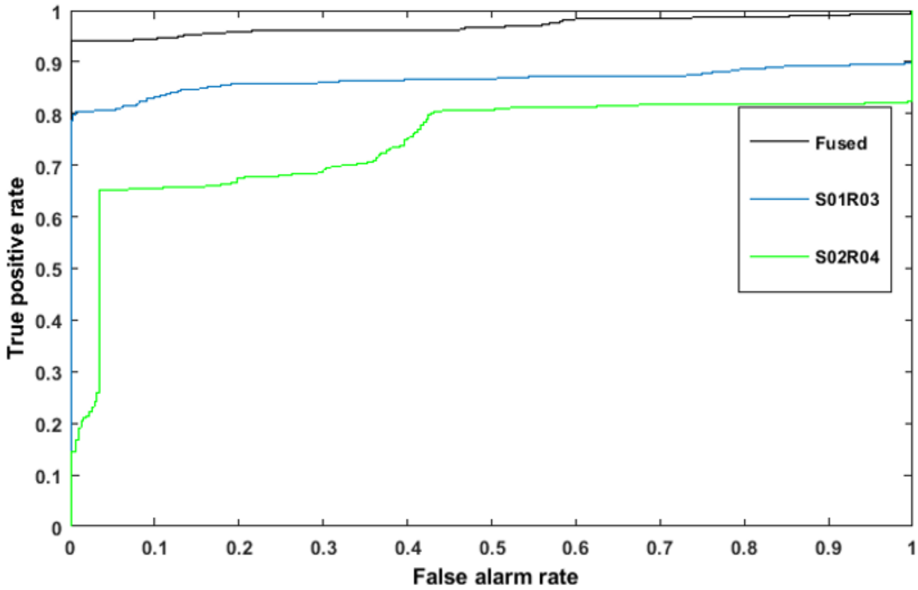

Figure 7.23: Overall results for signal from different pair of sensors and fused signal

7.4.4 Proposed fusion methodology for full scale experiment

The purpose of the field test was to reveal the sensitivity of the presented fusion methodology to detect internal changes in the reference real structure (tensile and compressive stresses).

In order to illustrate the effectiveness of the fusion methodology described above, the CWT features are computed from the time-domain signals collected from two pairs of ultrasonic sensors located on the cross-section E-D (named zone A, see Figure 7.24) and cross-section A-B (named zone B, see Figure 7.24) in the BLEIB structure during the quasi-static load experiment depicted in Figure 7.24. Cross-section E-D was chosen due to location of control cracks (see Figure 6.28) in one of the beams (near to sensor S12R14). However, increase of ultrasonic wave velocity and attenuation is an indicator of initiating cracks, and can be considered as damage index (section 4.2.1). Therefore, the interpretation of the CWT feature comparing with the reference signal, and if there are no operational effects in the structure, then the coefficient of the feature remains low, but sudden decrease of coefficient during different loading stages due to attenuation of the signal, and it considered as a crack opening.

During loading stage, a quasi-static load (39.85 kN) was slowly driven ($12:55 \leq t \leq 14:00$) in several positions of the structure (schedule of the quasi-static loads and positions in the structure are shown in Figure 6.31). The load was driven from the edge of the structure (25 m).

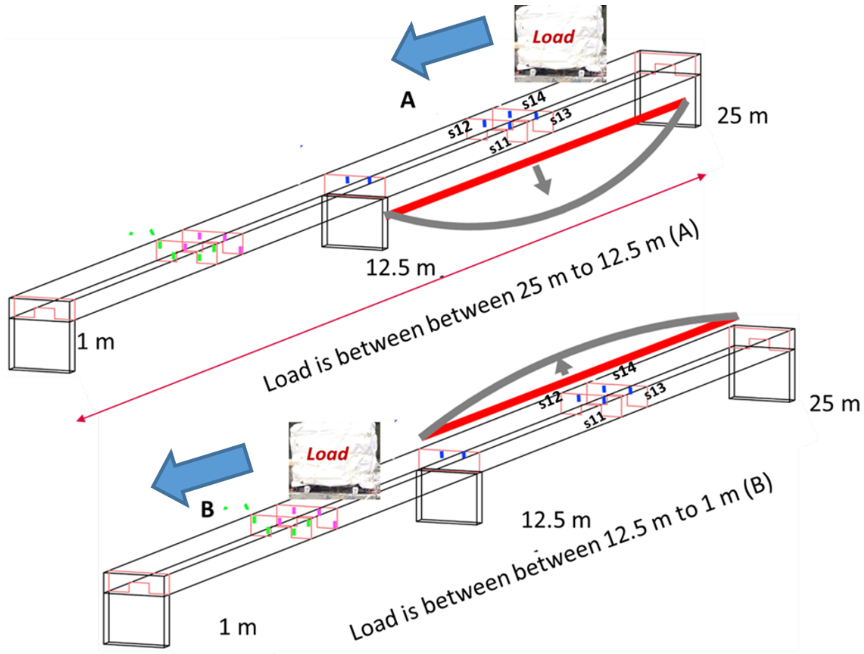

Figure 7.24: Quasi-static load position in the two cross section A and B of BLEIB structure

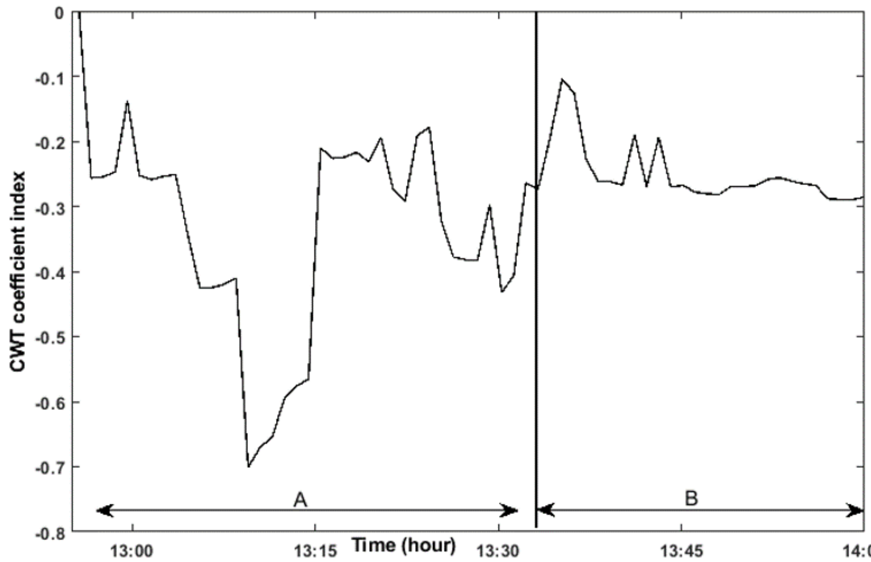

Figure 7.25: CWT coefficient index for S12R14

It can be observed that the CWT feature from both pair of the sensors located in the structure perform well in their ability to detect load. From sensors pair S11R13, one can observe the coefficient changes due to load moving toward the sensor position and even when the load is in zone B (see Figure 7.26). The CWT coefficient from sensor pairs S12R14 is increasing up to a highest value in the zone A (see Figure 7.25), when the load moved to the top sensor pair. On the other hand, CWT coefficient suddenly drops when load comes to near of the sensor pair (sensor pair S12R14). The energy of the signal drops due to attenuation of the recorded signals. Therefore, the anomalies are detected that indication of crack opening. However, when the load driven to cross-section B, still the coefficient is less comparing to sensor pair S11R13.

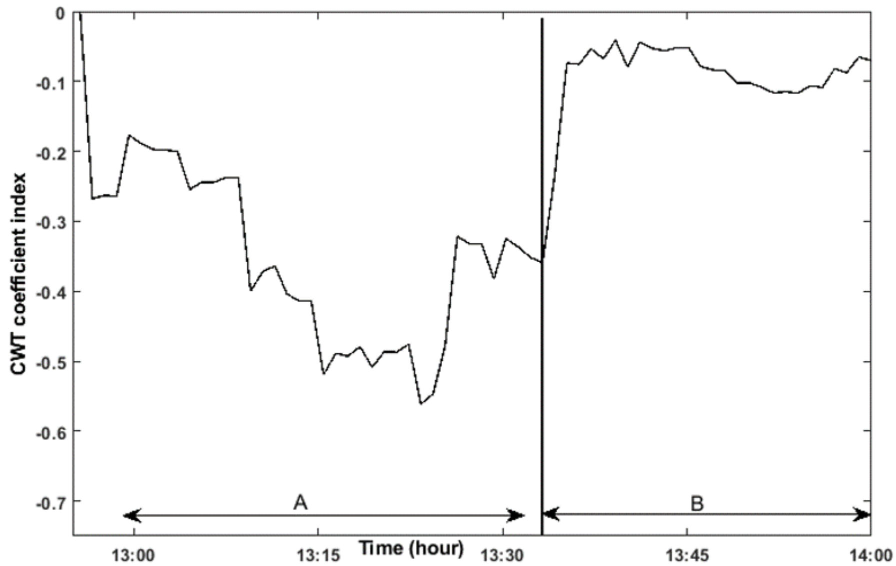

Figure 7.26: CWT coefficient index for S11R13

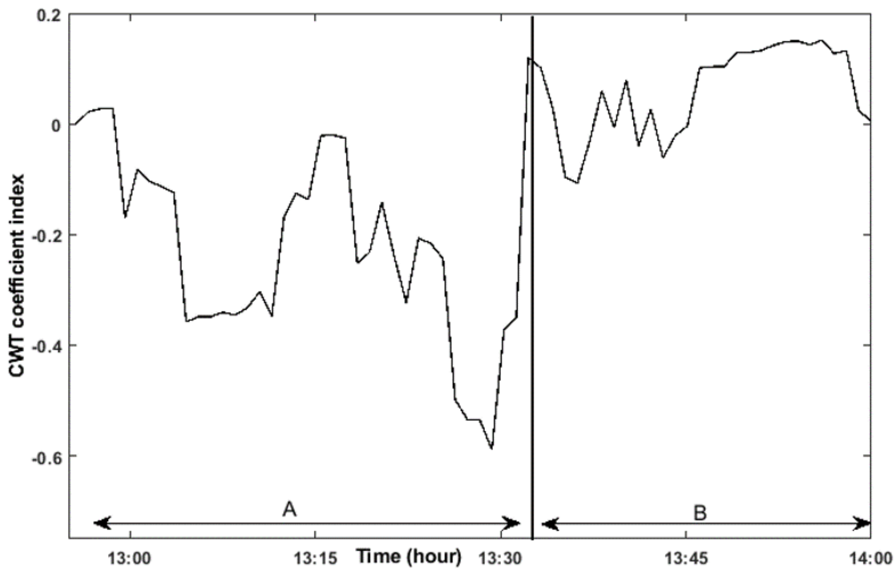

Figure 7.27: Fused coefficient index (S12R14&S11R13)

One can observe the results from both pairs of sensors. The evaluation from single pair of sensors are not comprehensive, as pair S11R13 don't indicate any signature of cracks, and S12R14 shows the crack opening but the coefficient does not increase even when the cracks is closed. Therefore, it can be useful to use proposed fusion methodology detailed in section 7.4.2 to get comprehensive result. The signal from both pair of the sensors is fused using fusion rules indicated in Figure 7.17. To evaluate the fused signals, the CWT feature is computed from the same time histories. One can observe three things from Figure 7.27: the coefficient increases (load moves towards the sensors), then suddenly drops (load on both top sensor pairs) where the crack is visible, and coefficient increases when the cracks are closed (especially load in cross-section B) basing on the CWT coefficient, one the can observe the changes due to tension and compression of the structure.

7.5 Conclusion

The study has shown that the use of features, information, and signal-based fusion improves the overall performance based on the detection capability of a multisensor system, with sensors located in different places of the structure. A technique to declaration of damage and undamaged state was implemented to improve overall decision making. Combining features with FIS was implemented in case of feature based fusion, and its effectiveness was assessed using ROC curves. To determine the fusion strategy for different sensors, the distribution of their values from the strain data could be obtained by computing the percentage of strain changes for the traffic load, and it worked well, detecting not only the mass of the truck but also high traffic load. Further, the signal level fusion was implemented to improve the performance of the feature (where a feature was computed from the same type sensors, but located in different geometrical position). A novel sensor fusion approach was presented to improve damage detection capability based on NDWT. The ability of the sensor fusion to detect cracks in the tested structure was verified.

8. Conclusion and future work

8.1 Concluding remarks

The purpose of the thesis was to increase the possibilities of tools for assessing the technical condition and monitoring of reinforced concrete civil structures, in particular bridges, which are made of concrete and constitute a major part of the transport infrastructure. The diagnosis of such constructions is of key importance in the process of extending their exploitation time, and, consequently, limiting the expenditure of funds for their repair or reconstruction. Therefore, the accuracy of permanently installed embedded ultrasonic sensors was investigated. Various features were extracted from time-domain signals and evaluated using a measurement protocol, and suggestions were made to benefit from extracting multiple features. The overall performance that can be achieved with the data fusion methodology was verified by laboratory destructive experiments, as well as tests on different real objects. One of the most significant and complex parameters (environmental) affecting the precision was also investigated. A signal processing and signal based fusion method were proposed to improve the accuracy of estimated cracks/changes in the structure. A technique of combining features with FIS was implemented for the fusion, and its effectiveness was assessed using ROC curves. To evaluate the fusion strategy for different sensors, the distribution of values from the strain data was obtained by computing the percentage of strain changes for traffic load in the real structure.

This research covered two topics of non destructive ultrasonic testing. After the general background and motivation, the remaining part of this thesis was devoted to new ultrasonic sensors and feature extraction procedures, data acquisition system, experimental validation, and data fusion. In each section, primary research was carried out covering these topics and methodologies for testing based on experimental data were proposed.

The context and basic theory of ultrasonic wave propagation were presented to support this research. It was demonstrated that embedded coupled ultrasonic sensors (permanently installed) had the potential to carry out active measurements better than traditional sensors. The experimental system, allowing transmitting, receiving and scaling the parameters of ultrasonic signals using a Labview application was specially developed for these applications. The author described the first few steps of building an energy model that tunes detection capacity to energy related sensor parameters, such as sample frequency. Although the entire extracted feature performed well detecting changes in all the structures under different load in the presence of noise, a single feature may not be a suitable approach in a real structure. Some of the features failed to detect changes during the load test performed on the real structure due to the complex geometry of the structure. The proposed information based fusion using the voting index provided more accurate results allowing distinguishing between the damaged and undamaged stage. The study has furthermore shown that the use of features and feature-based fusion improves the overall decision making process based on the detection capability of a multi sensor system, with sensors located in different places of the structure. The results were validated using ROC. The capability of the sensor fusion methodology (where signals coming from different locations were combined) to detect cracks in the tested structure was verified.

The contributions and remarks of this study can be summarized as follows:

- An integrated monitoring system which includes traditional gauges and novel ultrasonic measurements was presented.
- The study showed that the sensors location and the crack opening were the two significant factors affecting the fluctuation of the coefficients/index of the embedded sensors.
- The damage was not previously detected by analysing raw signals, but using the proposed algorithm it became detectable.
- Although a feature extracted from a signal may provide suitable detection results, the usage of a single feature may not be the optimal approach for quantifying structural damage due to different influences (such as temperature and humidity) on the measurement.
- The data fusion study shows very interesting results. It has been shown that different levels of fusion improve detectability. Experimental results using proposed fusion methodology showed a probability of detection greater than 94% when detecting cracks initiated by quasi static load.
- This research presented an effective tool using an embedded monitoring system to diagnose large structures, such as real bridges.
- The large-scale bridge structure was tested to verify the sensitivity of the embedded sensors. The applied approach allowed to precisely observe various loading scenarios, which proves their superiority in structural health monitoring. Moreover, the applied sensor network revealed its durability and high measurement precision, which additionally proves the possibility of long term monitoring of concrete structures.

- The developed methodology (in the thesis proposed in section 3.3) can effectively monitor large structure and is suitable for long term monitoring.

Considering the above-presented findings and contributions, one can state that the developed methodology, which is based on a combination of signal processing and data fusion from measurement devices, can be used for effective monitoring and early detection of structural changes of large concrete structures. This justifies the thesis presented in section 3.3.

8.2 Recommendations for future work

Although it was shown that sensors and proposed methodology presented in this thesis were capable of accurately monitoring the structure. Nevertheless, the optimal distance between ultrasonic sensors and their effect on detectability needs to be investigated. There is significant potential in using these sensors for bridge monitoring. However, in the future, it will be useful to design wireless data acquisition equipment for active measurements, which can scale the energy based on requirements (using the presented research knowledge). In further studies, an automatic application that can provide a threshold-based alarm should be taken into consideration. Data fusion shows promising results. However, more research work is needed with respect to the use of different types of required data fusion for particular circumstances. The influence of sensor fusion on long term monitoring needs to be investigated. In addition, data from more than two transducer pairs located in the same area can be investigated to study the boundaries of signal-level fusion. The parameters of ultrasonic sensors for long term monitoring in the real structure will be in the focus of further studies. Advanced signal processing for digital noise reduction (with oversampled signals) and classification should be considered as the focus of further studies.

Bibliography

Abdel-Qader I., Pashaie-Rad S., Abudayyeh O. and Yehia S. (2006): *PCA-Based algorithm for unsupervised bridge crack detection.* Advances in Engineering Software **37**(12): pp. 771–778.

Accelerometer Description (2017): `https://www.dimensionengineering.com/info/accelerometers`. Accessed: 2017-09-30.

Al-Adnani N. N. A., Mustapha F., Sapuan S. and Saifulnaz M. R. (2016): *Structural health monitoring and damage identification for composite panels using smart sensor.* Journal of Intelligent Material Systems and Structures **27**(17): pp. 2313–2323.

Alfalou A., Brosseau C., Abdallah N. and Jridi M. (2011): *Simultaneous fusion, compression, and encryption of multiple images.* Optics Express **19**(24): pp. 24023.

Alguri K. S., Michaels J. E. and Harley J. B. (2017): *Robust baseline subtraction for ultrasonic full wavefield analysis.* AIP Conference Proceedings **1806**(1).

Aliustaoglu C., Ertunc H. M. and Ocak H. (2009): *Tool wear condition monitoring using a sensor fusion model based on fuzzy inference system.* Mechanical Systems and Signal Processing **23**(2): pp. 539–546.

Allen D. W., Sohn H., Worden K. and Farrar C. R. (2002): *Utilizing the sequential probability ratio test for building joint monitoring.* In: Nondestructive Evaluation and Health Monitoring of Aerospace Materials and Civil Infrastructures, A. L. Gyekenyesi, S. M. Shepard, D. R. Huston, A. E. Aktan and P. J. Shull (Eds). Vol. 4704. SPIE.

Aranguren G., Etxaniz J., Barrera E., Ruiz M., A Olivares M., Taboada I., Urrutia A. and Melendez R. (2016): *Structural Health Monitoring Ultrasound System.* 8th European Workshop On Structural Health Monitoring. EWSHM 2016. Spain, Bilbao.

Atorod Azizinamini, Sharon S. Baum Kuska P. B. and Hatfield E. (1994): *Seismic behavior of square high-strength concrete columns.* ACI Structural Journal **91**(3): pp. 336–345.

Bakhshizade A. and Reza, Ashory M. (2015): *Root mean square error criterion using operational deflection shape curvature for structural damage detection.* Mathematical Models in Engineering **1**(2): pp. 96–101.

Bao Y., Li H., An Y. and Ou J. (2019): *Dempster-Shafer evidence theory approach to structural damage detection.* Structural Health Monitoring **11**(1): pp. 13–26.

Barai R. K., Tjahjowidodo T. and Pappachan B. K. (2015): *Fuzzy inference system based intelligent sensor fusion for estimation of surface roughness in machining process.* 2015 9th International Conference on Sensing Technology (ICST). IEEE. Auckland, New Zealand: pp. 799–802.

Barnby J. T., Nadkarni A. S. and Cresswell S. L. (2014): *Experimental determination of crack tip angles (CTOA) and their applicability to instability prediction in structures.* International Journal of Materials and Product Technology **10**(1–2): pp. 161–170.

Barua A., Mudunuri L. S. and Kosheleva O. (2014): *Why trapezoidal and triangular membership functions work so well: towards a theoretical explanation.* Journal of Uncertain Systems **8**: pp. 164–168.

Bastidas-Arteaga E. (2018): *Reliability of reinforced concrete structures subjected to corrosion-fatigue and climate change.* International Journal of Concrete Structures and Materials **12**(1).

Bastien Masse M. (2015): *Structural Behavior of R-UHPFRC - RC Composite Slabs.*

Benavent-Climent A., Gallego A. and Vico J. M. (2011): *An acoustic emission energy index for damage evaluation of reinforced concrete slabs under seismic loads.* Structural Health Monitoring **11**(1): pp. 69–81.

Berriman J., Hutchins D., Neild A., Gan T. and Purnell P. (2006): *The application of time-frequency analysis to the air-coupled ultrasonic testing of concrete.* IEEE Transactions on Ultrasonics, Ferroelectrics and Frequency Control **53**(4): pp. 768–776.

Bień J. (2010): *Uszkodzenia i diagnostyka óbiektow mostowych (Polish Edition).* Wydawnictwa Komunikacji i Łacznosci WKŁ.

Bień J., Kużawa M., Gładysz-Bień M. and Kamiński T. (2016): *Quality control of road bridges in Poland.* CRC Press. Foz do Iguacu, Brazil.

Brigante M. and Sumbatyan M. A. (2013): *Acoustic methods for the nondestructive testing of concrete: A review of foreign publications in the experimental field.* Russian Journal of Nondestructive Testing **49**(2): pp. 100–111.

Burdet O. L. (2010): *Thermal Effects in the Long-Term Monitoring of Bridges.* IABSE Symposium Report **97**(19): pp. 62–68.

Büyüköztürk O. and Taşdemir M. A. (2013): *Nondestructive Testing of Materials and Structures.* Springer Netherlands.

Capineri L., Giannelli P., Calabrese G., Granato M. and Frattini G. (2018): *Design, realization and characterization of a differential charge amplifier for ultrasonic piezopolymer transducers.* 2018 IEEE International Ultrasonics Symposium (IUS): pp. 1–5.

Casas J. R. and Rodrigues F. (2015): *Bridge Condition and Safety Based on Measured Vibration Level*. IABSE Symposium Report **103**(8): pp. 12–29.

Catbas N., Susoy M. and Frangopol D. (2008): *Structural health monitoring and reliability estimation: long span truss bridge application with environmental monitoring data*. Engineering Structures **30**: pp. 2347–2359.

Cavalline T. L., Calamusa J. T., Kitts A. M. and Tempest B. Q. (2017): *Field-Observed Cracking of Paired Lightweight and Normalweight Concrete Bridge Decks*. International Journal of Concrete Structures and Materials **11**(1): pp. 85–97.

Cegla F. B., Cawley P., Allin J. and Davies J. (2011): *High-temperature (500°C) wall thickness monitoring using dry-coupled ultrasonic waveguide transducers*. IEEE Transactions on Ultrasonics, Ferroelectrics and Frequency Control **58**(1): pp. 156–167.

Chakraborty J. and Katunin A. (2019a): *Detection of structural changes in concrete using embedded ultrasonic sesnsors based on autoregressive model*. Diagnostyka **20**(1): pp. 103–110.

Chakraborty J. and Katunin A. (2019b): *Sensor fusion approach for damage detection in RC structures*. Journal of Nondestructive Evaluation . submitted (under review).

Chakraborty J., Katunin A., Klikowicz P. and Salamak M. (2019): *Early Crack Detection of Reinforced Concrete Structure Using Embedded Sensors*. Sensors **19**(18): pp. 3879.

Chakraborty J., Katunin A., Klikowicz P. and Salamak M. (2019a): *Embedded ultrasonic transmission sensors and signal processing techniques for structural change detection in the Gliwice bridge*. Procedia Structural Integrity **17**: pp. 387–394.

Chakraborty J., Ottoy G., Gelaude M., Goemaere J.-P. and Strycker L. D. (2014): *Acoustic localization of unknown sources with wireless sensor nodes*. 2014 17th International Conference on Computer and Information Technology (ICCIT). IEEE: pp. 488–493.

Chakraborty. J., Ottoy G., Goemaere J.-P. and Strycker L. D. (20-2): *Modeling acoustic localization accuracy for scalable energy consumption in wireless sensor swarms*. 2014 Ubiquitous Positioning Indoor Navigation and Location Based Service (UPINLBS): pp. 164–169.

Chakraborty J., Stoliński M. and Katunin A. (2019b): *Addressing the detection capability for scalable energy consumption using primary data acquisition system of embedded ultrasonic sensors in SHM*. Proceedings of the 5th International Conference on Advances in Electrical Engineering (ICAEE). IEEE. Dhaka, Bangladesh. Accepted.

Chakraborty J., Varma J. V. K. C. and Erman M. (2013): *ANFIS based opportunistic power control for cognitive radio in spectrum sharing*. 2013 International Conference on Electrical Information and Communication Technology (EICT). Khulna, Bangladesh: pp. 1–6.

Chen J., Li P., Song G. and Ren Z. (2016): *Piezo-based wireless sensor network for early-age concrete strength monitoring*. Optik **127**(5): pp. 2983–2987.

Chen W. and Lui E. (Eds) (2005): *Handbook of Structural Engineering*. CRC Press. New York, US.

Chidambaram R. S. and Thirugnanam G. S. (2012): *Comparative Study on Behaviour of Reinforced Beam-Column Joints with Reference to Anchorage Detailing*. Journal of Civil Engineering Research **2**(4): pp. 12–17.

Choi M. (2006): *A new intensity-hue-saturation fusion approach to image fusion with a tradeoff parameter*. IEEE Transactions on Geoscience and Remote Sensing **44**(6): pp. 1672–1682.

Chong S. Y., Shrestha M. and Lee J.-R. (2014): *Development of Wireless Ultrasonic Propagation Imaging System for In-Situ Aircraft Inspection*. 7th European Workshop on Structural Health Monitoring. EWSHM. Nantes, France.

Claisse P. A. (2016): Strength of materials. Civil Engineering Materials. Butterworth-Heinemann. Boston, US. chapter 2, : pp9–22.

Clark G. A. (2008): *Cable Damage Detection Using Time Domain Reflectometry and Model-Based Algorithms*. Sixth Annual Sensors Workshop. Lawrence Livermore National Laboratory. Livermore, CA (United States).

Concu G. and Trulli N. (2018): *Concrete Defects Sizing by Means of Ultrasonic Velocity Maps*. Buildings **8**(12): pp. 176.

Connor J. J. and Faraji S. (2016): *Fundamentals of Structural Engineering*. 2 edn. Springer. Switzerland.

Croxford A., Wilcox P., Drinkwater B. and Konstantinidis G. (2007): *Strategies for guided-wave structural health monitoring*. Proceedings of the Royal Society A: Mathematical, Physical and Engineering Sciences **463**(2087): pp. 2961–2981.

D'Ambrosio A., Aria M. and Siciliano R. (2012): *Accurate Tree-based Missing Data Imputation and Data Fusion within the Statistical Learning Paradigm*. Journal of Classification **29**(2): pp. 227–258.

D'Antino T., Carloni C., Sneed L. H. and Pellegrino C. (2015): *Fatigue and post-fatigue behavior of PBO FRCM-concrete joints*. International Journal of Fatigue **81**: pp. 91–104.

de Vera C. P. and Güemes J. A. (1998): *Embedded Self-Sensing Piezoelectric for Damage Detection*. Journal of Intelligent Material Systems and Structures **9**(11): pp. 876–882.

Deng L. and Cai C. S. (2007a): *Applications of fiber optic sensors in civil engineering*. Structural Engineering and Mechanics **25**.

Deng L. and Cai C. S. (2007b): *Applications of fiber optic sensors in civil engineering*. Structural Engineering and Mechanics **25**(5): pp. 577–596.

Ellmauthaler A., Pagliari C. L. and da Silva E. A. B. (2013): *Multiscale Image Fusion Using the Undecimated Wavelet Transform With Spectral Factorization and Nonorthogonal Filter Banks*. IEEE Transactions on Image Processing **22**(3): pp. 1005–1017.

ElSafty A., Graeff M. K. and Fallaha S. (2014): *Behavior of Laterally Damaged Prestressed Concrete Bridge Girders Repaired with CFRP Laminates Under Static and Fatigue Loading*. International Journal of Concrete Structures and Materials **8**(1): pp. 43–59.

Ensminger D. and Bond L. J. (2011): *Ultrasonics: Fundamentals, Technologies, and Applications*. third edition edn. CRC Press.

Eurocode E. C. (2005): *EN 1992-1-1 Eurocode 2: Design of concrete structures - Part 1-1: General ruels and rules for buildings*. Eurocode 2 for Standardisation. EN. CEN. Brussels.

Fawcett T. (2006): *An introduction to ROC analysis*. Pattern Recognition Letters **27**(8): pp. 861–874.

Ferraris M. (2018): Immagine del Ponte Morandi. CC BY-SA 4.0 (https://creativecommons.org/licenses/by-sa/4.0). Retrieved from `https://commons.wikimedia.org/wiki/File:Il_Ponte_Morandi_dopo_il_crollo,_visto_da_Est,_panoramica.jpg`.

Figueiredo E., Figueiras J., Park G., Farrar C. R. and Worden K. (2010): *Influence of the Autoregressive Model Order on Damage Detection*. Computer-Aided Civil and Infrastructure Engineering **26**(3): pp. 225–238.

Fröjd P. and Ulriksen P. (2017): *Frequency selection for coda wave interferometry in concrete structures*. Ultrasonics **80**: pp. 1–8.

Fu G. (Ed.) (2005): *Inspection and Monitoring Techniques for Bridges and Civil Structures*. Woodhead. Cambridge, England.

Gajewski T. and Garbowski T. (2014): *Calibration of concrete parameters based on digital image correlation and inverse analysis*. Archives of Civil and Mechanical Engineering **14**(1): pp. 170–180.

Galal K., Arafa A. and Ghobarah A. (2005): *Retrofit of RC square short columns*. Engineering Structures **27**(5): pp. 801–813.

Garzón-Roca J., Ruiz-Pinilla J., Adam J. M. and Calderón P. A. (2011): *An experimental study on steel-caged RC columns subjected to axial force and bending moment*. Engineering Structures **33**(2): pp. 580–590.

Ghosh S. N. (1991): *Cement and concrete science and technology.*. ABI Books Private Ltd. New Delhi.

Grattan-Bellew P. E. (1996): *Microstructural investigation of deteriorated Portland cement concretes*. Construction and Building Materials **10**(1): pp. 3–16.

Graybeal B. A., Phares B. M., Rolander D. D., Moore M. and Washer G. (2002): *Visual Inspection of Highway Bridges*. Journal of Nondestructive Evaluation **21**(3): pp. 67–83.

Grêt A., Snieder R. and Scales J. (2006): *Time-lapse monitoring of rock properties with coda wave interferometry*. Journal of Geophysical Research: Solid Earth **111**(B3): pp. n/a–n/a.

Gros X. (1997): Data Fusion – A Review. NDT Data Fusion. Elsevier. chapter 2, : pp5–42.

Gros X. E. (2001): Pixel Level NDT Data Fusion. Applications of NDT Data Fusion. Springer US. Boston, MA: pp. 25–57.

Gros X., Liu Z., Tsukada K. and Hanasaki K. (2000): *Experimenting with pixel-level NDT data fusion techniques*. IEEE Transactions on Instrumentation and Measurement **49**(5): pp. 1083–1090.

Gu H., Song G., Dhonde H., Mo Y. L. and Yan S. (2006): *Concrete early-age strength monitoring using embedded piezoelectric transducers*. Smart Materials and Structures **15**(6): pp. 1837–1845.

Hallaji M., Seppänen A. and Pour-Ghaz M. (2014): *Electrical impedance tomography-based sensing skin for quantitative imaging of damage in concrete*. Smart Materials and Structures **23**(8): pp. 085001.

Harding J. E., Parke G. A. R. and Ryall M. J. (Eds) (1990): *Bridge Management*. Springer. Dordrecht, Netherlands.

Heideklang R. and Shokouhi P. (2013): *Application of data fusion in nondestructive testing (NDT)*. Proceedings of the 16th International Conference on Information Fusion. Istanbul, Turkey: pp. 835–841.

Heideklang R. and Shokouhi P. (2015): *Multi-sensor image fusion at signal level for improved near-surface crack detection*. NDT & E International **71**: pp. 16–22.

Hellier C. (2012): *Handbook of Nondestructive Evaluation*. second edn. McGraw-Hill Education - Europe.

Hoła J. (1999): *Acoustic-emission investigation of failure of high strength concrete*. Archives of Acoustics **24**(2): pp. 233–244.

Holnicki-Szulc J. and Soares C. (Eds) (2004): *Advances in Smart Technologies in Structural Engineering*. 1 edn. Springer. Berlin Heidelberg.

Hoon S., Czarnecki Jerry A. and Farrar Charles R. (2019): *Structural Health Monitoring Using Statistical Process Control*. Journal of Structural Engineering **126**(11): pp. 1356–1363.

Hossny M., Nahavandi S. and Crieghton D. (2008): Feature-Based Image Fusion Quality Metrics. Intelligent Robotics and Applications. Springer Berlin Heidelberg: pp. 469–478.

Hsu H.-H., Yang A. C. and Lu M.-D. (2011): *KNN-DTW Based Missing Value Imputation for Microarray Time Series Data*. Journal of Computers **6**(3): pp. 418–425.

Hu X., Wang B. and Ji H. (2012): *A Wireless Sensor Network-Based Structural Health Monitoring System for Highway Bridges*. Computer-Aided Civil and Infrastructure Engineering **28**(3): pp. 193–209.

Huang X.-Y., Li W., Chen K., Xiang X.-H., Pan R., Li L. and Cai W.-X. (2013): *Multi-Matrices Factorization with Application to Missing Sensor Data Imputation*. Sensors **13**(11): pp. 15172–15186.

Hughes D. S. and Kelly J. L. (1953): *Second-Order Elastic Deformation of Solids*. Physical Review **92**(5): pp. 1145–1149.

Hui L. I. and Jinping O. U. (2011): *Structural Health Monitoring: From Sensing Technology Stepping to Health Diagnosis*. Procedia Engineering **14**: pp. 753–760.

Hwang S.-J., Lee H.-J., Liao T.-F., Wang K.-C. and Tsai H.-H. (2005): *Role of hoops on shear strength of reinforced concrete beam-column joints*. ACI Structural Journal **102**: pp. 445–453.

Iffland J. S. B. and Birnstiel C. (1993): *2- Causes of bridge deterioration*. Thomas Telford: pp. 8–18.

Islam M. M., Soualihou N. N. and Faizullah S. (2018): *Structural Health Monitoring by Payload Compression in Wireless Sensors Network: An Algorithmic Analysis*. International Journal of Engineering and Management Research **8**(3): pp. 184–190.

Jiang R., Jauregui D. and White K. (2008): *Close-range photogrammetry applications in bridge measurement: literature review*. Measurement **41**: pp. 823–834.

Jin J., Moreno M. G., Riviere J. and Shokouhi P. (2017): *Impact-Based Nonlinear Acoustic Testing for Characterizing Distributed Damage in Concrete*. Journal of Nondestructive Evaluation **36**(3): pp. 51.

Jinsong Z. and Qingling M. (2019): *Effective and Fine Analysis for Temperature Effect of Bridges in Natural Environments*. Journal of Bridge Engineering **22**(6): pp. 04017017.

Karaiskos G., Deraemaeker A., Aggelis D. G. and Hemelrijck D. V. (2015): *Monitoring of concrete structures using the ultrasonic pulse velocity method*. Smart Materials and Structures **24**(11): pp. 113001.

Karaiskos G., Tsangouri E., Aggelis D. G., Van Tittelboom K., De Belie N. and Van Hemelrijck D. (2016): *Damage detection and healing performance monitoring using embedded piezoelectric transducers in large-scale concrete structures*. 19th World Conference on Non-Destructive Testing. Munich, Germany: pp. 1–8.

Karlsson B. (1998): *Fuzzy measures for sensor data fusion in industrial recycling*. Measurement Science and Technology **9**(6): pp. 907–912.

Katunin A. (2014): *Damage identification based on stationary wavelet transform of modal data*. Modelowanie Inżynierskie **20**(51): pp. 35–41.

Katunin A. (2015a): *Diagnostics of Composite Structures Using Wavelets*. The Publishing House of the Institute for Sustainable Technologies – National Research Institute. Gliwice.

Katunin A. (2015b): *Nondestructive Damage Assessment of Composite Structures Based on Wavelet Analysis of Modal Curvatures: State-of-the-Art Review and Description of Wavelet-Based Damage Assessment Benchmark*. Shock and Vibration **2015**: pp. 735219.

Ketelaar V. B. H. G. (2009): *Satellite Radar Interferometry*. Springer. Heidelberg, Germany.

Kindrachuk V. M., Thiele M. and Unger J. F. (2015): *Constitutive modeling of creep-fatigue interaction for normal strength concrete under compression*. International Journal of Fatigue **78**: pp. 81–94.

Klikowicz P., Salamak M. and Poprawa G. (2016): *Structural Health Monitoring of Urban Structures*. Procedia Engineering **161**: pp. 958–962.

Knitter-Piątkowska A., Guminiak M. J. and Przychodzki M. (2016): *Application of Discrete Wavelet Transformation to Defect Detection in Truss Structures with Rigidly Connected Bars*. Engineering Transactions **64**(2): pp. 157–170.

Kolsky H. (1964): *Stress waves in solids*. Journal of Sound and Vibration **1**(1): pp. 88–110.

Komlos K., Popovics S., Nürnbergerová T., Babál B. and Popovics J. S. (1996): *Ultrasonic pulse velocity test of concrete properties as specified in various standards*. Cement and Concrete Composites **18**(5): pp. 357–364.

Kozicki J. and Tejchman J. (2007): *Experimental Investigations of Strain Localization in Concrete using Digital Image Correlation (DIC) Technique*. Archives of Hydroengineering and Environmental Mechanics **54**(1): pp. 3–24.

Krautkraamer J. and Krautkraamer H. (1990): *Ultrasonic Testing of Materials*. Springer. Berlin, Heidelberg, Germany.

Kwon S.-J., Shin S., Lee H. S. and Park Y.-H. (2003): *Design of accelerometer layout for structural monitoring and damage detection*. KSCE Journal of Civil Engineering **7**(6): pp. 717–724.

L. Rose J. and Nagy P. (2000): *Ultrasonic Waves in Solid Media*. Journal of The Acoustical Society of America **107**(4): pp. 1807–1808.

Larose E. and Hall S. (2019): *Monitoring stress related velocity variation in concrete with a 2×10-5 relative resolution using diffuse ultrasound*. The Journal of the Acoustical Society of America **125**(4): pp. 1853–1856.

Li H. and Ou J. (2016): *The state of the art in structural health monitoring of cable-stayed bridges*. Journal of Civil Structural Health Monitoring **6**(1): pp. 43–67.

Li H., Dong Z., Ouyang Z., Liu B., Yuan W. and Yin H. (2019): *Experimental Investigation on the Deformability, Ultrasonic Wave Propagation, and Acoustic Emission of Rock Salt Under Triaxial Compression*. Applied Sciences **9**(4): pp. 635.

Liggins M. E., Hall D. L. and Llinas J. (2017): *Handbook of multisensor data fusion : theory and practice*. CRC Press. Boca Raton, Florida, US.

Liu Q. C. and Wang H.-P. B. (2001): *A case study on multisensor data fusion for imbalance diagnosis of rotating machinery*. Artificial Intelligence for Engineering Design, Analysis and Manufacturing **15**(3): pp. 203–210.

Lorenzi A., Tisbierek F. and Silva Filho L. C. (2007): *Ultrasonic pulse velocity analysis in concrete specimens*. IV Conferencia Panamericana de END Buenos Aires. Buenos Aires.

Lu G., Feng Q., Li Y., Wang H. and Song G. (2017): *Characterization of Ultrasound Energy Diffusion Due to Small-Size Damage on an Aluminum Plate Using Piezoceramic Transducers*. Sensors **17**(12): pp. 2796.

Lu Y. and Michaels J. E. (2005a): *A methodology for structural health monitoring with diffuse ultrasonic waves in the presence of temperature variations*. Ultrasonics **43**(9): pp. 717–731.

Lu Y. and Michaels J. E. (2005b): *A methodology for structural health monitoring with diffuse ultrasonic waves in the presence of temperature variations.* Ultrasonics **43**(9): pp. 717–731.

Luo J. and Konofagou E. E. (2010): *A fast normalized cross-correlation calculation method for motion estimation.* IEEE Transactions on Ultrasonics, Ferroelectrics, and Frequency Control **57**(6): pp. 1347–1357.

Maizuar M., Zhang L., Miramini S., Mendis P. and Thompson R. G. (2017): *Detecting structural damage to bridge girders using radar interferometry and computational modelling.* Structural Control and Health Monitoring **24**(10): pp. e1985.

Malekjafarian A., Golpayegani F., Moloney C. and Clarke S. (2019): *A Machine Learning Approach to Bridge-Damage Detection Using Responses Measured on a Passing Vehicle.* Sensors **19**(18): pp. 4035.

Malhotra V. and Carino N. J. (2003): *Handbook on Nondestructive Testing of Concrete.* CRC Press. West Conshohocken, US.

Matsagar V., Eslamian S., Ostad-Ali-Askari K., Raeisi M., Lee G., Pazdar S. and Bagheri-Basmenji A. (2018): Bridges. Encyclopedia of Earth Sciences Series. Springer International Publishing. Cham: pp. 1–20.

Mcneill D. K. (2009): 9 - Data management and signal processing for structural health monitoring of civil infrastructure systems. Structural Health Monitoring of Civil Infrastructure Systems. Elsevier: pp. 283–304.

Menn C. (1990): *Prestressed Concrete Bridges.* Springer-Verlag. Vienna, Austria.

Metz C. E. (2019): *Receiver Operating Characteristic Analysis: A Tool for the Quantitative Evaluation of Observer Performance and Imaging Systems.* Journal of the American College of Radiology **3**(6): pp. 413–422.

Michaels J. E. (2008): *Detection, localization and characterization of damage in plates with anin situarray of spatially distributed ultrasonic sensors.* Smart Materials and Structures **17**(3): pp. 035035.

Miller S., Chakraborty J., van der Vegt J., Brinkerink D., Erkens S., Liu X., Anupam K., Sluer B. and Mohajeri M. (2017): *Smart sensors in asphalt: monitoring key process parameters during and post construction.* SPOOL **4**(2): pp. 45–48.

Mina M., Udpa S. S., Udpa L. and Yim J. (1997): *A New Approach for Practical Two Dimensional Data Fusion Utilizing a Single Eddy Current Probe.* Springer US. Boston, MA.

Moll J., Kexel C., Pötzsch S., Rennoch M. and Herrmann A. S. (2019): *Temperature affected guided wave propagation in a composite plate complementing the Open Guided Waves Platform*. Scientific Data **6**(1): pp. 191.

Morandi Genoa bridge: Towers demolished after evacuations (2019): `https://www.bbc.com/news/world-europe-48790056`. Accessed: 2019-03-27.

Mosley W. H. and Bungey J. H. (1987): Properties of Reinforced Concrete. Reinforced Concrete Design. third edn. Macmillan Education. Hampshire, UK: pp. 1–14.

Moughty J. J. and Casas J. R. (2017): *Performance assessment of vibration parameters as damage indicators for bridge structures under ambient excitation*. Procedia Engineering **199**: pp. 1970–1975. X International Conference on Structural Dynamics, EURODYN 2017.

Murnaghan F. D. (1937): *Finite Deformations of an Elastic Solid*. American Journal of Mathematics **59**(2): pp. 235.

Nassif H. H., Gindy M. and Davis J. (2005): *Comparison of laser Doppler vibrometer with contact sensors for monitoring bridge deflection and vibration*. NDT & E International **38**(3): pp. 213–218.

Nguyen V. H., Mahowald J., Golinval J.-C. and Maas S. (2014): Damage Detection in Civil Engineering Structure Considering Temperature Effect. Dynamics of Civil Structures. Vol. 4. Springer. London, UK: pp. 187–196.

Ni F., Zhang J. and Chen Z. (2018): *Pixel-level crack delineation in images with convolutional feature fusion*. Structural Control and Health Monitoring **26**(1): pp. e2286.

Niederleithinger E. and Wunderlich C. (2013): *Influence of small temperature variations on the ultrasonic velocity in concrete*. AIP Conference Proceedings **1511**(1): pp. 390–397.

Niederleithinger E., Wolf J., Mielentz F., Wiggenhauser H. and Pirskawetz S. (2015): *Embedded Ultrasonic Transducers for Active and Passive Concrete Monitoring*. Sensors **15**(5): pp. 9756–9772.

Njoku E. G. (Ed.) (2014): *Encyclopedia of Remote Sensing*. Springer. New York, US.

Osman A., Kaftandjian V. and Hassler U. (2014): *Improving the reliability of NDT inspection through information fusion: applications in X-ray and ultrasound modalities*. European Conference on Non Destructive Testing. Prague, Czech Republic: pp. 1–6.

Pagani R., Bocciarelli M., Carvelli V. and Pisani M. A. (2014): *Modelling high temperature effects on bridge slabs reinforced with GFRP rebars*. Engineering Structures **81**: pp. 318–326.

Payan C., Garnier V. and Moysan J. (2010): *Potential of Nonlinear Ultrasonic Indicators for Nondestructive Testing of Concrete.* Advances in Civil Engineering **2010**(238472): pp. 1–8.

Pedersen A., Mikkelsen E., Cronin-Fenton D., Kristensen N., Pham T. M., Pedersen L. and Petersen I. (2017): *Missing data and multiple imputation in clinical epidemiological research.* Clinical Epidemiology **9**: pp. 157–166.

Peng Z. and Chu F. (2004): *Application of the wavelet transform in machine condition monitoring and fault diagnostics: a review with bibliography.* Mechanical Systems and Signal Processing **18**(2): pp. 199–221.

Peterson M. L., Landis E. and Achenbach J. D. (1995): Ultrasonic Evaluation of Damage in Concrete Bridge Deck Pavements. Review of Progress in Quantitative Nondestructive Evaluation. Springer. New York, US: pp. 2169–2176.

Poupinet G., Ratdomopurbo A. and Coutant O. (1996): *On the use of earthquake multiplets to study fractures and the temporal evolution of an active volcano.* Annals of Geophysics **39**(2): pp. 253–264.

Priestley M. J. N. (1985): *Long term observations of concrete structures analysis of temperature gradient effects.* Materials and Structures **18**(4): pp. 309–316.

Proceq products web-site (2019): `https://www.proceq.com/compare/pundit-ultrasonic-pulse-velocity-and-pulse-echo-testing`. Accessed: 18/09/2019.

Qiao L. and Esmaeily A. (2011): *An Overview of Signal-Based Damage Detection Methods.* Applied Mechanics and Materials **94-96**: pp. 834–851.

Roach G. F. (2007): *Wave Scattering by Time-Dependent Perturbations.* Princeton University Press. New Jersey, US.

Rozsypalová I., Vyhlídal M., Dvořák R., Majda T., Topolář L., Pazdera L., Šimonová H. and Keršner Z. (2018): *Characterization of cement-based composite exposed to high temperatures via ultrasonic pulse method.* Acta Polytechnica CTU Proceedings **15**: pp. 99–103.

Rässler S. (2004): *Data Fusion: Identification Problems, Validity, and Multiple Imputation.* Austrian Journal of Statistics **33**(1&2): pp. 153–171.

Salamak M., Weseli J. and Radziecki A. (2007): *Monitoring of highway bridges in areas under mining exploitation influence.* 5th international Conference on Current and future Trends in Bridge design, Construction and maintenance. Beijing, China: pp. 469–478.

Salmanpour M., Khodaei Z. S. and Aliabadi M. (2016): *Guided wave temperature correction methods in structural health monitoring.* Journal of Intelligent Material Systems and Structures **28**(5): pp. 604–618.

Satour A., Montrésor S., Bentahar M., Elguerjouma R. and Boubenider F. (2013): *Acoustic emission signal denoising to improve damage analysis in glass fibre-reinforced composites.* Nondestructive Testing and Evaluation **29**(1): pp. 65–79.

Schickert G. (1984): *Critical reflections on non-destructive testing of concrete.* Matériaux et Constructions **17**(3): pp. 217–223.

Scruby C. and Moss B. (1993): *Non-contact ultrasonic measurements on steel at elevated temperatures.* NDT & E International **26**(4): pp. 177–188.

Sharma V. and Davis J. W. (2009): Feature-Level Fusion for Object Segmentation Using Mutual Information. Augmented Vision Perception in Infrared. Springer. London, UK: pp. 295–320.

Simon K. M. and Kishen J. M. C. (2016): *Influence of aggregate bridging on the fatigue behavior of concrete.* International Journal of Fatigue **90**: pp. 200–209.

Singh C., Singh A., Bharathi V. S., Bansal A. and Chadha R. (2012): *Frequency-dependent body wave attenuation characteristics in the Kumaun Himalaya.* Tectonophysics **524-525**: pp. 37–42.

Skalny J. P. (1985): *Instructional modules in cement science.* Cement and Concrete Research **15**(6): pp. 1087–1088.

Smith B., Scherer B. and Conklin J. (2003): *Exploring Imputation Techniques for Missing Data in Transportation Management Systems.* Transportation Research Record **1836**(01): pp. 132–142.

Solaiman B., Pierce L. E. and Ulaby F. T. (1999): *Multisensor data fusion using fuzzy concepts: application to land-cover classification using ERS-1/JERS-1 SAR composites.* IEEE Transactions on Geoscience and Remote Sensing **37**(3): pp. 1316–1326.

Song H., Popovics J. S. and Park J. (6-9): *Development of an automated contactless ultrasonic scanning measurement system for wavefield imaging of concrete elements.* 2017 IEEE International Ultrasonics Symposium (IUS). Washington, DC, US: pp. 1–3.

Sousa H. and Wang Y. (2018): *Sparse representation approach to data compression for strain-based traffic load monitoring: A comparative study.* Measurement **122**: pp. 630–637.

Staszewski W. J. (2000): *Advanced data pre-processing for damage identification based on pattern recognition*. International Journal of Systems Science **31**(11): pp. 1381–1396.

Stepinski T., Uhl T. and Staszewski W. (2013): *Advanced Structural Damage Detection*. Wiley. West Sussex, UK.

Stähler S. C., Sens-Schönfelder C. and Niederleithinger E. (2011): *Monitoring stress changes in a concrete bridge with coda wave interferometry*. The Journal of the Acoustical Society of America **129**(4): pp. 1945–1952.

Strauss R. E., Atanassov M. N. and Oliveira J. A. D. (2003): *Evaluation of the principal-component and expectation-maximization methods for estimating missing data in morphometric studies*. Journal of Vertebrate Paleontology **23**(2): pp. 284–296.

Sun M. and Butar Butar F. (2007): *Bayesian Multiple Imputation and Maximum Likelihood Methods for Missing Data*. In JSM Proceedings, Survey Research Methods Section. Alexandria, Virginia, US: pp. 3174–3180.

Sun Y., Kang Y. and Qiu C. (2011): *A new NDT method based on permanent magnetic field perturbation*. NDT & E International **44**(1): pp. 1–7.

Tabsh S. W. and Abdelfatah A. S. (2009): *Influence of recycled concrete aggregates on strength properties of concrete*. Construction and Building Materials **23**(2): pp. 1163–1167.

Tepfers R., Hedberg B. and Szczekocki G. (1984): *Absorption of energy in fatigue loading of plain concrete*. Matériaux et Construction **17**(1): pp. 59.

Tiwari K. A., Raisutis R. and Samaitis V. (2017): *Signal processing methods to improve the Signal-to-noise ratio (SNR) in ultrasonic non-destructive testing of wind turbine blade*. Procedia Structural Integrity **5**: pp. 1184–1191.

Tsai D.-M. and Lin C.-T. (2003): *Fast normalized cross correlation for defect detection*. Pattern Recognition Letters **24**(15): pp. 2625–2631.

Tsiskreli G. D. and Dzhavakhidze A. N. (1970): *The effect of aggregate size on strength and deformation of concrete*. Hydrotechnical Construction **4**(5): pp. 448–453.

Tsonos A. G. (2004): *Improvement of the earthquake resistance of R/C beam-column joints under the influence of P-Δ effect and axial force variations using inclined bars*. Structural Engineering and Mechanics **18**(4): pp. 389–410.

Turgut P. and Kucuk O. F. (2006): *Comparative relationships of direct, indirect, and semi-direct ultrasonic pulse velocity measurements in concrete*. Russian Journal of Nondestructive Testing **42**(11): pp. 745–751.

Unaldi N. and Asari V. K. (2010): *Undecimated Wavelet Transform-Based Image Interpolation*. Springer Berlin Heidelberg.

Unnthorsson R. (2013): Hit Detection and Determination in AE Bursts. Acoustic Emission - Research and Applications. InTech: pp. 1–19.

Vasshaug H. (2019): Revit and Reinforcement. Retrieved from `https://vasshaug.net/2014/06/04/revit-and-reinforcement/`.

Vateekul P. and Sarinnapakorn K. (2009): *Tree-Based Approach to Missing Data Imputation*. 2009 IEEE International Conference on Data Mining Workshops. Miami, US: pp. 70–75.

Vialatte F. B., Solé-Casals J., Dauwels J., Maurice M. and Cichocki A. (2009): *Bump time-frequency toolbox: a toolbox for time-frequency oscillatory bursts extraction in electrophysiological signals*. BMC Neuroscience **10**(1): pp. 46.

Wang S., Li D., Song X., Wei Y. and Li H. (2011): *A feature selection method based on improved Fisher's discriminant ratio for text sentiment classification*. Expert Systems with Applications **38**(7): pp. 8696–8702.

Wang X., Foliente G., Su Z. and Ye L. (2019): *Multilevel Decision Fusion in a Distributed Active Sensor Network for Structural Damage Detection*. Structural Health Monitoring **5**(1): pp. 45–58.

Weaver R. (1998): *Ultrasonics in an aluminum foam*. Ultrasonics **36**(1-5): pp. 435–442.

Weaver R. L. and Lobkis O. I. (2000): *Temperature dependence of diffuse field phase*. Ultrasonics **38**(1-8): pp. 491–494.

Wight J. K. (2015): *Reinforced Concrete: Mechanics and Design (7th Edition)*. Pearson.

Wolf J., Pirskawetz S. and Zang A. (2015): *Detection of crack propagation in concrete with embedded ultrasonic sensors*. Engineering Fracture Mechanics **146**: pp. 161–171.

Wu T. and Liu P. (1998): *Advancement on the nondestructive evaluation of concrete using transient elastic waves*. Ultrasonics **36**(1): pp. 197–204.

Xia Y., Chen B., Weng S., Ni Y.-Q. and Xu Y.-L. (2012): *Temperature effect on vibration properties of civil structures: a literature review and case studies*. Journal of Civil Structural Health Monitoring **2**(1): pp. 29–46.

Yan J., Downey A., Cancelli A., Laflamme S., Chen A., Li J. and Ubertini F. (2019): *Concrete Crack Detection and Monitoring Using a Capacitive Dense Sensor Array*. Sensors **19**(8): pp. 1843.

Yang Z. and Mueller R. (2007): *Spatial-spectral cross-correlation for change detection : A case study for citrus coverage change detection.* ASPRS 2007 Annual Conference. Tampa, FL: pp. 767–777.

Yaphary Y. L., Lam R. H. W. and Lau D. (2017): *Chemical Technologies for Modern Concrete Production.* Procedia Engineering **172**: pp. 1270–1277.

Yi T.-H., Li H.-N. and Zhao X.-Y. (2012): *Noise smoothing for structural vibration test signals using an improved wavelet thresholding technique.* Sensors **12**(8): pp. 11205–11220.

Yilmaz Ç. and Wasti S. T. (Eds) (1984): *Analysis and Design of Bridges.* Springer. The Hague, Netherlands.

Yu L. and Giurgiutiu V. (2005): *Advanced signal processing for enhanced damage detection with piezoelectric wafer active sensors.* Smart Structures and Systems **1**(2): pp. 185–215.

Yu X. and Kwon E. (2009): *A carbon nanotube/cement composite with piezoresistive properties.* Smart Materials and Structures **18**(5): pp. 055010.

Yun H.-B., Kim S., Wu L. and Lee J. J. (2013): *Development of Inspection Robots for Bridge Cables.* The Scientific World Journal **2013**: pp. 967508.

Zahiri-Azar R. and Salcudean S. (2006): *Motion Estimation in Ultrasound Images Using Time Domain Cross Correlation With Prior Estimates.* IEEE Transactions on Biomedical Engineering **53**(10): pp. 1990–2000.

Żak G., Wyłomańska A. and Zimroz R. (2017): *Local damage detection method based on distribution distances applied to time-frequency map of vibration signal.* 2017 IEEE 11th International Symposium on Diagnostics for Electrical Machines, Power Electronics and Drives (SDEMPED). IEEE. Tinos, Greece: pp. 134–140.

Zakić B. D., Ryzynski A., Guo-Hong C. and Jokela J. (1991): *Classification of damage in concrete bridges.* Materials and Structures **24**(4): pp. 268–275.

Zapłotny M., Katunin A. and Dragan K. (2017): *Enhancement of Damage Detectability in Aircraft Structures Using the Fusion of NDT Results.* Fatigue of Aircraft Structures **2017**(9): pp. 55–74.

Zhang Y., Abraham O., Grondin F., Loukili A., Tournat V., Duff A. L., Lascoup B. and Durand O. (2012): *Study of stress-induced velocity variation in concrete under direct tensile force and monitoring of the damage level by using thermally-compensated Coda Wave Interferometry.* Ultrasonics **52**(8): pp. 1038–1045.

Zhang Y., Abraham O., Larose E., Planes T., Duff A. L., Lascoup B., Tournat V., Guerjouma R. E., Cottineau L.-M., Durand O., Thompson D. O. and Chimenti D. E. (2011): *Following stress level modification of real size concrete structures with coda wave interferometry (CWI)*. Vol. 1335. AIP: pp. 1291–1298.

Zhang Y., Abraham O., Tournat V., Duff A. L., Lascoup B., Loukili A., Grondin F. and Durand O. (2013): *Validation of a thermal bias control technique for Coda Wave Interferometry (CWI)*. Ultrasonics **53**(3): pp. 658–664.

Zhou G.-D. and Yi T.-H. (2013): *Recent Developments on Wireless Sensor Networks Technology for Bridge Health Monitoring*. Mathematical Problems in Engineering **2013**: pp. 1–33.

List of figures